PEOPLE'S DEMOCRATIC REPUBLIC OF ALGERIA
MINISTRY OF HIGHER EDUCATION AND SCIENTIFIC RESEARCH

UNIVERSITY OF SAAD DAHLAB BLIDA 1
FACULTY OF TECHNOLOGY
MECHANICAL ENGINEERING DEPARTMENT

To obtain the Master's Degree in Mechanical Engineering, Major:

Materials Engineering

Laboratory for studies and research in industrial technology

Title

Tribological investigations on the lubricious properties of exfoliated kaolinite

By :

ChananeSihame

MamecheImene

Proposed and led by:

Dr. BenamorAbdessabour

Year: 2022/2023

THANKS

Above all, we would like to praise Allah the Almighty for the benefits he has granted us during our studies and during the realization of this thesis.

This thesis is the result of a long research work. As a preamble, I want to address all my thanks to the members of the jury Dr. AbdessabourBenamor Dr Hadji Mohamed Dr. Chiker Nabil Dr.NemriYacin Dr. Haddad Adel Dr. AbderrahmenAbderrahmen for their interest in my research by accepting to examine my work and enrich it with their proposals. I would like to thank the faculty and administrative staff of our department (Department of Mechanical engineering), I would like to express my deep gratitude to our promoter Dr. ABDESSABOUR BENAMOR for his precious helppositive energy, and patience with us.

I would like to thank all the members of the Laboratory for studies and research in industrial technology (LERTI) for their help and sympathy shown during my presence at LERTI. Without forgetting all the teachers whether primary, middle, high school or Higher Education.

To any human being who added a piece to my Knowledge.

Finally, I would like to extend my most sincere thanks to everyone who has contributed directly or by far to the realization of this work.

Thank you to all of you.

Dedication

A merency meetig of feeling

To my father Abd-el-Kader and my mother Houria

To the most beautiful and truest friend I ever knew Siham

To a very special person with his pure thoughts and soul Abdessabour

To me for never giving up even in the face of challenges and obstacles Imene

To all the people who are dear to my heart I'm so thankfull to having known you

One day ….

Dedication

This work is dedicated to To my dear parents chanane abdelbasire & chaibe fatmazohra. To my brothers ABEDELMADJID, habiba, fella rachida to my nephews.

To my best friend Mameche Imene

To the nicest teacher I met in college Mr.Benamore Abdessabore

To all university families

One Day....

Table Des Matières :

CHAPTER III : COMPOSITE MATERIALS GENERAL

FIGURE S CONTENTS

Chapter 1

Chapter2

Chapter3

Chapter 4

Chapter 5

Figure 5.5:wear trace for worn surfaces lubricated by oil and oil + different concentration of KNT

Figure 5.6: a). b). c.) d). e). f) shows the optical microscopy of the wear marks for the different samples a of KNT 1% 0.7% 0.5% 0.2% 0.1%

Figure 5.7: a). b). c.) d). e). f) shows the optical microscopy of the wear marks for the different samples of pawderkaoilniteexfolié.

Figure 5.8: Optical microscopy of wear marks of 100Cr6 steel balls a) Kno_3b) DMSO C) Raw d) kuera

Figure5.9: image from inkscape present optical microscope result showing the FSP of Al2024 Cr2 AlC

Figure5.10: image from inkscape present optical microscope result showing the FSP of Al2024 KUrea

Figure5.11: The varaition hardness changes in each of these samples witness not heat treated, witness heat treated Al2024 530 °, Cr_2AlC not heat treated and Al2024 Cr_2AlC heat treat530°

Figure5.12: The varaition hardness changes in each of these samples witness not heat treated, witness heat treated 530 °, Al2024 + KUrea not heat treated and Al2024+KUrea heat treat 530°.

Figure5.13: The varaition hardness changes in each of these samples witness not heat treated, witness heat treated 480 °, Al2024 + KUrea not heat treated and Al2024+KUrea heat treat 480°.

Figure 5.14: The varaition hardness changes in each of these samples witness not heat treated, witness heat treated 500 °, Al 2024 KUrea not heat treated and Al 2024 KUrea heat treat500°.

Figure 5.15:variation in coefficient of friction for Al 2024 witout friction stir processing and Al 2024 +KUrea with FSP

Figure5.16: wear trace for worn surfaces for Al 2024 witout friction stir processing and Al 2024 +KUrea with FSP

Abstract:

This work focuses on the study of the lubricating properties of peeled kaolin. This work consists mainly ofTry several detailing methods and choose the best method in terms of dergified exfoliationClay (Kaolin) in its natural state. The study will then consist in characterizing the tribological properties of thisClay as an additive in paraffin oil for tribological applications, then we used the best result as a solid reinforcement lubricant in friction stir processing to improve the properties of Al 2024

Key Words:kaoilnite, two-dimensional materials, tribology , lubrication

Résumé :

Ce travail porte sur l'étude des propriétés lubrifiantes du kaolin pelé. Ce travail consiste principalement à Essayez plusieurs méthodes détaillées et choisissez la meilleure méthode en termes d'exfoliation certifiée Argile (Kaolin) à l'état naturel. L'étude consistera ensuite à caractériser les propriétés tribologiques de ceL'argile comme additif dans l'huile de paraffine pour les applications tribologiques, nous avons ensuite utilisé le meilleur résultat comme lubrifiant de renforcement solide dans le traitement par friction-malaxage pour améliore les propriétés de Al 2024

Mots clefs :kaoilnite, matériaux bidimensionnel, , lubrification, tribologie

ملخص :

يركز هذا العمل على دراسة خصائص تشحيم الكاولين المقشر. يتكون هذا العمل بشكل أساسي من تجربة العديد من الطرق التفصيلية واختيار أفضل طريقة من حيث تقشير الطين المعتمد (كاولين) في الحالة الطبيعية. ستتألف الدراسة بعد ذلك من وصف الخصائص القبلية لهذا الطين على أنها مادة مضافة في زيت البارافين للتطبيقات القبلية، ثم استخدمنا أفضل نتيجة كمزلق تقوية صلب في خلط علاج الاحتكاك لتحسين خصائصAl 2024

GENERAL ITRODUCTION

In Chapter 1 we talked about kaolin, a two-dimensional material that has some similarities to graphene. Kaolin is a clay mineral that is widely used in various fields thanks to its remarkable properties.

In the second chapter, we talked about the special properties of two-dimensional materials, which are of great interest to the scientific community. A major breakthrough was made in this area in 2004, paving the way for extensive research on these materials. Since then, many new 2D materials have been discovered, further promoting research in this field in recent years

In the third chapter we talked about the study and design of composite materials, which have aroused great interest in various fields of modern chemistry for almost a century. These materials are characterized by their heterogeneous, isotropic, or anisotropic compositions, and often have superior performance in terms of chemical and mechanical properties compared to homogeneous materials.

In the experimental part, we will evaluate the performance of kaolin as a solid lubricant. We will conduct experiments to measure and analyze its effectiveness in reducing wear and friction.

The results obtained and their interpretation will then be presented in the corresponding section. We will discuss kaolin's performance as a solid lubricant, highlighting its advantages and potential limitations.

Finally, we will conclude our thesis by summarizing the main points discussed and highlighting the importance of kaolin as a solid lubricant, while suggesting avenues for future research .

CHAPTER 1

KAOLINITE

1.INTRODUCTION:

Kaolinite is a clay mineral that belongs to the phyllosilicate group. It is one of the most common minerals found in nature and is widely distributed around the world. Kaolinite is named after the Kao-ling mountain in China, where it was first discovered.

The structure of kaolinite consists of alternating layers of silicon (Si) and aluminum (Al) atomsbonded to oxygen (O) and hydroxyl (OH) groups. It is composed of one octahedral sheet and one tetrahedral sheet stacked together.

The phase transformation of kaolinite refers to the changes in its crystal structure and propertiesthat occur under certain conditions, such as heating or exposure to different environments.The key phase transformations of kaolinite are :

1.**Metakaolinite:** The decomposition process of kaolinite into metakaolinite takes place within a temperature range typically spanning from around 400°C to 630°C.

2.Spinel-Type Phase: At a temperature of 920°C, a distinct phase with a spinel-type structure originated and exhibited stability until at least 1150°C.

3.Mullite Phase: Observations revealed that the microcrystalline mullite exhibited a size of less than 10 nm, which remained constant until reaching a temperature of 1100°C. However, beyond 1200°C, a significant increase in the size of mullite was observed.

4.SiO2 Phase: The formation of the SiO2 phase is considered to be closely associated with the decomposition of metakaolinite. When metakaolinite is subjected to high temperatures, typically above 1000°C, it undergoes further transformations leading to the formation of silica (SiO2). During this process, the structure of metakaolinite breaks down, and the aluminum and silicon oxides rearrange to form SiO2. The resulting SiO2 phase can exhibit various crystal structures, such as quartz, cristobalite, or tridymite, depending on the specific conditions and cooling rates. The formation of SiO2 plays a crucial role in determining the properties and characteristics of materials derived from metakaolinite, particularly in refractory applications and the production of high-temperature-resistant materials.

5.Phase Transformation Sequence: The phase transformation sequence can be summarized as follows: Firstly, metakaolinite retains its structural integrity up to 920°C, with decomposition initiating at 940°C. Secondly, the spinel-type phase does not form directly

from the decomposition of metakaolinite but instead undergoes a topotactic process in relation to metakaolinite prior to decomposition. Thirdly, the breakdown of metakaolinite, starting around 940°C, facilitates the formation of mullite while preserving the previously formed spinel-type phase. Finally, the complete decomposition of the spinel-type phase takes place at approximately 1200°C.

Kaolinite possesses several distinctive properties that contribute to its versatility and usefulness invarious applications. These propertiesinclude:structure stability; cationexchange capacity;Adsorbtion; Charge Heterogeneity;Adsorbtion; Charge Heterogeneity; Electrokinetic Property.

Kaolinite possesses a wide range of physical and chemical properties that render it highly valuable in numerous applicationslike paper, ceramics ,catalysts ,florideabsorbtion ,fondry,flame retardant…ext

2.DEFINITION AND STRUCTURE OF KAOLINITE:

Kaolinite was first proposed as a mineral by Johnson and Blake (1867) the word kaolinite derived from kaolin relative to the region kauling in chaina[1].

Kaolinite is a type of clay mineral that is formed by the weathering and erosion of rocks rich in feldspar. It is a white or grayish mineral that is soft and earthy in texture, and it has a plate-like structure. Kaolinite is composed of aluminum silicate hydroxide with the chemical formula $Al_2Si_2O_5(OH)_4$. It is typically found in soils, sediments, and sedimentary rocks, and it is an important constituent of many types of clay, including porcelain clay, china clay, and ball clay. Kaolinite has many industrial uses, including in the production of paper, ceramics, and refractory materials.

Kaolinite is an inorganic silicate clay mineral that occurs naturally with a layer structure. The mineral has the chemical formula $Al_2Si_2O_5(OH)_4$. The siloxane layer of kaolinite is composed of SiO_4 tetrahedra arranged in a hexagonal array. The apical oxygen atoms of the tetrahedra are connected to a second layer containing aluminum ions and OH groups, known as the gibbsite-type layer[2]. This arrangement forms a dioctahedral 1:1 phyllosilicate structure, with interlayer spaces between adjacent layers held together by van der Waals forces and hydrogen bonding. These interlayer spaces restrict access to the interlamellar aluminol groups (Al-OH), which can be used for grafting reactions (fig 1). The most reactive

functional groups in kaolinite are hydroxyl groups, which can participate in various chemical reactions and ion exchange processes [3-4].

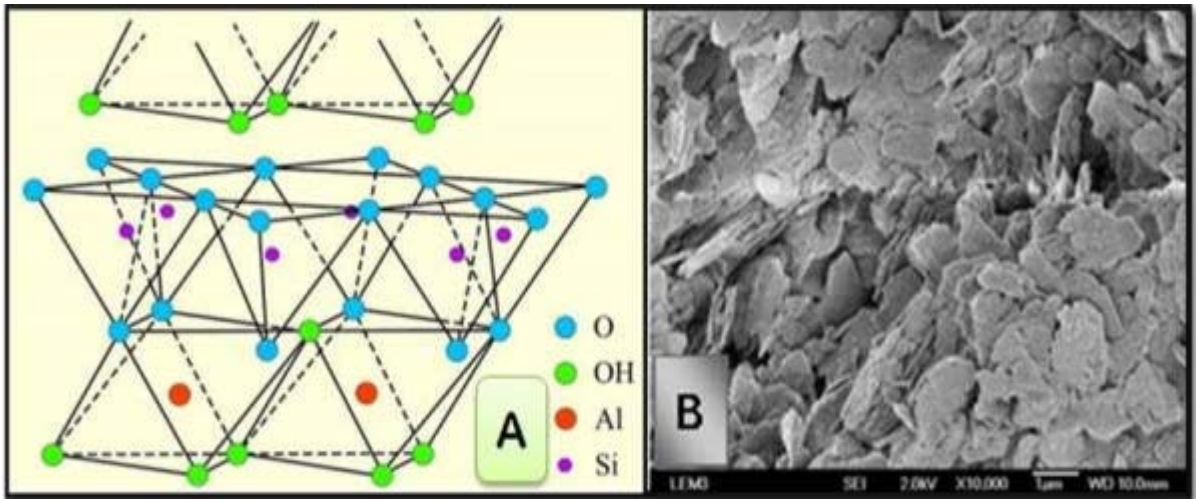

Figure 1-1 :(A)Kaolinite structure (El Hachmi, 2013), (B) SEM photo of kaolinite (Wei et al., 2013; Wei, 2014).

The alumina-oxygen octahedral sheet contains two types of hydroxyl groups: the outer and inner hydroxyl groups [3-5]. The outer hydroxyl groups are positioned on the unshared plane of the alumina hydroxyl sheet, while the inner hydroxyl groups are found on the plane shared with and adjacent to the silica-oxygen tetrahedral sheet. The bonding between the silica-oxygen and alumina-oxygen sheets limits the mobility of the inner hydroxyl groups.

Kaolinite's structure, which includes three surface hydroxyl groups, is vertically aligned with the layer, creating three interlayer hydrogen bonds. Additionally, kaolinite has several reactive groups on its surface [6,7]. The exposed hydroxyl groups and strong groups (>Al2OH) on the O faces are formed from ruptured alumina octahedra, and oxygen atoms are exposed on the SiO2 surface of the crystal. In addition, there are (>Al-OH) groups that result from ruptured alumina octahedra and (>SiO) groups from broken silica tetrahedra.

Kaolinite particles present an anisotropic nature that makes it difficult to predict their behavior, as they are composed of three distinct surfaces. One surface consists of a siloxane surface formed by tetrahedral units with inert Si-O-Si bonds. The basal surface comprises an octahedral gibbsite (Al (OH)3) sheet, and the edge planes (110) and (010) [8]. To better understand kaolinite properties, it is necessary to determine the characteristics of each surface [5, 9-11]. Various factors influence the surface activity of kaolinite, such as its chemical composition, the nature of its surface atoms, the type and extent of defect sites, layer charge,

and the type of exchangeable cations. These factors play a critical role in optimizing physicochemical properties and expanding potential applications.

The diverse and distinct structural characteristics of kaolinite can be attributed to its formation during long, complex geological processes such as construction, migration, and deposition. These processes have led to the formation of structural defects in kaolinites,which

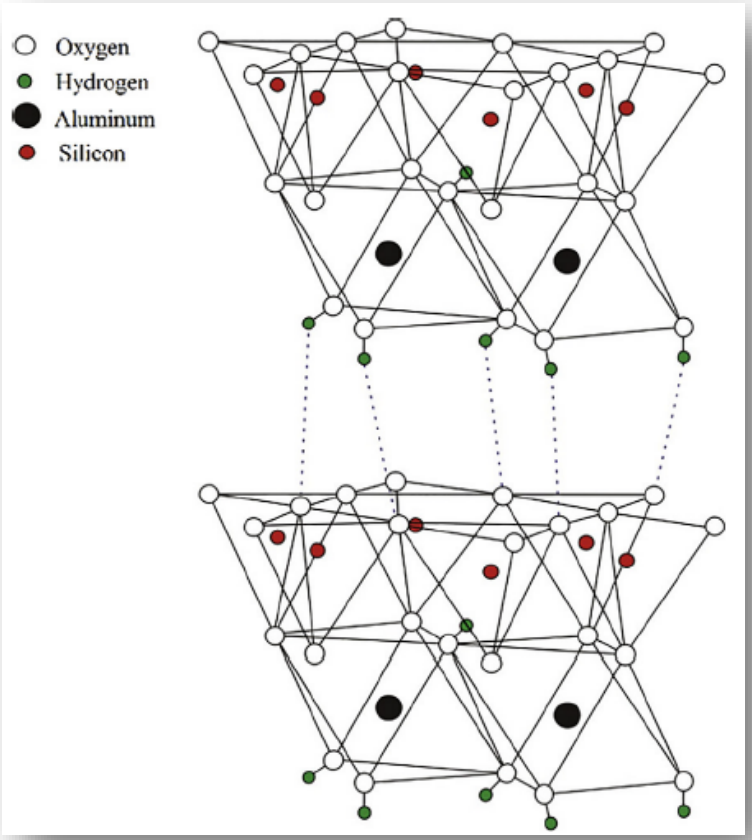

Figure 1-2: Schematic view of the structure of kaolinite. Reproduced with permission from H. Cheng, Q. Liu, J. Yang, S. Ma, R.L. Frost, The thermal behavior of kaolinite intercalation complexes—a review, Thermochim. Acta 545 (2012) 1–13.

are linked to various geological factors like chemical composition, temperature, pressure, and formation process [12-15]. The chemical composition of kaolinite, which includes impurities like mica, quartz, and metal oxides (K2O, CaO, TiO2, Fe2O3, Na2O, MgO, MnO, and P2O5), plays a significant role in affecting the degree of disorder and particle size of kaolinite [0]. Kaolinitehas a tendency to form a wide range of ordered and disordered polytypes, with a higher number of structural defects corresponding to a lower crystallizationdegree.

2.CHEMICAL AND THERMAL ANALYSES OF KAOLINITE:

The chemical composition of the kaolinite sample was 44.80wt% SiO_2, 39.02 wt% Al_2O_3, 0.05 wt% Fe_2O_3, 0.04 wt% MgO,0.05 wt% CaO, 0.04 wt% Na_2O, 0.03 wt% K_2O, and 0.04 wt%TiO_2.

3.PROPERTIES:

Urrent research on kaolinite focuses on its surface, interlayer, and structure, which are interconnected and play important roles in determining its properties. Kaolinite possesses a wealth of physical and chemical properties that make it highly useful in numerous applications such as paint, paper, rubber, plastic, cable, ceramic, enamel, refractory, textile, cement, automotive, chemical, environmental, agricultural, and many others [1, 3, 12, 16].Therefore, developing a comprehensive understanding of the properties of kaolinite is crucial for optimizing itsstructural characteristics and expanding its potential applications.

3.1. STRUCTURE STABILITY:

Due to its tightly packed structure and limited or non-existent isomorphous substitution, kaolinite particles are difficult to break down, and its layers are difficult to separate [17]. Furthermore, kaolinite exhibits exceptional molecular stability, even under harsh acid and alkali conditions, except under long-term mechanical action or roasting. Additionally, its unique surface structure prevents kaolinite from expanding in kaolinite/water dispersions or other media. [18]

3.2. CATAION EXCHANGE CAPACITY:

The cation exchange capacity (CEC) measures the ability of kaolinite to exchange cations and retain nutrients, which is crucial for assessing its adsorption capacity and understanding the interaction between plants and nutrients [19, 20]. The CEC of kaolinite is affected by its pH level and the quantity of impurities present. Kaolinite with high impurity or high pH levels generally exhibit high CEC values. Furthermore, the degree of structural order also affects the CEC of kaolinite, with a negative correlation between the degree of order and the CEC value.Compared to other 2:1 type clay mineral, kaolinite has a low cation exchange capacity (CEC) of approximately 5 meq/100 g.

3.3. ADSORPTIONA:

He adsorptive capacity of kaolinite for basic ions or groups is augmented by its Bronsted and Lewis type of acidity and acidic sites [21]. Adsorption is a surface phenomenon that occurs due to interactions between individual atoms, ions, or molecules of an adsorbateand those present on the adsorbent surface. The process involves separating matter from onephase and accumulating it at the surface of another phase.

The adsorption activity of solids mainly occurs at the edges or surfaces [21,22], and kaolinite is a mineral with unique surface features that enable it to adsorb a wide range of substances, including metal ions. Metal ion adsorption is usually accompanied by the release of hydrogen ions from the mineral's edge sites [23]. Additionally, adsorption can also take place on the flat exposed planes of the silica and alumina sheets. Adsorption of F, Cr, As, Cd, Co, Cu, Fe, Pb, Mn, Ni, and Zn shows great potential [24]. Many studies have also examined the adsorption of molecules, such as CH4 and N2 gases.

3.4. CHARGE HETEROGENEITY:

Kaolinite has a layer charge generally close to zero, and variable surface charges, including permanent structural charge and surface charge[25,26]. Negative structural charges are associated with undefined isomorphic substitutions in crystal structures. The surface charge is the result of physicochemical processes in different media, leading to the decomposition of Si-O and Al-OH on the edge surfaces and Al2OH on the octahedral gibbsite layer (Al(OH)3), leading to unique results leading to the charge Heterogeneity[27]. Protonation of the aluminum alcohol groups occurs when kaolinite is placed in an aqueous medium at a pH below the point of zero net proton charge at the primary (amphoteric) edge site.Conversely, deprotonation of silanol and aluminum alcohol groups occurs at pH values greater than the point of zero net proton charge at the primary (amphoteric) edge site. As the pH increases, the surface charge changes from positive to zero and then negative. The surface charge of kaolinite is affected by factors such as pH value, ionic strength, solid-liquid ratio, crystallinity and particle size of the surrounding medium. [29-30].

The surface of kaolinite exhibits two types of charges: a permanent charge resulting from isomorphic substitution of Al/Si, and a variable charge resulting from protonation or deprotonation of an end group. At a pH where the surface charge is zero, it is referred to as

the surface zero charge point (pHpzc). When the suspension pH is below the pHpzc, the surface of kaolinite is positively charged. Conversely, when the pH is above the pHpzc, the surface is negatively charged. Based on acid-base titration results, the pHpzc of the kaolinite surface is determined to be 5.1.

3.5. ELECTROKINETICPROPERTYE:

The interfacial properties of inorganic solids and liquids are of significant interest due to their impact on the stability of colloidal kaolinite dispersions. These properties have a dominant influence on a broad range of interfacial processes. In aqueous suspension, kaolinite experiences ion exchange and group dissociation on its surface, leading to ionic conductance. Thus, the properties of the aqueous phase have a critical influence on the electro-osmotic permeability and zeta potential of kaolinite particles[31]. The Zeta potential of kaolinite is influenced by various factors, such as pH, ionic strength, solid-liquid ratio, and concentration and type of electrolytes in the medium. Additionally, the crystallinity of kaolinite plays a crucial role in determining its Zeta potential.

3.6. PHYSICO-CHIMICAL PROPERTIES:

Kaolinite is characterised by several physico-chemical properties that aredifferentiated from other groups of kaolins. Table 04 shows some of the physico-chemical properties ofproperties of kaolinite:

Tab. 01: Physico-chemical properties of kaolinite (Ledoux .R. and White J.L, 1965).

Density	hardness	Molar mass (g/mol)	Specific surface(m^2/g)
2.4 - 2.65	2 - 2.5	258	10 - 22

4.PHASE TRANSFORMATION OF KAOLINITE:

4.1. METAKAOLINITE:

The decomposition of kaolinite into metakaolinite occurs within the temperature range of approximately 400°C to 630°C. The X-ray diffraction analysis of metakaolinite reveals the absence of distinct diffraction peaks, indicating its amorphous nature. However, electron

diffraction patterns show that it still retains some crystalline characteristics(Figs. 2(c,d)). Specifically, the six nearest spots surrounding the direct beam remain visible after heating, suggesting the preservation of short-range order while the long-range order is disrupted. This indicates that metakaolinite undergoes structural changes during decomposition, retaining certain degrees of order at a local scale while losing its overall crystalline arrangement.

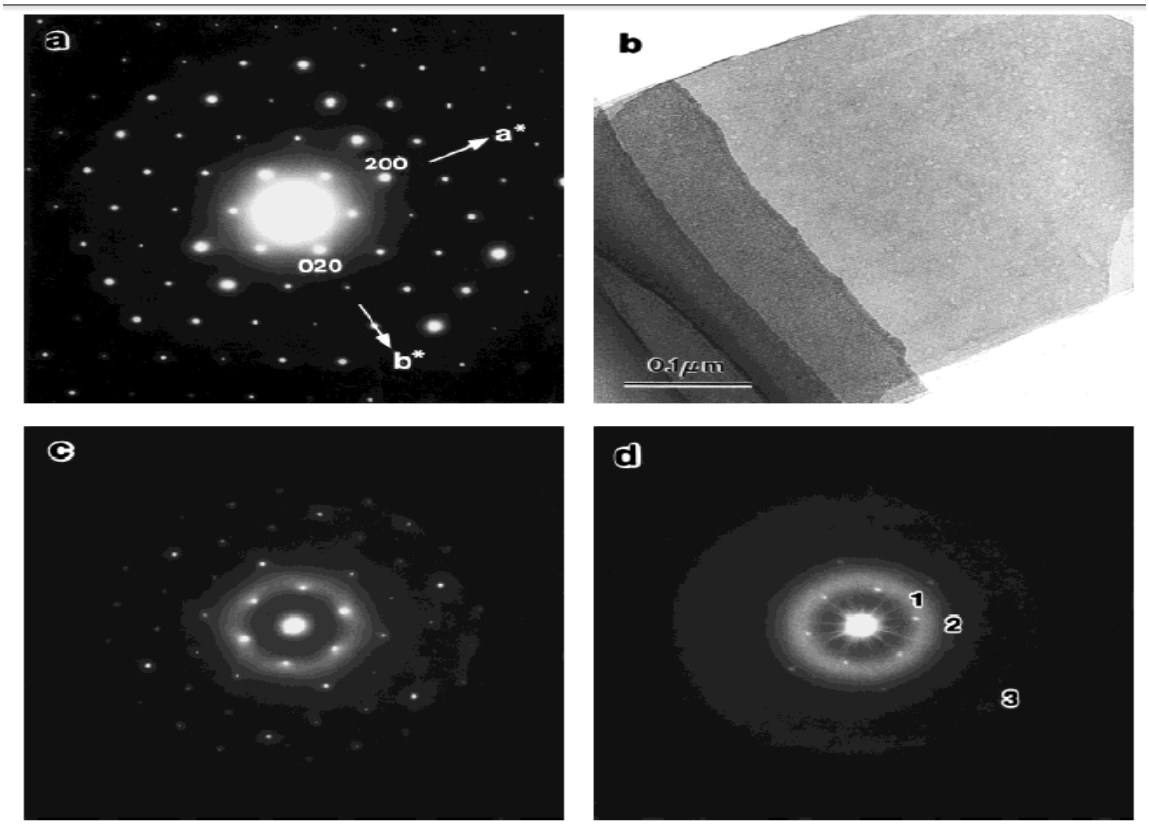

Fig 1.3: (a) The [001] electron diffraction pattern and (b) the bright-field image of the unheated kaolinite, and the electron diffraction patterns of the heated kaolinite at (c) 500° and (d) 630°C. The diffuse halos in (d) are designated with numbers.

When subjected to heat, the weakest chemical bonds within a crystal structure are susceptible to breaking or disruption, initiating a phase transformation in that specific region. In the case of kaolinite, the dehydroxylation process primarily affects the $Al(O,OH)_6$octahedral sheet while having minimal impact on the SiO_4 tetrahedral sheet. It is suggested that the outer hydroxyl groups are situated in a more reactive environment compared to the inner hydroxyl groups, which are relatively shielded(figure 3)[33.34]. Consequently, the outer hydroxyl groups are more easily eliminated through heating compared to the inner hydroxyl groups. The remaining hydroxyl groups play a crucial role in providing support to the overall

structure of metakaolinite, particularly in conjunction with the SiO4 tetrahedral sheets. This may explain why the characteristic electron diffraction pattern of metakaolinite persists even at high temperatures, such as 920°C.(MacKenzie*et al* 9.Rocha and Klinowski,[14][29]. Studies utilizing Fourier transform infrared spectroscopy (FT-IR) and solid-state[29,27]**Si** and Al nuclear magnetic resonance spectrometry (NMR) .MacKenzie*et al*.9. have demonstrated that approximately 10% of the hydroxyl groups remain in the metakaolinite structure. Furthermore, the use of cross polarization (CP) NMR, which detects silicon atoms in proximity to protons, has revealed that the residual hydroxyl groups in metakaolinite become associated with various Si environments as indicated by their chemical shift.

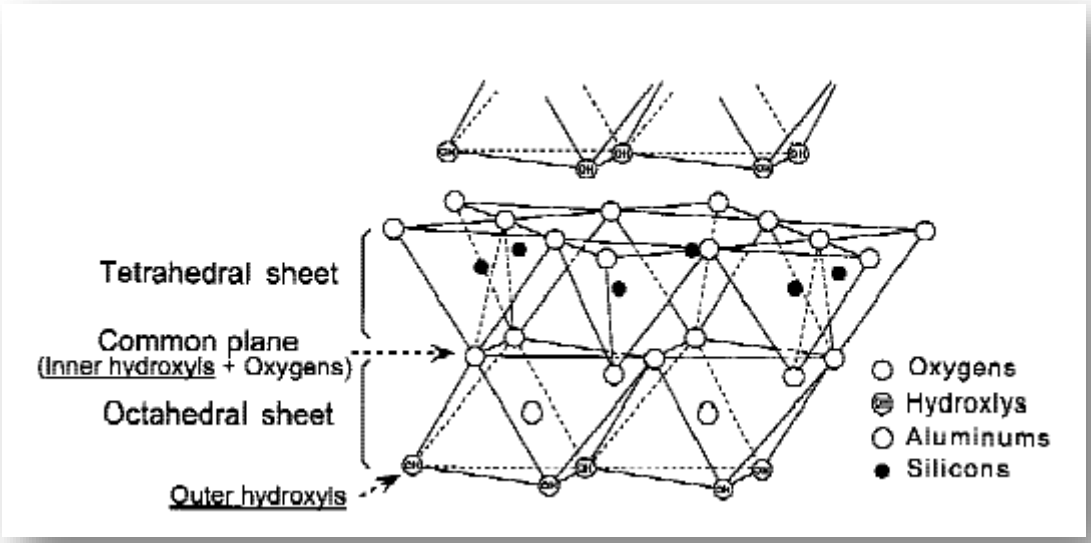

Fig. 1.4:Schematic drawing of kaolinite structure (after Gruner32).

4.2. SPINEL-TYPE PHASE:

At a temperature of 920°C, a spinel-type phase emerged and remained stable until at least 1150°C.Traditionally, this phase is known to form simultaneously with mullite following the initial exothermic reaction. However, our recent electron diffraction data revealed that the spinel-type phase appeared before the mullite phase, even before the occurrence of an exothermic peak (Figs. 4(a,c)). The electron diffraction patterns of the newly formed spinel-type phase exhibited pseudohexagonal symmetry, supporting the notion that it displayed a preferred orientation towards the parent kaolinite structure, as previously proposed by various studies [2, 4, 22, 24, 25].

Based on investigations by Brindley and Nakahira [reference 3], the cube axis [111] was determined to be perpendicular to the (001) plane of kaolinite, while the cube-face diagonal [110] aligned with the b-axis of kaolinite, as observed through rotation and oscillation photographs. Nonetheless, in(Fig. 4(a)),

the diffraction spots of the spinel-type phase (with a d-spacing of approximately 1.4 Å) did not precisely intersect at 60°, and the d-spacings were not uniform, suggesting that this phase might not possess the previously assumed high cubic symmetry.

In an attempt to compare the spinel-type phase, Brindley and Nakahira also synthesized γ-alumina; however, the exact structure of γ-alumina remains unclear. Nevertheless, it can be confidently concluded that the spinel-type phase resulted from a topotactic transformation of metakaolinite due to its simultaneous presence with metakaolinite at 920°C.

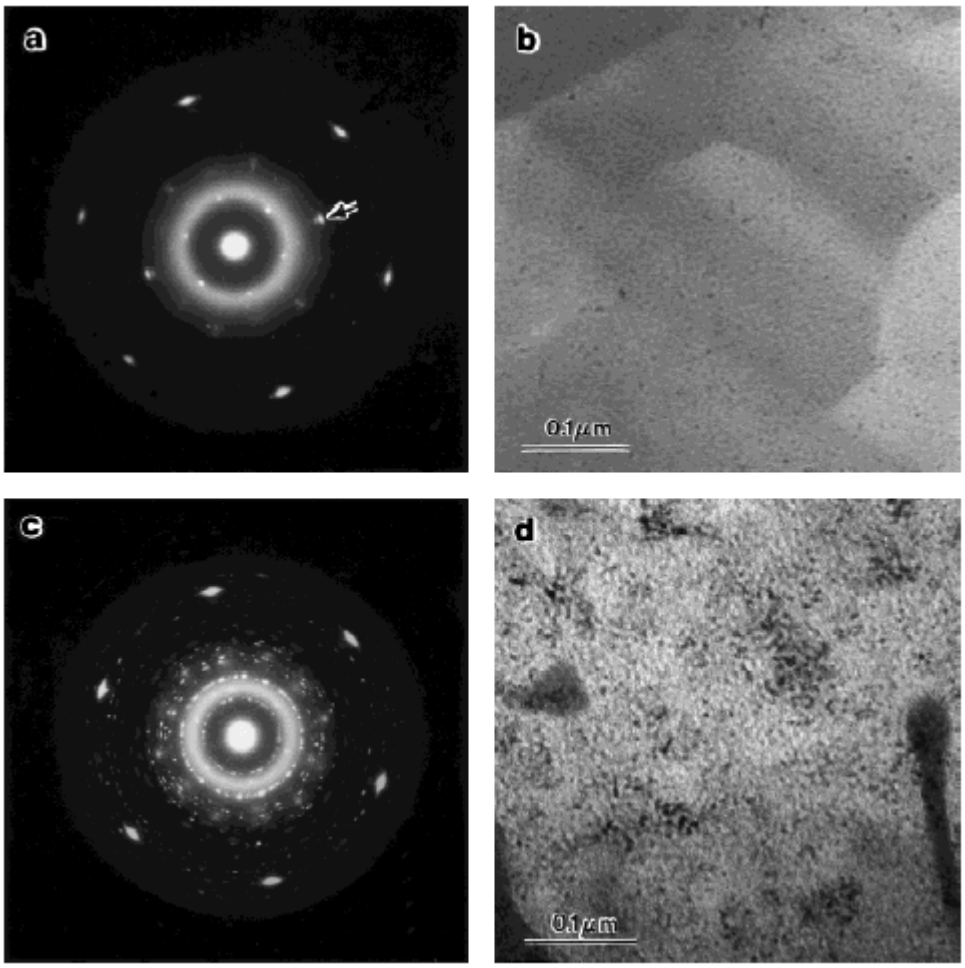

Fig. 1.5:(a) The electron diffraction pattern and (b) the bright-field image of the heated kaolinite at 920°C. One of the newly formed faint spots located at the edge of the second halo is indicated with an arrow. (c) The electron diffraction pattern and (d) the bright-field image of the heated kaolinite at 940°C.

The electron diffraction pattern of the spinel-type phase was intriguing as it displayed characteristics similar to that of a single crystal rather than the typical ring pattern observed in microcrystals. However, the diffuse nature of each spot indicated the presence of three possible orientations of the newly formed spinel-type microcrystals, which were related by 3-fold symmetry. Since the cubic spinel with [111] orientation exhibits 3-fold symmetry, it is

likely that the spinel-type phase on metakaolinite possessed lower symmetry with a domain structure resulting from rotational relationships [30].

Although the chemical composition of the spinel-type phase has been examined using EDS (energy dispersive spectrometry), it has not been conclusively determined. The electron beam used for analysis had a minimum possible diameter of 1.6 nm, but to obtain sufficient intensity, a beam size of at least 5 nm was necessary. Both Al and Si were detected in all parts of the grain, and although small variations were observed, the ratio of Al to Si remained constant. However, it is important to note that the presence of Si does not necessarily indicate that the spinel-type phase is an Al-Si spinel. In the case of topotaxy, even if the spinel-type phase corresponds to γ-alumina, the detection of Si could originate from metakaolinite or amorphous silica in the surrounding area. It is challenging to eliminate the effects of beam size restrictions and beam spreading during the analysis.

4.3. MULLITEPHASE:

Based on the findings of [3], who proposed that the c-axis of mullite aligns with the α110β orientation of the spinel-type phase, it was observed that the microcrystalline mullite initially had a size of less than 10 nm, which remained consistent until 1100°C. However, beyond 1200°C, the size of mullite experienced a sudden increase (Figs. 5(b,d)).

While the formation of the spinel-type phase did not require the collapse of the metakaolinite structure, it is believed that the breakdown of metakaolinite, commencing at 940°C, facilitated the growth of mullite nuclei. The subsequent growth of mullite was temporarily hindered, likely due to the coexistence of the spinel-type phase and mullite. Both phases necessitated the availability of Si from amorphous silica for their growth. As a result, the initial strong exothermic peak at approximately 1000°C is likely attributed to the nucleation of mullite rather than the formation of the spinel-type phase from metakaolinite. Ongoing investigations are focused on understanding the chemical compositional changes of mullite with respect to temperature.

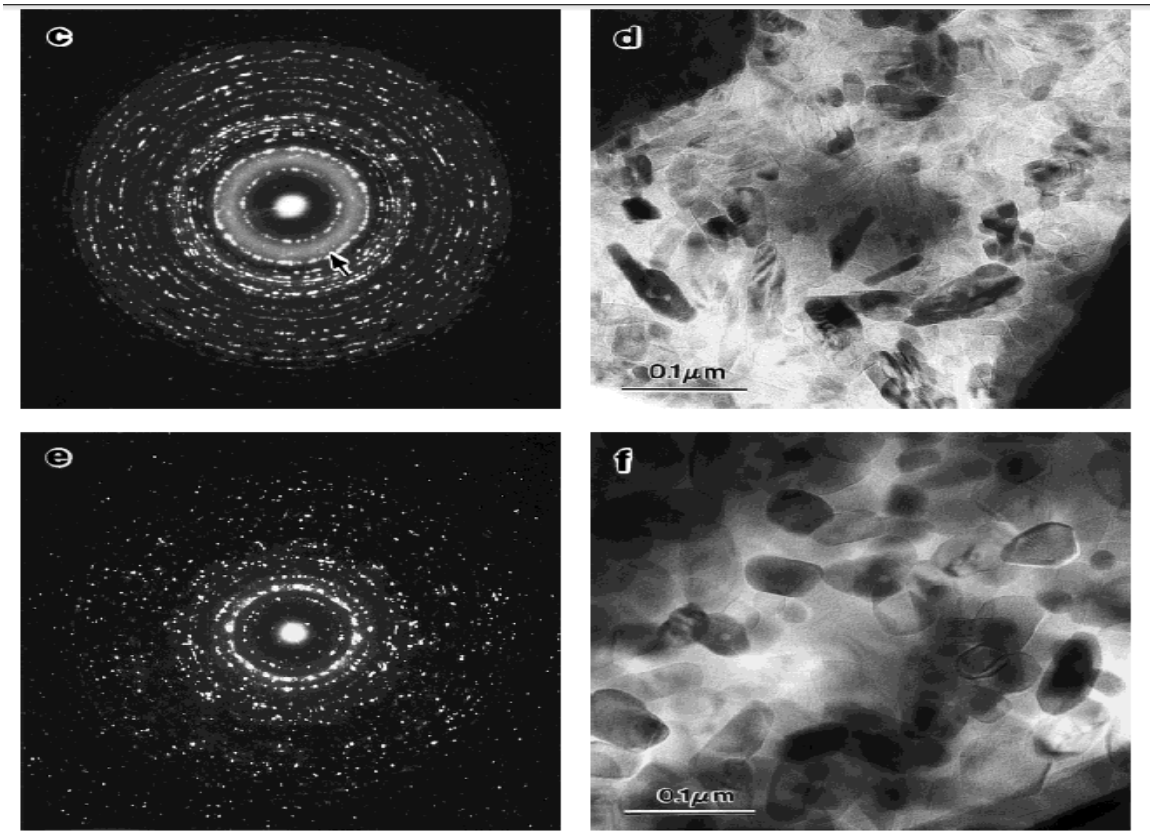

Fig. 1.6.: The electron diffraction patterns and the bright-field images of the heated kaolinite at (a,b) 1100°, (c,d) 1200°, and (e,f) 1300°C. Some scattered spots of cristobalite within the first diffuse ring in (c) are indicated with an arrow.

4.4. SiO2 Phase:

The formation of the SiO2 phase is believed to be closely linked to the decomposition of metakaolinite. The separation of the Si tetrahedral sheet and the Al octahedral sheet provides ample opportunity for the generation of amorphous silica. This hypothesis is supported by several pieces of evidence. Firstly, the diffraction spots of metakaolinite weakened at 940°C, while the intensity of the first diffuse ring increased. Furthermore, the center of the broad background in the XRD patterns shifted from 23° 2θ to 21.5° 2θ, which corresponds to the characteristic diffraction pattern of amorphous silica (Figs. 6(b) and 4(c)).

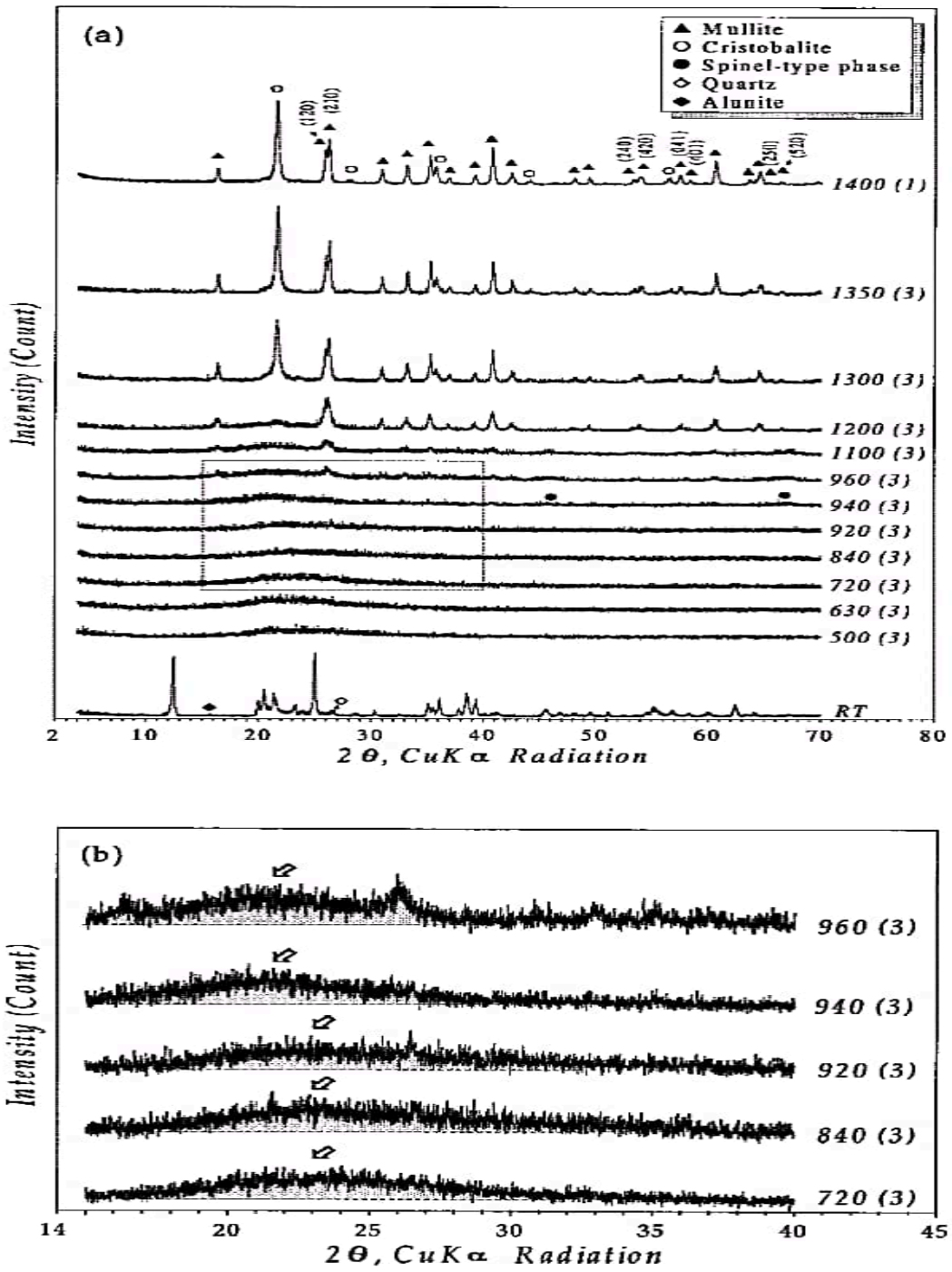

Fig. 1.7 :(a) X-ray diffraction patterns of the unheated and heated kaolinite at various temperatures with heating times in parentheses. (b) Enlarged patterns of the portion indicated by the dotted rectangle in (a). Arrows show that the center of the broad background shifted to a lower angle from 940°C.

In addition, distinct chemical shifts of Si were observed within the Q4(0) range in the NMR spectral data at this stage. The crystalline SiO2 phase, cristobalite, began to form at approximately 1200°C in a random orientation, which coincided with the disappearance of the spinel-type phase. It is hypothesized that the complete elimination of the residual hydroxyls

trapped by the spinel-type phase triggeredthe crystallization of cristobalite from amorphous silica. The disintegration of the spinel-type phase promoted the supply of SiO2, leading to accelerated mullite growth and the precipitation of cristobalite.

4.5. PHASE TRANSFORMATION SEQUENCE:

The sequence of phase transformations can be summarized as follows: (1) Metakaolinite remains structurally intact up to 920°C, and its decomposition initiates at 940°C. (2) The spinel-type phase is not formed through the decomposition of metakaolinite, but rather through a topotactic process in relation to metakaolinite before its decomposition. (3) The breakdown of metakaolinite, starting around 940°C, promotes the formation of mullite while retaining the previously formed spinel-type phase. (4) The complete decomposition of the spinel-type phase occurs at approximately 1200°C, triggering the crystallization of cristobalite from amorphous silica and significant growth of mullite crystals. Although the chemical composition ofthe spinel-type phase was not determined in this study, it is plausible topropose that the early-formed spinel-type phase originates from metakaolinite, which coexists with it up to at least 920°C. The disturbance caused by dehydroxylation, particularly in the Al octahedral sheet, suggests that the early-formed spinel-type phase could be enriched in Al (such as γ-alumina). As temperature increases, Si may be incorporated into its defective structure, eventually forming an Al-Si spinel phase.

In contrast, the disintegration of metakaolinite is necessary for the crystallization of mullite. The removal of residual hydroxyls from metakaolinite at 940°C appears to initiate the breakdown of its structure, leading to the separation of a significant amount of amorphous silica and the formation of poorly crystalline mullite. It is likely that silicon combines with the aluminum octahedral sheet of the decomposed metakaolinite, forming nuclei for mullite. The growth of these nuclei is delayed by the presence of the spinel-type phase but is promoted when the spinel-type phase breaks down, coinciding with the onset of cristobalite formation. Similar to the spinel-type phase, the early-formed mullite exhibits a defective structure, and its composition may change with temperature. Initially, an aluminum-rich mullite, such as 2/1-mullite, is believed to form, which then transforms into a more stable form, such as 3/2-mullite, with the incorporation of silicon. The phase transformation process of kaolinite with increasing temperature is depicted in (Figure 7).

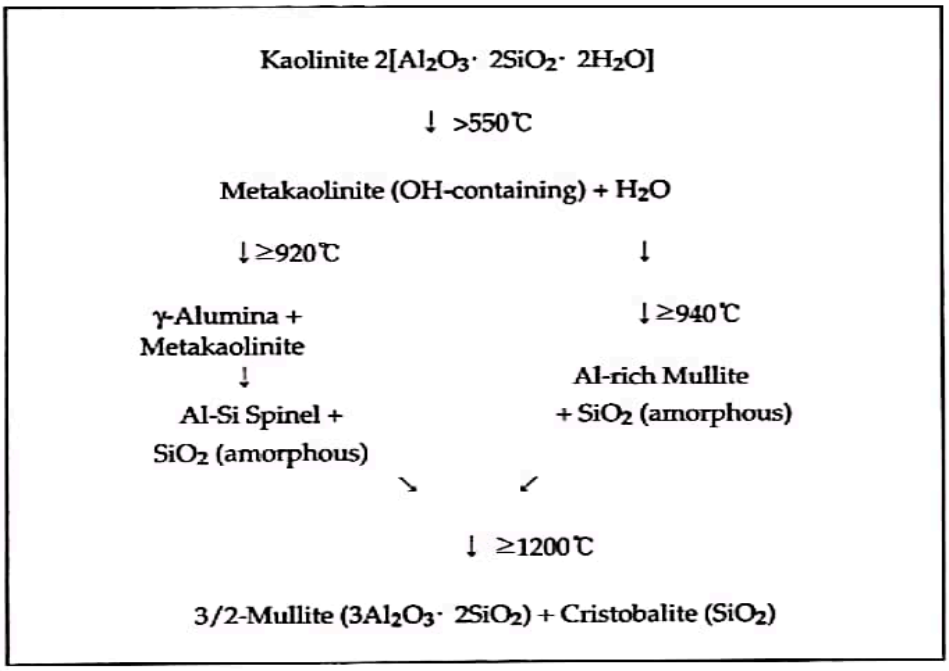

Fig. 1.8: Reaction scheme for the phase transformation of kaolinite to mullite proposed in this study.

The notable difference from (Figure 8) lies in the transformation pathway from metakaolinite and the spinel-type phase to mullite.Theobservation that the spinel-type phase is formed prior to the appearance of the mullite phase is supported by the electron diffraction data obtained in this study.

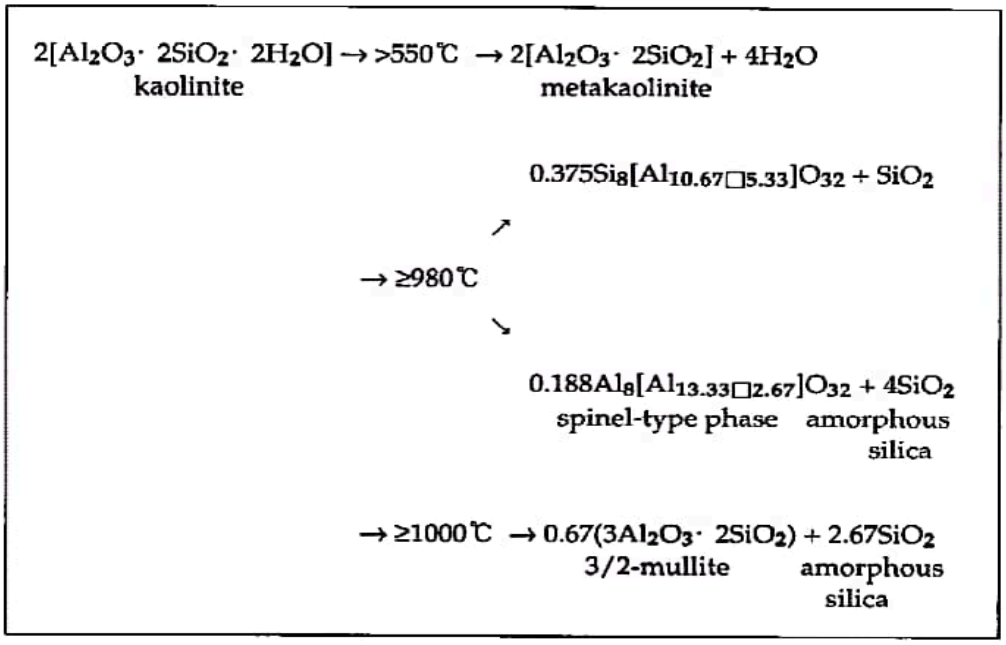

Fig. 1.9: Schematic reaction series for the phase transformation from kaolinite to mullite (after Schneider *et al.*22)

5.KAOLINITE APPLICATION:

Kaolinite possesses a wide range of physical and chemical properties that render it highly valuable for numerous applications. Unlike smectites, palygorskite, and sepiolite, kaolinite exhibits lower reactivity when incorporated into various industrial formulations, thereby contributing to its significant applications.The combination of its low surface charge, relatively low surface area, white color, low ion exchange capacity, and distinctive particle shape positions kaolinite as a highly desirable pigment and extender in applications such as paper coating, paints, and various specialty uses.Clay minerals exhibit distinct differences in their viscosity when dispersed in water. Pure kaolinite, in particular, demonstrates a low viscosity even at high solids content, reaching levels of 70% or slightly higher. On the other hand, sodium montmorillonite exhibits a significantly higher viscosity at a solids content of just 5% due to its elevated surface charge, surface area, ion exchange capacity, and extremely fine particle size.

5.1. PAPER:

The ideal combination of fine particle size and platy shape in kaolinite contributes to the creation of a smooth and dense surface with uniform porosity. This desirable surface characteristic of kaolinite enables the paper to exhibit consistent ink receptivity throughout, resulting in a more uniform ink absorption.

Due to its hydrophilic nature, kaolinite exhibits excellent dispersibility in aqueous systems. Coating formulations typically comprise pigment, binder, water, and small quantities of additional additives. Known as coating color, this formulation is applied onto the paper surface using a trailing blade coater or similar equipment. At the interface between the coatingblade and the paper, shear forces are extremely high due to the paper's high speeds of up to 1500 m/min. To ensure optimal spreading on the paper, the rheology of the coating color should be either Newtonian or thixotropic, as depicted in (Figure 9). If the clay within the formulation exhibits dilatant behavior, the formation of pinheads may occur, resulting in streaks on the coated paper.

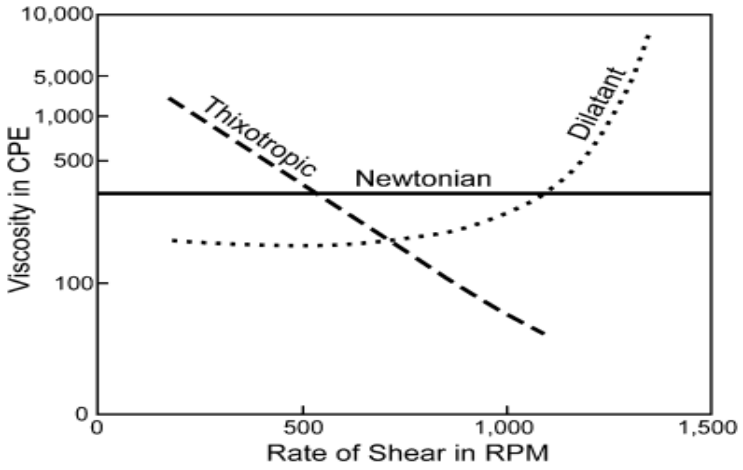

Fig. 1.10: Rheology—dilatant, Newtonian, and thixotropic.

5.2. CERAMICS:

Kaolinite finds extensive applications in the field of ceramics, encompassing a diverse range of products. These include dinnerware, sanitaryware, tiles, electrical porcelain, pottery, and refractories. The versatile properties of kaolinite make it a valuable component in the manufacturing processes of these ceramic products.Kaolinite holds paramount significance among clay minerals utilized in ceramic applications due to its distinct physical and chemical properties, which greatly contribute to ceramic processing and the quality of finishedproducts.

5.3. CATALYSTS:

Kaolinite exhibits a highly acidic nature on its dry surface (Solomon and Murray, 1972), which finds applications in various chemical processes. It serves as a catalyst for promoting the polymerization of styrene, the heterolytic breakdown of organic peroxides, the dehydration of alcohols, the hydrolysis of esters, and the isomerization of alkenes (Solomon et al., 1971).

5.4. Fluoride Absorption:

Kaolinite possesses a highly acidic dry surface. One interesting manifestation of this property is its affinity for fluoride, which can react with and potentially replace hydroxyl groups within the kaolinite structure. In the context of drinking water with elevated fluoride levels, kaolinite canbe employed to effectively absorb and reduce the fluoride content. This highlights its potential application in fluoride removal or reduction processes. Furthermore, there is a

possibility of utilizing kaolinite in scrubbers to mitigate fluorine emissions in certain ceramic and clay manufacturing facilities.

5.5. Foundry:

Kaolinitic plastic clays find extensive application in the formulation of bonding molding sands, especially in scenarios where a high refractoriness is necessary, particularly during the pouring of molten metals at elevated temperatures. Ball clays, known for their excellent plasticity, are commonly employed for this purpose. However, it should be noted that these fine particle kaolinitic clays exhibit lower bond strength compared to montmorillonite clays. In certain foundries dealing with extremely high temperatures and molten metals, there is a requirement for the use of calcined kaolin granules, which have been subjected to temperatures around 1300°C to form mullite, as an alternative to silica sand.

5.6. For Flame Retardant:

In recent years, there has been a significant focus on polymer-layered silicate nanocomposites due to their notable impact on flame retardancy. These nanocomposites consist of polymer clay (layered silica) introduced into the matrix in intercalated or exfoliated states. During combustion, they can accumulate on the polymer surface, forming a barrier layer that hinders the release of degradation products and incoming gases. Research has shown that even small amounts of nanoclay (1%–4%) can reduce the peak heat release rate in a cone calorimeter by approximately 30%.

Furthermore, studies have demonstrated that certain additives, such as kaolinite and nanohydroxyl aluminum oxalate, exhibit synergistic effects on flame retardancy when incorporated into low-density polyethylene/ethylene propylene diene rubber composites. Modified kaolinite has been found to enhance the fire-retardant properties of polypropylene.

Additionally, the addition of kaolinite has been observed to improve the fire performance of composites containing 20 wt% compared to the neat polymer, specifically in terms of peak heat release rate. A novel approach involved fabricating a superhydrophobic surface on lignocellulose composites by coating them with polydimethylsiloxane@stearic acid modified kaolinite particles. This composite coating demonstrated excellent water repellency, with a contact angle of 156 degrees, and exhibited flame retardancy. It holds promise as a potential alternative for protecting lignocellulose composites.

6.METHODSE USDE MADE BEFORE ELARBI HADJALA WALIDE AND DARWICHE MOHAMAD RIDA:

- method 1

We took a mixture of 50g of purified kaolin with 100 ml of dmso, the mixture was subjected to mechanical treatment(Grinding), we took a 50 ml sampling box and recovered rolling balls with a diameter of 8 and 10 mm Then we did the grinding manually for 10 hoursWe recover the powder which has been put in sampling boxes to put them in the oven at 120° for 2 hours.
Then the recovered powder was filtered and washed with ethanol for 5 series to remove excess molecules of DMSO (Dymethyl sulfoxide).Then, the samples were dried under vacuum at 50° for 48 to obtain a k1M10I2 kaolin powder.

-method 2

We took 25g of kaolin purified with a solution of 50 ml Dmso (20% distilled water + 80% Dmso) with stirring for 24 hours to obtain a hybrid material, then filtration was done to separate the kaolin and the dmso which was then wash with methanol for 5 times for about 20 minutes then we went to drying for 5 hours.
Thanks to this process, methoxykaolinite was obtained.
We recover 12g of methoxykaolinite we mix it with 100 ml of ctab of concentration 0.1 mol and we agitate it for 12 hours in the ultrasonic bath In addition to 3 hours with the probe sonicator (homogenizer of solution). After that we made a filtration of the solution using filter paper with distilled water and methanol.

- method 3

We took 25 g of purified kaolin mixed with 12.5 g of uric acid The mixture was subjected to a temperature of 95° Then we did 3 series of washing with filtration with distilled water
To recover the powder, we dry it at 60° for 24 hours.

-method

We took 25g of purified kaolin mix at 480 mol kno3 of concentration of 2mol put in the stirrer for 48 hours at a temperature of 90°We went to filtering with distilled water then we let it dry for 1 hour at a temperature of 120°.

CHAPTER2:

APPLICATION OF 2D MATERIAL IN OIL LUBRICATION SYSTEM

1.INTRODUCTION:

2D materials are a relatively new class of materials that have gained significant attention in recent years. Graphene, the first 2D material to be discovered, was isolated in 2004 by Andre Geim and Konstantin Novoselov at the University of Manchester. For their groundbreaking work on graphene, Geim and Novoselov were awarded the Nobel Prize in Physics in 2010.

The discovery of graphene sparked interest in other 2D materials, leading to the discovery of many other materials with unique properties. 2D materials are composed of a single layer or a few layers of atoms, and have a thickness of just one or a few atoms. Despite their small size, they can extend over large areas in the two-dimensional plane, which gives them unique properties and functionalities that differ from their bulk counterparts.

2D materials exhibit a wide range of properties, including exceptional mechanical strength, high electrical conductivity, and thermal conductivity, as well as unique electronic, optical, and magnetic properties. These properties make 2D materials promising candidates for various applications in electronics, photonics, energy, and biotechnology.

Overall, the development of 2D materials has the potential to revolutionize various fields, and has already led to many exciting discoveries and innovations. Ongoing research into 2D materials will continue to uncover new properties and applications, and will help to address the challenges of our rapidly changing world.

I .2D MATERIALS:

1.DEFINITION:

2D materials are a specific class of nanomaterials

1.1. NANOMATERIALS:

Nanomaterials are materials with a size between 1 and 100 nanometers, composed of various materials such as metals, polymers, ceramics, and composites. They can be produced through different means, including chemical synthesis, lithography, spraying, and crystal growth.

Due to their small size, nanomaterials possess unique properties different from their macroscopic counterparts, such as higher specific surface area, chemical reactivity, electrical and thermal conductivity, optical properties, mechanical strength, and magnetic properties. They have numerous applications in areas such as electronics, medicine, energy, composite materials, and catalysis.

1.2.2D MATERIALS:

2D materials are thin layers of material with atoms or particles arranged in a 2D pattern, often referred to as "monolayers" because they contain only one layer of atoms or particles. Graphene, composed of carbon atoms arranged in a hexagonal mesh, is one of the most famous 2D materials. However, there are many other types of 2D materials, including transition metal dichalcogenides (TMDs), black phosphorus, and boron nitride.

2D materials have unique features such as photoelectric, optical, and mechanical properties, which have attracted interest from physicists and engineers. They have potential applications in fields such as electronics, energy storage, and catalysis, among others.

2.STRUCTURE OF 2D MATERIALS:

Two-dimensional (2D) materials are materials that possess an extremely thin thickness, usually on the order of one or a few atoms. Unlike three-dimensional materials, 2D materials have unique physical and chemical properties due to their restricted atomic structure in two dimensions.

There are several two-dimensional materials, such as graphene (the best known), molybdenum disulfide (MoS_2), tungsten diselenide (WSe_2), boron nitride (BN) and black phosphorus (BP). Each of these materials has specific properties that make them interesting for different applications.

2.1. GRAPHENE:

Graphene is a single layer of carbon atoms arranged in a two-dimensional honeycomb lattice. It is the basic structural element of other carbon allotropes, such as graphite and carbon nanotubes. Graphene possesses exceptional properties, including high electrical and thermal conductivity, mechanical strength, and optical transparency. It has a wide range of potential applications in various fields, such as electronics, energy storage, sensors, and materials science.

2.2. STRUCTURE AND COPOSITION OF GRAPHENE:

Graphene is a two-dimensional allotrope of carbon, consisting of a single layer of carbon atoms tightly arranged in a hexagonal lattice pattern. Each carbon atom is bonded to three neighboring carbon atoms through strong covalent bonds, resulting in a flat, honeycomb-like structure.

The carbon-carbon bonds in graphene are exceptionally strong, giving it remarkable mechanical properties. It is one of the thinnest and strongest materials known, with a tensile strength about 200 times greater than steel.Graphene is composed entirely of carbon atoms, making it a pure form of carbon. The carbon atoms are sp^2 hybridized, meaning they form three sigma bonds in a trigonal planar arrangement. This unique bonding structure contributes to its exceptional electrical and thermal conductivity properties.

Due to its single-layer structure, graphene is considered a two-dimensional material with a thickness of only one atom. It can be viewed as an individual atomic layer extracted from bulk graphite, which is composed of stacked layers of graphene.

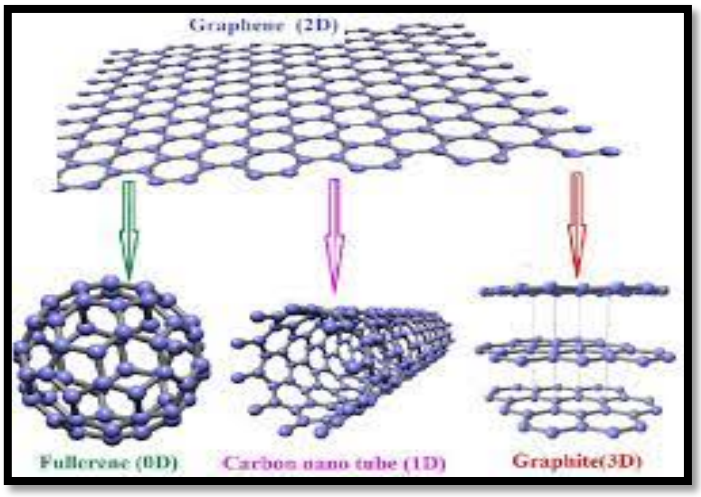

Figure2.1: Strucrur of grapheme

2.3. PROPERTIES OF GRAPHENE:

Graphene possesses a multitude of exceptional properties, making it a highly sought-after material for various applications. Here are some key properties of graphene:

- Electrical conductivity: Graphene is an excellent conductor of electricity, even surpassing copper. Its high electron mobility allows for fast electron transport, making it ideal for applications in electronics, such as transistors and flexible displays.
- Thermal conductivity: Graphene exhibits exceptional thermal conductivity, enabling efficient heat transfer. This property is crucial for applications involving heat management, such as thermal interface materials and heat sinks.
- Mechanical strength: Graphene is incredibly strong and has a tensile strength that exceeds most other materials. It is also very flexible and can be stretched without breaking. These properties make it suitable for applications requiring strong yet lightweight materials.
- Transparency: Despite being a single layer of atoms, graphene is highly transparent, allowing over 97% of light to pass through. This characteristic makes it useful for applications in optoelectronics, touchscreens, and solar cells.

- Flexibility: Graphene is highly flexible and can be bent or folded without losing its properties. This flexibility enables its integration into flexible electronic devices and wearable technologies.
- Chemical stability: Graphene is chemically inert and has high resistance to many chemicals, making it stable in a variety of environments. This property ensures its durability and longevity in applications that require resistance to corrosion or chemical reactions.
- Large surface area: Graphene has an extremely high surface area-to-volume ratio due to its two-dimensional structure. This feature makes it advantageous for energy storage applications, such as batteries, supercapacitors, and fuel cells.
- Optical properties: Graphene exhibits unique optical properties. It absorbs only a small fraction of light across a broad range of wavelengths. It also has the ability to tune its optical properties through doping or applying external stimuli, making it suitable for optical modulators and sensors.

These properties, combined with its thinness and versatility, contribute to the immense potential of graphene in various fields, including electronics, energy, materials science, biomedical applications, and more.

2.4. GRAPHENE HISTORY:

The history of graphene is closely tied to the scientific understanding of carbon and the development of nanotechnology. Here are the key milestones in the history of graphene:

- Theoretical Prediction (1947): In 1947, physicist P.R. Wallace theoretically described a two-dimensional sheet of carbon atoms with a honeycomb lattice structure. This laid the foundation for the concept of graphene.
- Experimental Observations (1962): Graphene was indirectly observed for the first time by scientists Hanns-Peter Boehm and Ernst O. Fischer when they examined the surface of graphite using electron microscopy. They observed the thin layers that would later be recognized as graphene.

- Isolation and Identification (2004):AndreGeim and Konstantin Novoselov, researchers at the University of Manchester, successfully isolated and identified graphene for the first time. They used a simple "Scotch tape" method to peel off thin layers of graphite until they obtained single-layer graphene. Their breakthrough discovery was published in 2004.
- Further Characterization (2005-2008): Researchers expanded on the understanding of graphene's properties, including its electrical, thermal, and mechanical characteristics. They conducted experiments to measure its conductivity, investigated its band structure, and explored its interactions with light and other materials.
- Development of Scalable Production Methods (2009-present): Efforts were made to develop scalable methods for producing graphene. Various techniques, such as chemical vapor deposition (CVD), epitaxial growth, and exfoliation methods, have been explored to enable large-scale production of high-quality graphene sheets.
- Nobel Prize in Physics and Advances in Applications (2010): In recognition of their groundbreaking work, Geim and Novoselov were awarded the Nobel Prize inPhysics in 2010 for their "groundbreaking experiments regarding the two-dimensional material graphene.

Since its isolation (2004) graphene has become a subject of intense scientific research and exploration. Scientists worldwide have made significant advancements in understanding its properties and exploring its potential applications. Ongoing research focuses on improving production methods, uncovering new properties, and developing practical uses for graphene in various fields.

The discovery of graphene has sparked a new era of nanomaterials and has the potential to revolutionize technology and various industries. Its exceptional properties have opened up possibilities for applications in electronics, energy, materials science, biomedicine, and more.

2.5. GRAPHENE PRODUCTION TECHNIQUE:

Several techniques have been developed for the production of graphene. Here are some of the commonly used methods:

- Mechanical Exfoliation (Scotch tape method): This method, pioneered by Geim and Novoselov, involves repeatedly peeling off thin layers of graphite using adhesive tape.By applying the tape to the graphite surface and then peeling it off, individual graphene layers can be obtained. This technique produces high-quality graphene, but it is time-consuming and not suitable for large-scale production.

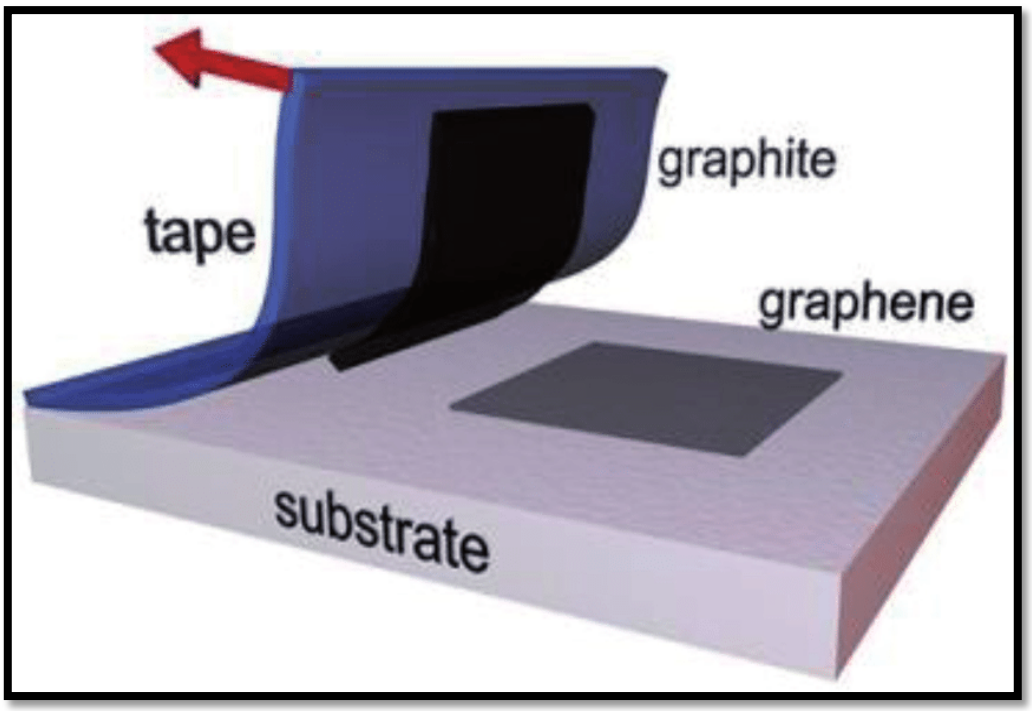

Figure 2.2: Mechanical Exfoliation of grapheme (Scotch tape method)

- Mechanical Exfoliation (Scotch tape method): CVD is a widely used method for large-scale graphene production. It involves exposing a substrate, typically copper or nickel, to a carbon-containing gas, such as methane. Under controlled conditions, carbon atoms deposit on the substrate and form a graphene layer. The substrate is then etched away, leaving graphene on the desired surface. CVD can produce high-quality graphene with good scalability.

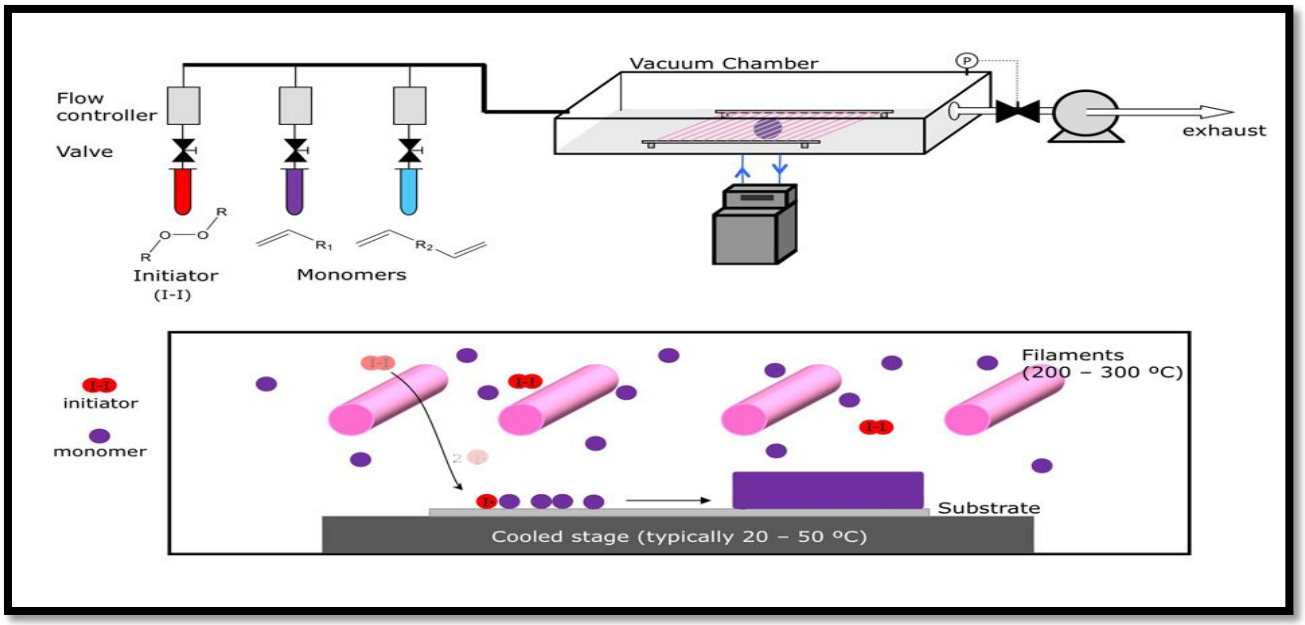

Figure2.3: Mechanical Exfoliation of graphene (Scotch tape method)

- Epitaxial Growth: In this method, graphene is grown on a crystalline substrate, such as silicon carbide (SiC). The substrate is heated to high temperatures, causing carbon atoms from the substrate to migrate and form a graphene layer on its surface. Epitaxial growth can result in large-area graphene, but it requires specialized equipment and precise control of growth conditions.
- Liquid Phase Exfoliation: This method involves dispersing graphite or graphite oxide in a liquid solvent and applying mechanical or ultrasonic energy to break down the graphite into individual graphene sheets. The resulting graphene dispersion can be further processed and used in various applications. Liquid phase exfoliation offers a scalable and relatively simple approach for graphene production.

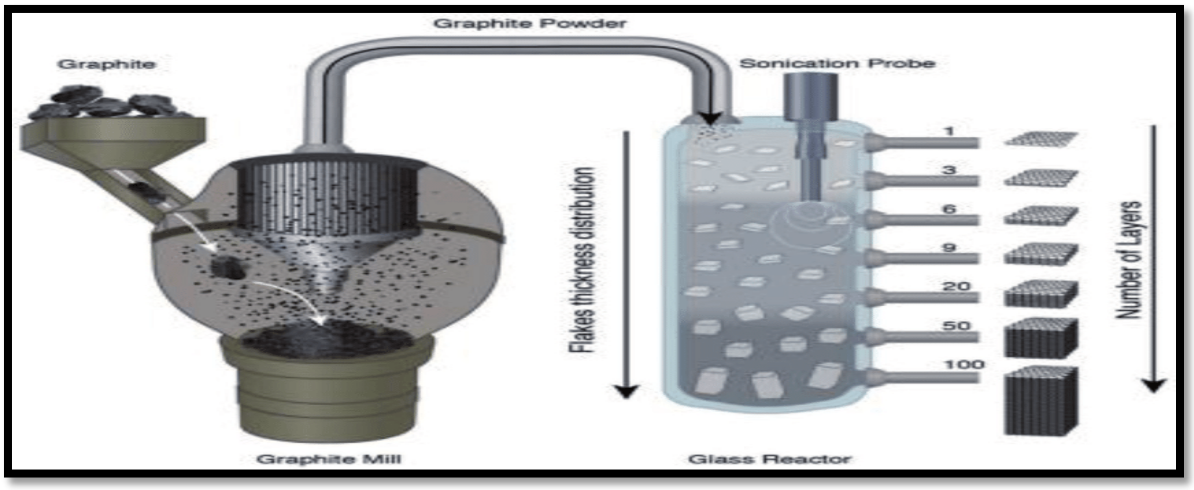

Figure2.4: Liquid Phase Exfoliation of grapheme.

- Graphite Oxide Reduction: Graphite oxide can be synthesized by oxidizing graphite, and then the resulting graphite oxide can be thermally or chemically reduced to produce graphene. The reduction process removes oxygen functional groups and restores the sp^2 carbon structure of graphene. Graphite oxide reduction can yield graphene in the form of sheets or powders.

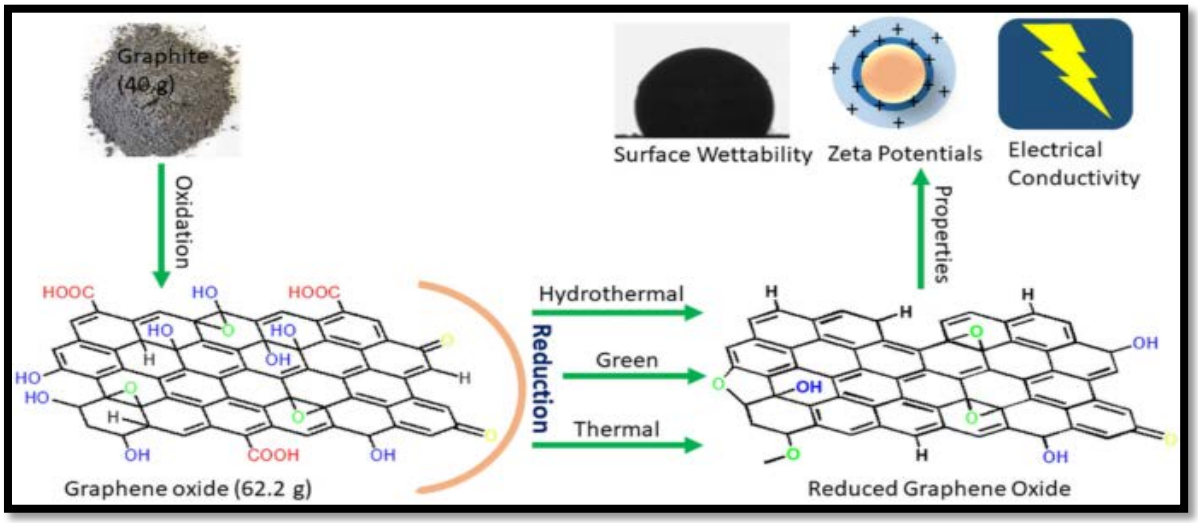

Figure2.5: Graphite Oxide Reduction.

- Electrochemical Exfoliation: This technique involves applying an electric field to a graphite electrode immersed in a suitable electrolyte. The electric field causes the

exfoliation of graphene layers from the graphite electrode, resulting in the production of graphene flakes in the electrolyte.

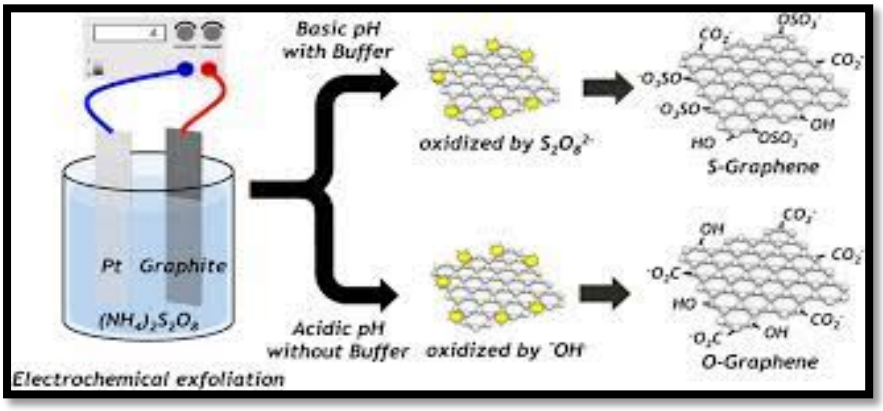

Figure 2.6: Electrochemical Exfoliation of grapheme.

These are some of the commonly employed methods for graphene production. Each technique has its advantages and limitations in terms of scalability, quality, and cost, and the choice of method depends on the specific requirements of the application. Ongoing research is focused on refining these techniques and developing new approaches to enhance graphene production efficiency and quality.

2.6. POTENTIAL APPLICATION OF GRAPHENEl:

Graphene's remarkable properties have sparked significant interest and exploration for a wide range of potential applications. Some of the notable areas where graphene shows promise are:

- Electronics and computing: Graphene's high electrical conductivity and electron mobility make it suitable for ultrafast transistors, flexible electronics, and high-frequency applications. It could lead to advancements in faster and more efficient electronic devices.
- Energy storage: Graphene's large surface area and high electrical conductivity make it ideal for energy storage devices. It has the potential to improve the performance of batteries, supercapacitors, and fuel cells, leading to longer-lasting and faster-charging energy storage solutions.

- Optoelectronics: Graphene's excellent optical properties, such as transparency and tunability, make it well-suited for optoelectronic applications. It can be used in the development of ultra-thin and flexible displays, photodetectors, solar cells, and sensors.
- Composite materials: Adding small amounts of graphene to composite materials can significantly enhance their mechanical strength, electrical conductivity, and thermal properties. Graphene composites have the potential to improve the performance of structural materials, coatings, and aerospace applications.
- Water filtration and desalination: Graphene membranes have shown promise in water filtration and desalination processes. The ultra-thin and porous structure of graphene allows for efficient sieving of molecules and ions, making it an excellent candidate for water purification technologies.
- Biomedical applications: Graphene's unique properties make it a promising material in biomedical applications. It can be used for drug delivery systems, bioimaging, tissue engineering scaffolds, and biosensors due to its biocompatibility, large surface area, and electrical conductivity.
- Environmental applications: Graphene-based materials can be employed in environmental applications, such as pollution sensing, air and water purification, and energy-efficient membranes for gas separation. Graphene's high surface area and chemical stability make it useful for addressing environmental challenges.
- Wearable technology: Graphene's flexibility, transparency, and conductivity make it suitable for wearable devices and smart textiles. It can be integrated into clothing and accessories to enable functions like sensing, energy harvesting, and communication.

These are just a few examples of the potential applications of graphene. Ongoing research and development continue to explore and uncover new uses for this versatile material.

3.AREAS OF USE 2D MATERIALS:

2D materials have a wide range of applications in various fields. Some key areas of use include:

- Electronics and Optoelectronics: 2D materials like graphene and transition metal dichalcogenides (TMDs) are used for developing high-performance transistors, flexible displays, and sensors due to their excellent electrical and optical properties.
- Energy Storage and Conversion: Graphene and other 2D materials are utilized in energy storage devices such as batteries, supercapacitors, and fuel cells. They offer enhanced charge storage capacity, faster charging rates, and improved efficiency.
- Catalysis: 2D materials can act as catalysts or support materials for catalytic reactions, enabling efficient and selective chemical transformations in areas such as hydrogen production, water splitting, and environmental remediation.
- Biomedicine and Biosensing: Graphene and other 2D materials are explored for applications in drug delivery, tissue engineering, biosensors, and bioimaging. They can be functionalized to interact with biological systems and enable targeted drug delivery or sensitive detection of biomolecules.
- Water Purification: 2D materials like graphene oxide exhibit excellent water filtration properties. They can remove contaminants and impurities from water, making them promising candidates for desalination, wastewater treatment, and water purification systems.
- Flexible and Wearable Devices: Due to their ultrathin nature and flexibility, 2D materials are suitable for creating flexible and wearable electronic devices, such as smart clothing, wearable sensors, and healthcare monitoring systems.
- Photonics and Optics: 2D materials possess unique optical properties that make them suitable for applications in photonics and optics. They can be used in lasers, photodetectors, photovoltaics, and light-emitting devices, enabling advancements in communication and imaging technologies.
- Coatings and Barrier Films: Thin films of 2D materials can serve as protective coatings and barrier films, providing corrosion resistance, moisture barrier properties, and chemical stability for applications in packaging, electronics, and aerospace industries.

It's important to note that ongoing research and development in the field of 2D materials continue to uncover new applications and expand their potential uses across various disciplines.

II.LUBRICATION SYSTEME

1.TRIBOLOGY:

Tribology is the science and engineering discipline that deals with the study of friction, wear, and lubrication between interacting surfaces in relative motion. It encompasses the understanding of how surfaces interact, the mechanisms of friction and wear, and the development and application of lubricants and surface treatments to minimize friction and wear. Tribology involves the investigation of the physical, chemical, and mechanical properties of materials in contact, as well as the study of surface roughness, adhesion, lubricant properties, and the effects of operating conditions on friction and wear. It plays a crucial role in various fields, including mechanical engineering, materials science, automotive and transportation industries, manufacturing, aerospace, and many others.

The goal of tribology is to improve the efficiency, reliability, and durability of mechanical systems and components by minimizing friction and wear, enhancing lubrication, and opimizing the design and materials selection. By understanding and controlling the tribological behavior of interacting surfaces, it is possible to reduce energy consumption, extend the lifespan of machinery, and improve overall performance.

2.LUBRICATION:

Lubrication is the process of introducing a lubricant between two surfaces in relative motion to reduce friction and wear. The lubricant, which can be in the form of a liquid, solid, or semi-solid, forms a thin film that separates the surfaces and provides a protective barrier. Lubrication helps to minimize the direct contact between the surfaces, preventing metal-to-metal contact and reducing frictional resistance. It also helps to dissipate heat, improve efficiency, and prolong the lifespan of mechanical systems and components. Lubrication is widely employed in various industries, including automotive, manufacturing, aerospace, and energy, to ensure smooth operation and prevent damage caused by friction and wear.

2.1. TYPE OF LUBRICATION:

There are several types of lubrication, including:

- Hydrodynamic Lubrication: In hydrodynamic lubrication, the lubricant is introduced between the surfaces in motion under sufficient pressure to create a wedge-shaped film that completely separates the surfaces. This type of lubrication is used in high-speed applications, such as in engines and turbines.
- Boundary Lubrication: In boundary lubrication, the lubricant film is thin, and the surfaces in motion are in direct contact. This type of lubrication is used in low-speed and high-pressure applications, such as in metal-forming processes.
- Elastohydrodynamic Lubrication: In elastohydrodynamic lubrication, the lubricant is introduced between two surfaces under high pressure, causing the surfaces to deform and create a temporary lubricant reservoir. This type of lubrication is used in applications with high contact pressures, such as in bearings.
- Solid Lubrication: In solid lubrication, a solid material, such as graphite or molybdenum disulfide, is introduced between the surfaces in motion. This type of lubrication is used in applications where high temperatures, vacuum, or clean-room environments prohibit the use of liquid lubricants.
- Mixed Lubrication: In mixed lubrication, both boundary and hydrodynamic lubrication are present. This type of lubrication is commonly found in industrial applications with varying operating conditions, such as in gears and rolling-element bearings.

The selection of lubrication type depends on factors such as the operating conditions, speed, load, temperature, and the type of surfaces in motion.

3.LUBRICANT:

A lubricant is a substance that is used to reduce friction and wear between two surfaces that arein relative motion. Lubricants can be in the form of liquids, such as oils, or solids, such as

graphite or molybdenum disulfide. They are commonly used in machinery and equipment to reduce friction, dissipate heat, and protect against wear and corrosion. Lubricants can also provide other benefits, such as improving energy efficiency and extending the life of equipment. The selection of a lubricant depends on the specific application and operating conditions, such as temperature, load, and speed.

3.1. TYPE OF LUBRICANT:

Grease, oil, and paste lubricant are three different types of lubricants commonly used in various applications.

- Grease is a lubricant that has a semi-solid or solid consistency at room temperature. It is made up of a base oil and a thickener, such as soap or a synthetic polymer, which gives it its characteristic texture. Grease is commonly used in bearings, gears, and other applications where a long-lasting lubrication is needed.
- Paste lubricant is a type of lubricant that is commonly used in applications where high pressure and extreme temperatures are present, such as in metal-forming processes or high-temperature machinery. It is made up of a solid lubricant, such as graphite or molybdenum disulfide, suspended in a carrier fluid.
- Oil is a liquid or semi-liquid lubricant that is commonly used in engines, hydraulic systems, and other machinery to reduce friction and wear between moving parts. It is typically made up of a base oil and additives, which are designed to improve the performance and properties of the oil.

The selection of lubricant type depends on the application, operating conditions, and the manufacturer's recommendations. Grease is often used in applications where a long-lasting lubrication is needed, while oil is commonly used in engines and hydraulic systems. Paste lubricants are often used in extreme temperature and high-pressure applications where other lubricants may break down.

3.2. TYPE OF OIL:

There are many types of oils used for various purposes. Here are some common types of oils:

- Mineral oil: a type of petroleum-based oil that is commonly used as a lubricant and in various industrial applications.

- Synthetic oil: a type of oil that is chemically engineered to have specific properties such as improved performance in high temperatures and resistance to oxidation.
- Vegetable oil: a type of oil that is derived from plant sources such as soybeans, corn, or canola. It is commonly used for cooking and as a biofuel.
- Motor oil: a type of oil specifically designed for use in engines, which helps to reduce friction, wear and tear, and keep the engine cool.
- Hydraulic oil: a type of oil used in hydraulic systems to transfer power.
- Compressor oil: a type of oil used in compressors to reduce friction and wear and improve efficiency.
- Turbine oil: a type of oil used in turbines to reduce friction, wear, and extend the life of the equipment.
- Transformer oil: a type of oil used in electrical transformers to insulate and cool the equipment.

These are just a few examples of the many types of oils available. The selection of the appropriate oil depends on the specific application and operating conditions.

EXMPEL: Paraffin oil, also known as white oil, is a type of mineral oil produced through the distillation of crude oil. It is primarily composed of paraffin, a saturated hydrocarbon, and finds wide usage as a lubricant, processing oil, baby oil, laxative, and skin emollient. It is also employed as a dielectric insulator in electrical transformers and as a heat transfer fluid in heating systems. Paraffin oil has low viscosity and is relatively inexpensive compared to other types of oils, making it popular in numerous industrial and commercial applications.

4. WEAR:

Wear refers to the process of gradual deterioration, damage, or reduction in the quality, functionality, or performance of an object, material, or system, caused by regular, prolonged, or repeated use, as well as environmental conditions or physical stresses.

Preventing wear can involve measures such as using more resistant materials, applying protective coatings, regular maintenance, lubrication, improving designs, optimizing manufacturing processes, or adopting good usage practices. In some cases, it may be

necessary to replace or repair worn objects to restore their functionality or extend their useful lifespan.

4.1. WEAR MECHANISMS:

Wear mechanisms refer to the specific processes or actions that contribute to the deterioration or damage of an object or material during the wear process. There are several commonly recognized wear mechanisms:

4.1.1. ABRASIVE WEAR:

This type of wear occurs when hard particles or surfaces come into contact with a softer material, causing the removal of material through scratching, plowing, or cutting actions. It is often encountered in situations involving the presence of solid contaminants or in applications involving sliding or rubbing surfaces.

4.1.2. ADHESIVE WEAR:

Adhesive wear happens when two surfaces come into direct contact and stick together, resulting in material transfer between the surfaces upon separation. It occurs due to the localized welding and subsequent tearing of microscopic surface asperities, leading to material loss.

4.1.3. FATIGUEWEAR:

Fatigue wear is caused by repeated cyclic loading and unloading, leading to the initiation and propagation of cracks within a material. It commonly occurs in high-stress applications and can result in surface pitting, spalling, or cracking.

4.1.4. EROSIVEWEAR:

Erosive wear is caused by the impact of solid particles, droplets, or high-velocity fluids on a material's surface. It typically occurs in environments with abrasive particles or high-velocity flow conditions, such as erosion of turbine blades by sand particles in a gas turbine

4.1.5. CORROSIVEWEAR:

Corrosive wear is the combined action of corrosion and mechanical wear. It occurs when a corrosive environment weakens the surface of a material, making it more susceptible to wear mechanisms such as abrasive or adhesive wear.

4.1.6. FRETTINGWEAR:

Fretting wear occurs in small-scale cyclic motion between two surfaces in contact, resulting in material removal due to repeated micro-slip, oxidation, and surface damage. It commonly affects components such as bolted joints, connectors, or bearings.

These wear mechanisms can often act in combination or influence each other, depending on the specific conditions and materials involved. Understanding the wear mechanisms at play is crucial for designing appropriate materials, lubrication systems, maintenance strategies, and wear-resistant coatings to mitigate or minimize wear effects.

4.2. WEARTESTS:

Wear tests are conducted to evaluate the performance and durability of materials, coatings, or lubricants under specific wear conditions. These tests help assess the resistance of a material

to various wear mechanisms and provide valuable information for product development, quality control, and performance optimization. Here are some commonly used wear tests:

4.2.1.PIN –ON-DISK TEST:

This test involves a rotating disk against which a pin or a specimen is pressed with a specific load. The pin or specimen undergoes sliding motion, simulating the contact and relative motion between two surfaces. The wear volume or weight loss is measured to evaluate the material's wear resistance.

4.2.2. BLOCK –ON-RING TEST:

Similar to the pin-on-disk test, the block-on-ring test involves a sliding contact between a stationary ring and a reciprocating block. The wear of the block or ring is evaluated based on wear volume or weight loss.

4.2.3. TABER ABRASION TEST:

This test measures the resistance of materials to abrasive wear. It involves rotating a specimen on a turntable while applying a specific load. Abrasive wheels or discs, such as H-18 or CS-10, with controlled abrasive particles are used to wear away the surface. The wear resistance is assessed by measuring the weight loss or evaluating surface roughness.

4.2.4. BALL –ON- PLATE TEST:

In this test, a spherical ball is pressed against a flat plate while subjected to a specific load. The ball rolls or slides across the plate, simulating rolling contact or sliding wear. The wear is evaluated based on wear volume or weight loss.

4.2.5. SLURRY EROSION TEST:

This test assesses the resistance of materials to erosive wear caused by solid particles suspended in a fluid (slurry). The material is exposed to a controlled slurry flow, and the wear is measured by weight loss or surface damage evaluation.

4.2.6. FOUR –BALL WEAR TEST:

This test evaluates the wear and friction characteristics of lubricants or lubricant additives. It involves three stationary balls held in a triangular arrangement, while a fourth ball rotates against them under a specific load. The wear scar diameter or wear volume is measured to assess the lubricant's performance.

These are just a few examples of wear tests, and various other tests exist depending on the specific application and wear mechanisms of interest. Wear testing provides valuable data for material selection, product development, and optimization of surface treatments or lubrication systems to enhance wear resistance and durability.

4.3. TYPES OF GRAPHS RELATED TO WEAR AND FRICTION:

When studying wear and friction, various types of graphs are commonly used to analyze and visualize the data. Here are some of the different types of graphs used in wear and friction studies:

- Friction coefficient vs. time graph: This graph represents the variation of the friction coefficient over time during a specific test or experiment. It helps to understand the changes in frictional behavior, such as transitions from static to kinetic friction or variations in friction during different stages of wear.
- Wear rate vs. time graph: This graph illustrates the wear rate, i.e., the amount of material loss or wear, as a function of time. It shows how the wear progresses over the duration of the test or experiment and helps to analyze the wear behavior and identify any trends or patterns.
- Load vs. wear graph: This graph depicts the relationship between the applied load and the wear observed. It helps to understand the effect of load on wear behavior and can

be used to determine the critical load or threshold load at which significant wear occurs.

- Wear volume vs. sliding distance graph: This graph represents the wear volume (amount of material loss) as a function of the sliding distance between the surfaces in contact. It helps to evaluate the cumulative wear and establish wear mechanisms over a specific distance.
- Surface roughness vs. wear graph: This graph shows the relationship between surface roughness (measured before or after the wear test) and the resulting wear. It helps to understand the impact of surface roughness on wear behavior and assess the effectiveness of different surface treatments or coatings in reducing wear.

These are some of the commonly used graphs in wear and friction studies. The choice of graph depends on the specific parameters being investigated and the data available from

experimental measurements. These graphs help researchers to analyze wear and friction phenomena, identify trends, and make informed decisions regarding lubrication strategies and material choices.

Chapitre 3
Composite material

GENERAL INFORMATION ON MATERIALS COMPOSITES:

1.INTRODUCTION:

The study and design of composite materials have attracted significant attention across various fields of modern chemistry for nearly a century. These materials, characterized by their heterogeneous, isotropic, or anisotropic structures, frequently exhibit superior performance in terms of chemical and mechanical properties compared to homogeneous materials. This includes properties such as optical, thermal, and dielectric characteristics. Consequently, composites hold immense potential and offer highly promising prospects for a wide range of applications.[61]

2.COMPOSITE MATERIALS:

Composite materials are engineered materials that consist of two or more distinct components, typically a matrix material and reinforcement elements, working together to create a new material with improved properties. The matrix material acts as a binder, surrounding and supporting the reinforcement elements, while the reinforcements enhance specific characteristics of the composite.[62]

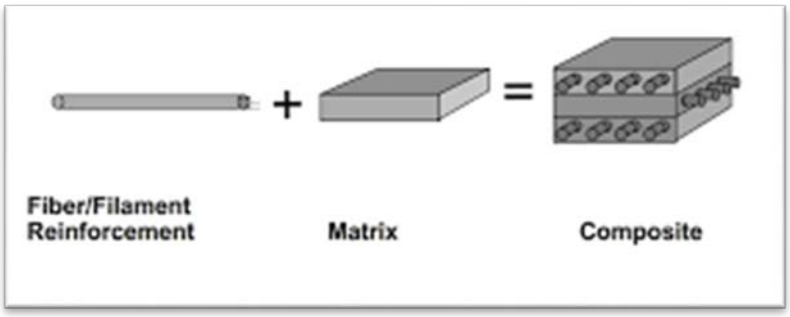

Figure3.1: Composite materials

3.THE MATRIX:

The matrix material, often a polymer resin, ceramic, or metal, provides the structure and cohesion for the composite. It distributes applied stresses, such as compressive or flexural loads, throughout the material and protects the reinforcement from environmental factors. The matrix material can also contribute additional properties, such as chemical resistance or electrical insulation.[63]

4.THE REINFORCEMENT:

The reinforcement elements are incorporated into the matrix to enhance specific properties of the composite. These reinforcements can take the form of fibers, particles, or flakes made from materials such as carbon, glass, aramid, or metal. The choice of reinforcement depends on the desired properties of the composite, such as strength, stiffness, thermal conductivity, or impact resistance. Reinforcements provide mechanical strength, stiffness, and other desired characteristics to the composite.

5.PROPERTIES:

The combination of the matrix material and reinforcement elements in a composite material leads to synergistic effects, resulting in improved properties compared to the individual components alone. Composite materials are known for their high strength-to-weight ratio, making them lightweight yet strong. They often exhibit excellent corrosion resistance, thermal stability, and fatigue resistance.

6.APPLICATION:

Composite materials find applications in a wide range of industries. In aerospace, they are used to manufacture aircraft components, such as wings, fuselages, and engine parts, where the high strength and lightweight properties are crucial for fuel efficiency and performance. In the automotive industry, composites are utilized for parts like body panels, chassis components, and interior parts, contributing to weight reduction and improved fuel economy. In construction, composites are employed in infrastructure applications, such as bridges,

buildings, and pipelines, due to their durability, corrosion resistance, and design flexibility. Additionally, composite materials are widely used in sports equipment, marine vessels, wind turbine blades, and various other applications where their unique properties offer advantages [64]

7.METAL MATRIX COMPOSITES:

Metal matrix composites are much more widely used in the automotive and aerospace industries, despite their cost and complexity. aerospace industry, despite the cost and complexity of forming them. complexity. In the aerospace industry, aluminium alloys tend to be used because of their low density and good resistance to corrosion. for their low density and good corrosion resistance. However, they do not resist well at high temperatures, so they need to be replaced by with high temperature resistance. For this reason, there is a tendency to to develop new composite materials, which are made up of a matrix (aluminium alloys) (aluminium alloys) and reinforcements (short, long or particulate fibres).

The first metal matrix composites (MMCs) were composed of an aluminium-based matrix. A metal matrix composite consists of a metal matrix into which are inserted fibres, particles or filaments known as whiskers [65]. As far as fibres are concerned, there are short fibres and continuous fibres (monofilament or multi-filament). The figure (Fig. 16) represents a cross-sectional view showing the arrangement of the fibres in a monofilament metal matrix. Figure illustrates one of the mono-filament fibres, the core in black is silicon carbide surrounded by boron.

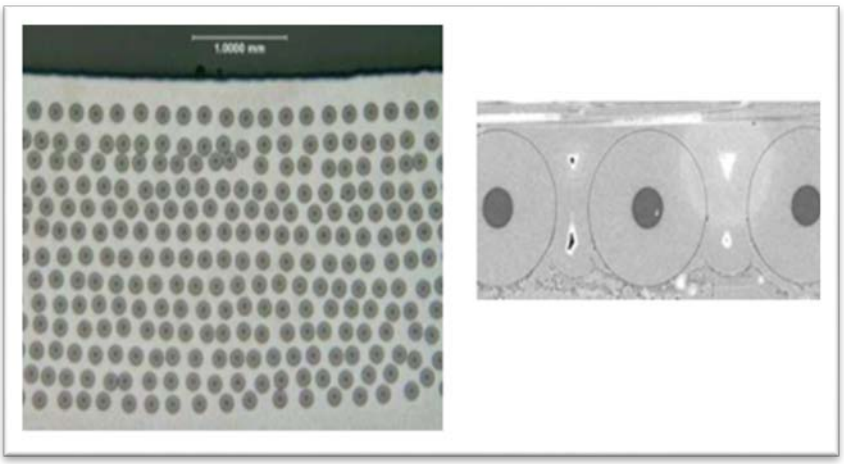

Figure3.2: Sectional view of a metal matrix composite with a single filament [2].

Composites containing a certain percentage of fibre (15% to 25%) generally contain silicon carbide (SiC) or alumina. This type of composite material improves maximum strength, specific rigidity, high-temperature resistance and reduces the coefficient of thermal expansion. However, it does have its drawbacks: the composite is brittle compared with the pure matrixabsorbs less energy during deformation, and the transformation and shapingprocesses are more expensive than those for polymers or simple metals. As a result, there are few applications using discontinuous fibres and almost none using fibres [3].

Metal matrix composites (MMCs) generally use a strong, rigid metal with reinforcement (fibres), giving it ductile behaviour. The advantages of pure matrix and polymer matrix composites [4] include rigidity, tensile strength, thermal resistance, fatigue resistance, impact resistance and no mould. On the other hand, their disadvantages include: manufacturing cost; little-known material; difficult to form ; corrosion problems.

Metal matrix composites (MMCs) generally use a strong, rigid metal with reinforcement (fibres), giving it ductile behaviour. The advantages of pure matrix and polymer matrix composites [4] include rigidity, tensile strength, thermal resistance, fatigue resistance, impact resistance and no mould. On the other hand, their disadvantages: manufacturing cost; little-known material; difficult to form; corrosion problems.

Metal matrix composites (MMCs) were developed in the 1960s and 1965s, with applications focused exclusively on the aerospace industry. Then, in the 1980s, new ceramic fibres made it possible to relaunch work in this field, with examples of industrial applications being developed in the automotive and electronics industries. electronics [66].

Metal matrix composites (MMCs) are made up of a metal matrix and reinforcements. So the choice of metals or metal alloys and reinforcements used in the manufacture of metal matrix composites (MMCs) depends on their specific properties in the un-reinforced state. reinforced state.

The metals most commonly used as matrices are aluminium, titanium and magnesium, and the inclusions most commonly used as reinforcements are particles of silicon carbide (SiC) and aluminium oxide (Al2O3), or sometimes titanium boride (TiB2), titanium carbide (TiC) or boron carbide (B4C). The manufacturing processes for metal matrix composites (CMM) depend on the state of the matrix when the reinforcements are introduced.

It can be in a liquid state (liquid forging, medium-pressure foundry), or in a semi-solid state (liquid forging, medium-pressure foundry). pressure foundry), or a semi-solid or solid state (powder metallurgy). The metal matrix composites (MMCs) generally have good specific mechanical characteristics specific mechanical properties, good resistance to temperature and thermal shock, as well as resistance to wear and abrasion ([67], [86]), depending on the nature of the dispersed elements. depending on the nature of the dispersed elements contained in the metal matrix.

Most of the research carried out in the field of metal matrix composites (MMC) is generally oriented towards the development of matrices based on light alloys of the type (Al, Mg, Ti), while there is some work oriented towards steel matrix-based metal matrix composites (MMC), which are mainly studied for their resistance to abrasion. In terms of the matrix most commonly used in metal matrix composites (MMCs), we find that aluminium matrix, which has a low density and relatively high mechanical and physical properties. relatively high mechanical and physical properties.

However, the most commonly used reinforcement is (SiC) [69], although reinforcements of type (Ai203, B4C) are also used. The choice of reinforcement depends on the following main parameters:

- Shape and dimensions (geometric properties);
- Young's modulus and tensile strength (mechanical properties);
- Density and coefficient of thermal expansion (physical properties);
- Compatibility of the reinforcement with the matrix;
- Cost of the reinforcement;

Metal matrix composites (MMCs) are a vast subject of research, and a great deal of work has been done on studying the elastoplastic behaviour of the composite, taking into account microscopic factors (volume fraction, slenderness ratio, different types of fibre (cylindrical, spherical, ellipsoidal), and fibre distribution). (cylindrical, spherical, ellipsoidal), and fibre distribution).

8. FABRICATION METHODES OF MMCs:

There are three primary categories for classifying the fabrication methods employed in the production of metal matrix composites (MMCs).

- Liquid State Fabrication
- Solid State Fabrication
- In-Situ Fabrication

8.1. LIQUID STATE FABRICATION:

Liquid phase processing is a method used in the fabrication of metal matrix composites (MMCs), where the reinforcement phase is incorporated into molten metal. A crucial objective is to achieve strong interfacial bonding between the reinforcements and the molten metal, resulting in improved mechanical properties. To enhance the wetting between the reinforcement particles or fibers and the molten metal, a coating process can be employed. This coating facilitates better adhesion and interaction between the two components, ultimately contributing to the desired mechanical enhancements.

8.1.1. STIR CASTING :

One commonly employed method for fabricating metal matrix composites (MMCs) is stir casting. In this technique, the reinforcement phase is mechanically stirred into a metal matrix. Stir casting is widely preferred by researchers for various applications of matrix composites. The process involves heating the base metal or alloy in a crucible above its melting point in a furnace. Once the matrix is melted, a stirrer is used to uniformly distribute heat throughout the liquid metal. Reinforcement particulates or fibers are then added, and stirring continues to ensure even distribution of the reinforcement phase. After solidification, the desired MMC is obtained. Thecontinuous stirring action during the process results in a more homogeneous and defect-free MMC [70]. MMCs produced through stir casting exhibit improved mechanical properties, making them suitable for diverse engineering applications [71]. The stirring of the liquid metal and dispersed phase is a crucial step in this method [72,73]. Researchers Lai and Chung [74] discovered that when SiC interacts with aluminum at high temperatures, it forms brittle aluminum carbide, which can impact the mechanical properties of the composite. To overcome this issue, surface modification processes have been employed. **Figure 17** illustrates the preparation of an MMC using the stir casting method, highlighting its detailed components.

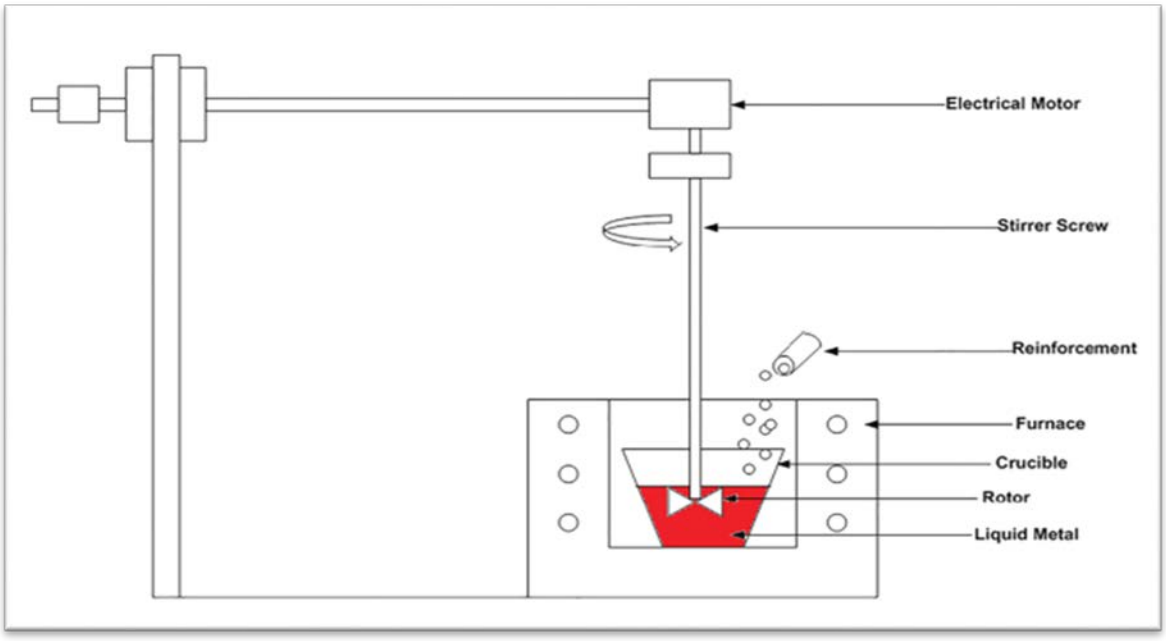

Figure 3.3:Stircasting method.

8.1.2 INFILTRATION:

The liquid state process of composite manufacturing involves immersing preformed reinforcement phases such as particulates or fibers into a liquid metal matrix. The liquid metal fills the gaps between the preformed reinforcement inclusions. Infiltration can be achieved either through the capillary force of the reinforcement phase or by applying external pressure to the molten matrix phase. [75] have identified certain limitations of this method, such as void formation during the infiltration of particle-reinforced metals. The formation of voids is attributed to high volume fractions of particulates and differences in the coefficients of thermal expansion between the matrix and reinforcement. Brief discussions on the three types of infiltration processes are provided Gas pressure infiltration; Squeeze Casting infiltration;Pressure die infiltration.

8.1.2.1.GAS PRESSURE INFILTRATION:

Gas Pressure Infiltration is a widely employed method for fabricating large composite parts. One advantage of this process is that it allows for the use of non-coated fibers due to their minimal contact time with the molten metal. Compared to processes involving mechanical force, Gas Pressure Infiltration causes less damage to the fibers. The process involves taking a container and filling it with a preform up to a specific level, followed by pouring molten metal onto it. Subsequently, gas pressure is applied, leading to the infusion of the molten metal into the preform and the formation of a metal matrix composite. The commonly used pressurized

gas is Nitrogen (N2), although inert gases can also be utilized to prevent any unwanted reactions between the gas and the metal matrix composite. For a detailed illustration of the gas pressure infiltration method, refer to Figure 18.

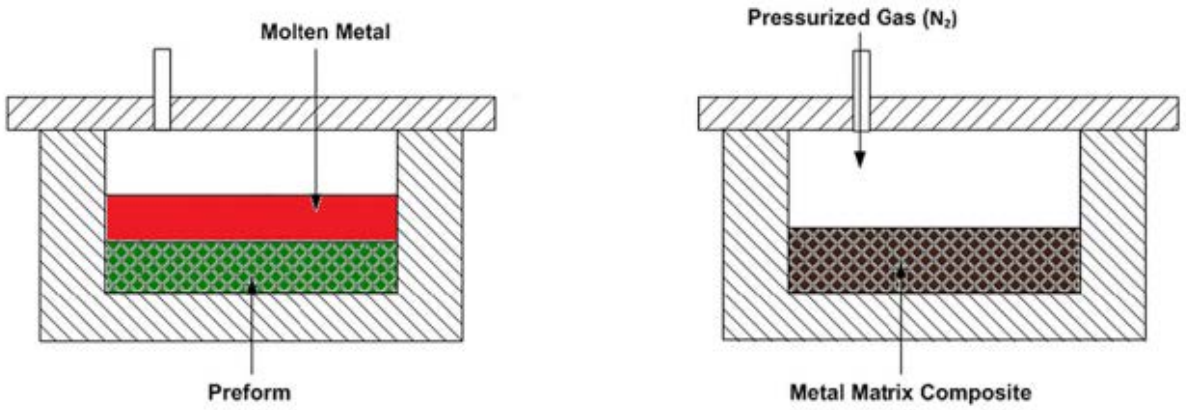

Figure 3.4:Gas Pressure Infiltration.

8.1.2.2. SQUEEZE CASTING INFILTRATION:

The forced infiltration process is a method used in the liquid state fabrication of metal matrix composites (MMCs). This process involves placing a preform of the reinforcement phase, such as particulates or fibers, in the lower section of a fixed mold part. As shown in Figure 19, the liquid metal is then forced to infiltrate the preform as the upper movable mold part (ram) moves downward. Under pressure, the infiltrated material undergoes solidification. Several process criteria play a crucial role in maintaining the quality of the squeeze casting composite, including mold temperature, pouring temperature, die temperature, time delay in pressurizing the melt, and filling velocity. Currently, there are no specific rules governing the control of these process variables [76,77].

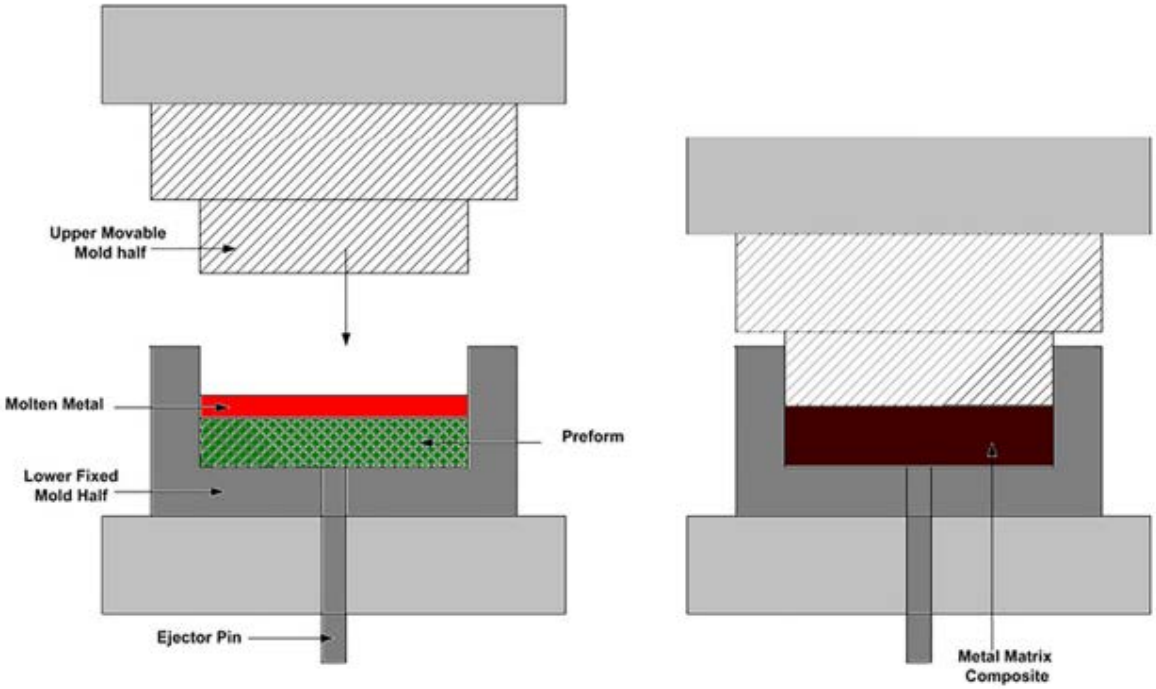

Figure 3.5: Squeeze Casting Infiltration method.

8.1.2.3.PRESSURE DIE INFILTRATION:

The forced infiltration process is utilized for the fabrication of metal matrix composites (MMCs) and employs die-casting technology. As depicted in **Figure 20**, molten metal is forcefully injected into a die by means of a movable piston or plunger. Within the die, a preformed reinforcement phase consisting of particles or fibers is carefully placed. The molten metal infiltrates the preform, resulting in the formation of a homogeneous metal matrix composite. However, placing the preform presents a challenge, as the high pressure involved can displace it. Any displacement of the preform would compromise the quality of the final product. To overcome this issue, spacers made of ceramic components are employed. These spacers serve as integral parts of the composite, preventing the displacement of the preform during the infiltration process.

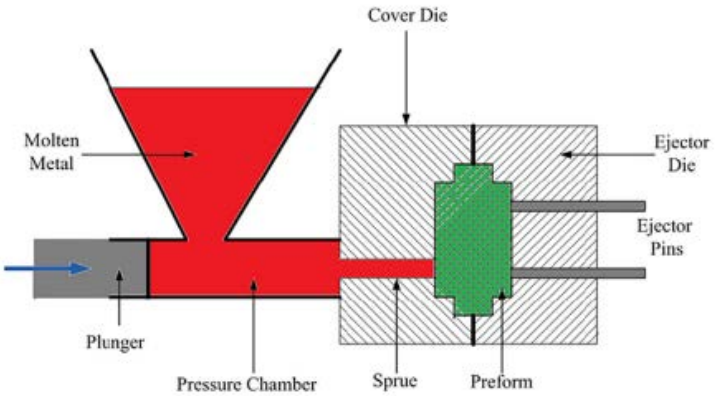

Figure 3.6:Pressure Die Infiltration method.

8.2. SOLID STATE FABRICATION MMC :

In these fabrication processes, the formation of metal matrix composites (MMCs) relies on the bonding between the metal matrix and the reinforcement phase. This bonding is essential for the creation of MMCs. During the manufacturing process, under high pressure and temperature conditions, bonding occurs between the metal matrix and the reinforcement phase through mutual diffusion. The combination of these factors facilitates the establishment of strong bonds between the metal matrix and the reinforcement, resulting in the formation of MMCs.

8.2.1.DIFFUSION BONDIN :

In this particular process, a specific arrangement is followed where the metal matrix, in the form of foils, and the dispersed phase, in the form of long fibres, are stacked in a predetermined order. This stack is then subjected to high temperature and pressure, as illustrated in **Figure 21**. As a result, a multilayer structure of laminate composite material is obtained. This process is particularly suitable for the fabrication of simple-shaped parts. However, challenges arise when manufacturing MMCs using distinct materials, mainly due to significant differences in deformation and melting temperatures [78]. To address these challenges, the diffusion bonding process offers an effective solution, ensuring the preservation of the microstructure without any deterioration [79].

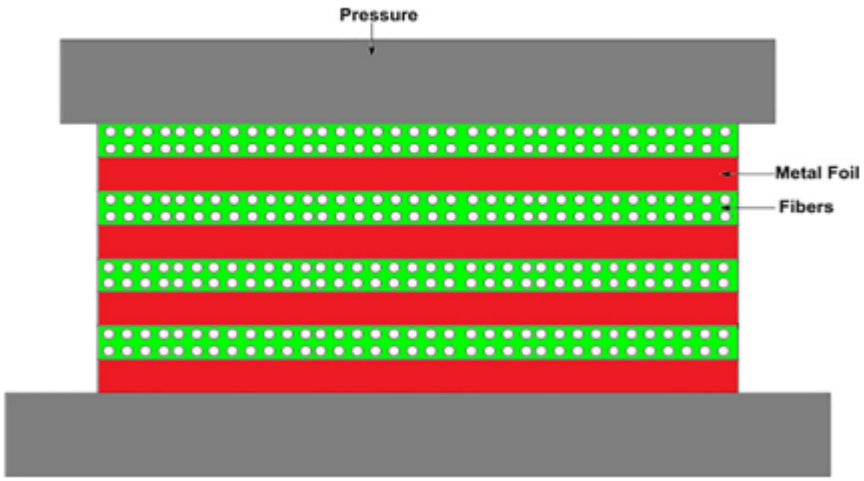

Figure3.7: Diffusion Bonding.

8.2.2.POWDER METALLURGY :

In the powder metallurgy process, metal or metal alloy powder is combined with reinforcement particles, whiskers, or short fibers. This mixture is then compacted into the desired shape using a die and punch at room temperature. Following compaction, the material undergoes heating, referred to as sintering. The powder metallurgy method begins with obtaining a homogeneous mixture of powders through ball milling. The mixed powder is then filled into a die and subjected to punching under load to form a solid-state or green state

material. This solid-state material is subsequently heated to a specific elevated temperature, a process known as sintering. During sintering, the powder particles fuse together without melting, resulting in an increase in the density of the composite material with longer sintering times. The powder metallurgy process finds extensive use in the production of magnesium alloy MMCs [80], MMCs of aluminum alloys [81,82], and copper matrix alloys [83–85]. Additional steps, such as forging and hot isostatic pressing, may be employed to further process the composite matrix that is formed [86–88]. Figure 8 illustrates the various steps involved in the powder metallurgy process.

8.3 IN-SITU FABRICATION OF MMCs:

The in-situ process allows for the production of matrix-dispersed phase in various types of metal matrix composites (MMCs), as illustrated in **Figure 22**. In this process, the dispersed phase is formed within the matrix through precipitation from the melt during the cooling andsolidification stages. This in-situ formation of the dispersed phase enables the fabrication of a wide range of MMCs with tailored properties and characteristics. By controlling the composition, processing conditions, and cooling rate, different types of MMCs can be prepared using the in-situ process. This method offers versatility and flexibility in designing MMCs with enhanced properties for specific applications.

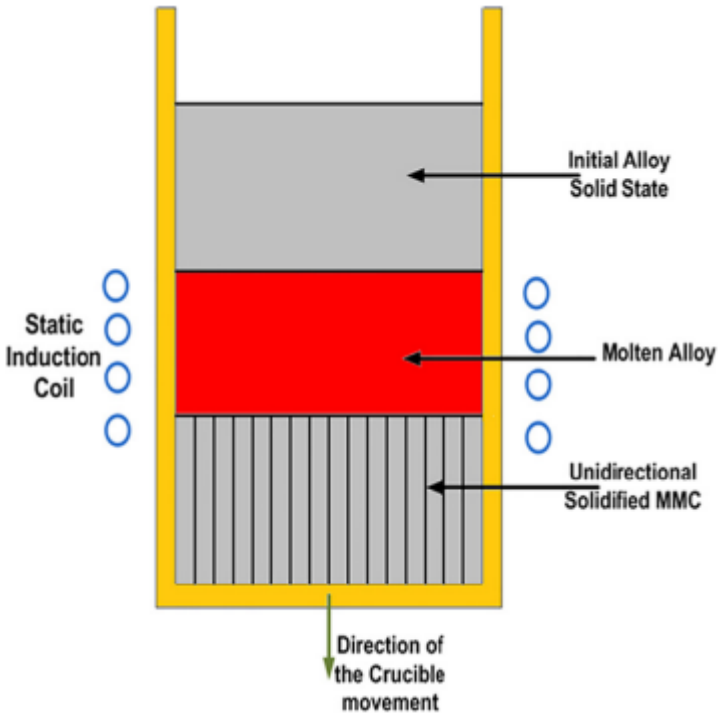

Figure 3.8:In-Situ Fabrication of MMC.

In the in-situ manufacturing process of metal matrix composites (MMCs), different types of composites can be fabricated based on the form of the reinforcement phase. These include:

- **Particulate-based in-situ MMC**: These composites are prepared by manufacturing the reinforcement phase in the form of particles directly within the matrix. During the fabrication process, the particles are generated in-situ, resulting in particulate-based MMCs.
- **Short fiber-based in-situ MMC:** Composites in this category are fabricated by in-situ manufacturing of the reinforcement phase in the form of whiskers or short fibers. The whiskers or short fibers are produced within the matrix during the fabrication process, leading to the formation of short fiber-based MMCs.
- **Long fiber-based in-situ MMC**: The composites in this group are manufactured by in-situ production of the reinforcement phase in the form of continuous fibers. The continuous fibers are generated within the matrix during the fabrication process, resulting in the formation of long fiber-based MMCs.

These different approaches of in-situ manufacturing allow for the production of MMCs with specific forms of reinforcement phases, providing versatility in tailoring the properties and characteristics of the composites for various applications.

In the in-situ manufacturing process of metal matrix composites (MMCs), a more homogeneous distribution of reinforcement phase particles is achieved. This method offers advantages such as lower cost equipment and technologies. **Table** 2presents an illustrative example of vector representation, demonstrating the fabrication of metal matrix composites with different compositions at varying temperature ranges. These MMCs undergo mechanical and thermal analysis to assess their performance, and the component exhibiting the most efficient results is selected for subsequent applications. Furthermore, **Table 3** showcases a compilation of commonly fabricated MMCs using different processes by various researchers. These tables serve as valuable references in understanding the wide range of MMCs that have been successfully produced.

TABLE 2 :vector representation of MMCs preparation.

temperature	X(matrix)	Y(reinforcement)	Z(reinforcement)
T_1°C	90%	5%	5%
T_2°C	88%	6%	6%
T_3°C	86%	7%	7%
T_4°C	87%	8%	5%

TABLE 3: Commonly fabricated MMCs through various processes:

Sr. No.	Matrix material and reinforcement	Preparationmethod	References
1	Al matrix with TiO2 reinforcement	Liquid Powder Metallurgy	[39]
2	NiAl with fiber reinforcement of W, Al, Mo etc.	Reactive Infiltration	[40.41]
3	Cu-Nb composites	Diffusion Bonding	[42.43]
4	Magnesium matrix with SiC reinforcement	Stir Casting	[44]
5	Al and Mg matrix using TiC and SiC as reinforcement	Pressure Infiltration	[45.48]
6	SiCreinforcement in Al matrix.	Vacuum PressurE	[49]
		Casting Stir Casting	
8	Cu with Gr particles as reinforcement	Powder Metallurgy	[50]
9	Al metal matrix using SiC particles and whiskers as reinforcement.		[49.51.53]
9	Al-Ni-Z where Z can be Cr, Fe, W, Mo reinforcements	In-Situ Method	[45]
10	Al356 alloy with Mica and SiC as reinforcement	Stir Casting	[55]
11	Ti matrix with SiCfibres as reinforcement, Al matrix using CF-coated with SiC as reinforcement Al alloys using SiC, Al2O3 or Gr particles as reinforcement, Ni3Al matrix using TiB2 particles as reinforcement, Ti-based matrix composites.		
12	Cu matrix with steel reinforcement	Stir Casting	[49.56.58] [60]

13	Stir Casting

9. SOME RECENT TECHNIQUES OF MMCs FABRICATION:

9.1. CONTINUOUS BINDER POWDERE COATING (CBPC): Continuous Binder Powder Coating (CBPC) is an innovative technique utilized for the production of composites. This method involves the continuous coating of reinforcing fibers with matrix powders. The process begins by cleaning the fibers with acetone and immersing them in a binder solution. The acetone and binder solution are maintained at ambient temperature. Subsequently, the fibers are passed through a vessel containing matrix powder, where the matrix grains adhere to the binder coating. Finally, the coated fibers are rolled out and dried. The CBPC technique finds significant application in the fabrication of titanium-based metal matrix composites (MMCs) [81]. This approach enables the creation of MMCs with enhanced properties and tailored characteristics**.**

9.2. METAL INJECTION MOLDING (MIM) :

Metal injection molding (MIM) is an advanced manufacturing technique employed for the production of metal and ceramic powders with near-net-shape accuracy. The MIM process consists of four stages: mixing, injection molding, debinding, and sintering. This method is particularly suitable for the high-volume production of small and intricate components. Unlike traditional powder metallurgy, MIM allows for the easy fabrication of complex shapes and geometries. The utilization of very fine powders in the feedstock facilitates optimal compaction during the final sintering process. By employing the MIM process for metal matrix composite (MMC) fabrication, the cost of composite materials used for commercial applications can be significantly reduced, making them more economically viable [82]. This technology offers tremendous potential for the production of MMCs with improved performance characteristics and cost-effectiveness.

9 .3. MECHANICALALLOYING:

To produce homogeneous material, mechanical alloying is asolid-state powder processing technique that involves repeatedcold welding, fracturing, and rewelding of blended powder particlesin a high energy ball mill. This technique was designed tomanufacture MMCs for application in aerospace industry. Mechanicalalloying is basically divided 3 steps:

1. The matrix and reinforcement materials are added in ball milland converted to fine powders.

2. To compress the powders a hot isostatic process is applied.

3. Finally, to remove the stresses induced during compaction sintering

technique is applied.

FRICTION STIR PROCESSING DEFINITION:

Friction Stir Processing (FSP) is a solid-state joining and material processing technique used to modify the microstructure and properties of metals and alloys. It is a variation of friction stir welding, which was originally developed for joining materials. In FSP, a specially designed rotating tool with a non-consumable pin is inserted into the workpiece, which is typically a metal plate or component. The tool is then traversed along the surface, generating heat and mechanical deformation in the material. As the tool moves, the frictional heat softens the material without reaching its melting point. The mechanical mixing action of the rotating pin breaks down the original grain structure and promotes the formation of a fine-grained, homogeneous microstructure. This can lead to various desirable changes in the material, such as grain refinement, dissolution of precipitates, redistribution of alloying elements, and improved mechanical properties. FSP has been widely used for enhancing the properties of metallic materials, including improving their strength, hardness, fatigue resistance, and corrosion resistance. It is particularly useful for processing difficult-to-weld materials, such as aluminum alloys and steels, as it avoids the drawbacks associated with conventional fusion-based welding processes, such as solidification defects and residual stresses.

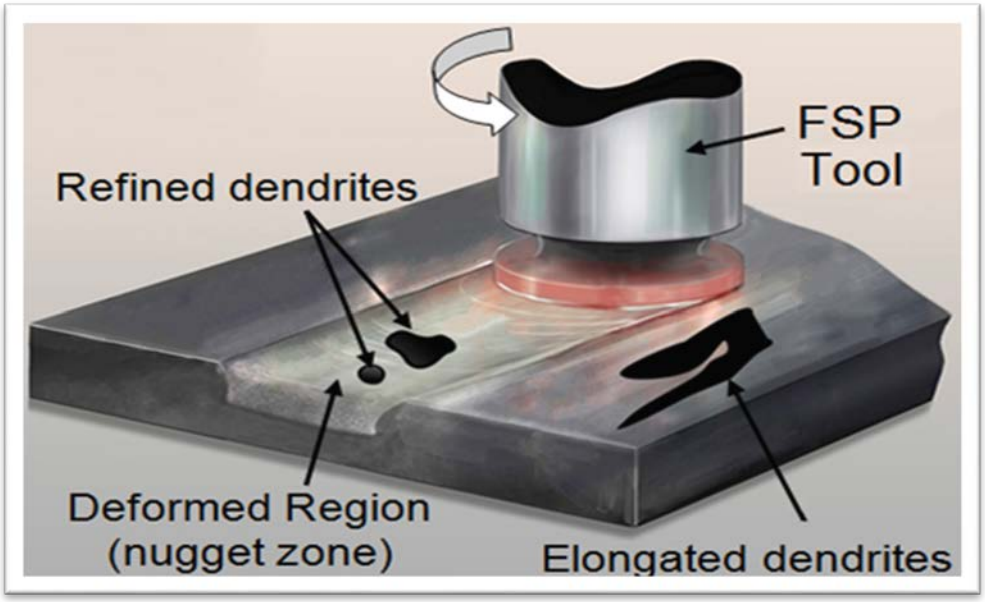

Figure 3.9: Schematic of friction stir processing

10. FSP PROCESS PARAMETERS:

The parameters that have the most significant influence on Friction Stir Welding/Friction Stir Processing (FSW/FSP) and greatly affect heat input, material flow, heat generation, peak temperature, and final surface quality include traverse speed, rotation speed, axial force, and tilt angle, as noted in reference [86]. The generation of heat during FSW/FSP primarily occurs due to the friction between the tool and the workpiece material. This friction is directly influenced by the contact area and pressure at the interface between the tool shoulder and the workpiece surface, which is controlled by the axial force. As a result of the rotational and translational motion of the tool, the material surrounding the pin experiences localized heating and subsequent softening, allowing it to move around the pin. In addition to heat generated by friction, the material also experiences heat generation through severe plastic deformation [63]. Studies have demonstrated that the axial force enhances heat generation, reduces the density of isotherms, and expands the Heat Affected Zone (HAZ) [87].

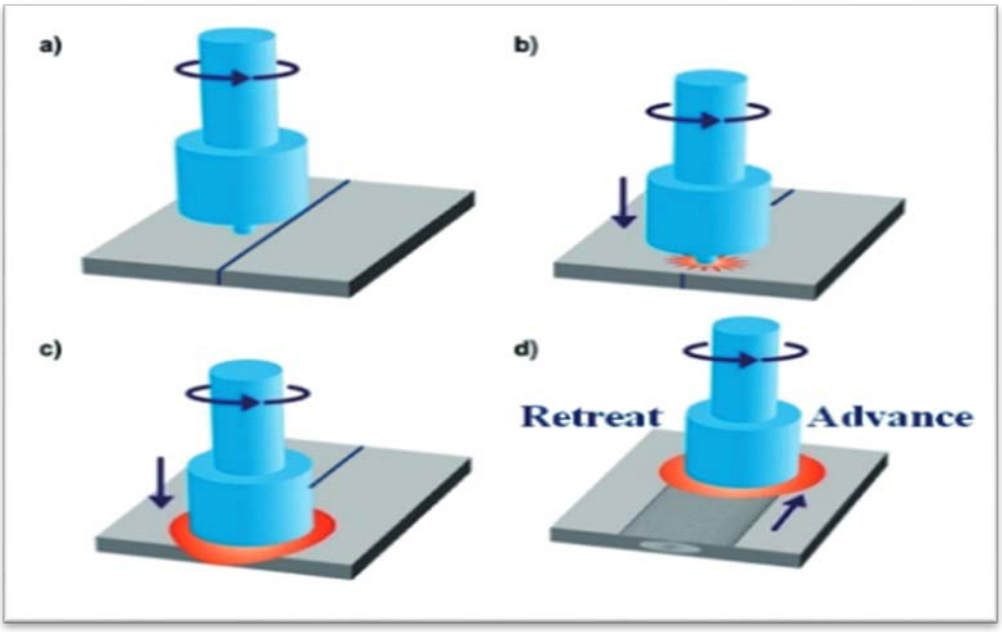

Figure 3.10:A schematic of FSP, showing the rotating,non-consomable tool in (a),frictional heating upon plunging into the work piece in (b) , frictional and adiabatic heating in (c) and traversing of the tool to weld / process the work piece in (d)

10.1.AXIAL FORCE:

Axial force, as defined in reference, refers to the downward force applied to the workpiece through the tool. The increase in axial force has a direct impact on surface quality by enhancing hardness and improving mechanical properties within the stirred zone . It is crucial to maintain consistency in axial force to ensure the production of high-quality microstructures, underscoring the utmost importance of force control [89].

10.2. ROTATIONAL AND TRAVERSE SPEED :

Rotational speed (ω), measured in rotations per minute (rpm) in either clockwise or counterclockwise directions based on the tool geometry, and traverse speed, or translational speed (v), measured in millimeters per minute (mm/min), are the primary parameters that significantly influence the material stirring process in FSW/FSP. The stirring of the material begins with the rotational motion of the tool, continues with a combination of rotational and translational movements, and concludes with pure rotational movement as long as the tool and specimen remain in contact . Research has demonstrated a substantial increase in generated temperature with an increase in rotational speed . Moreover, when the rotational speed remains constant, decreasing the translational speed leads to an increase in the average

welding temperature [31]. [32] conducted experiments with fixed rotational speed at 1600 rpm and tested traverse speeds of 0.37, 0.76, and 1.25 mm/s, concluding that the best tensile properties were achieved at a speed of 0.76 mm/s. [12] examined various rotational (800, 1000, 1200, 1400, and 1600 rpm) and traverse (20, 40, 60, 80, and 100 mm/min) speeds in surface composite fabrication using FSP. They found that the cross-sectional stirred zone area increased with higher rotational speeds (for a fixed traverse speed) but decreased with increasing traverse speed (for a fixed rotational speed). Additionally, they investigated the relationship between the stirred zone and groove size, revealing that the stir zone area decreased as the groove width increased. [11] fabricated a surface composite with an Al 7075 matrix and B4C powder reinforcements. Their findings indicated that lower traverse speeds resulted in better powder distribution, higher hardness, finer microstructure, and enhanced wear resistance. Another study ,with fixed traverse speed and varying rotational speed, observed that decreasing the rotational speed led to increased hardness, while higher rotational speeds provided better uniformity of microhardness. , high tensile strength was achieved at lower rotational speeds of 900 and 1200 rpm, combined with a medium traverse speed of 15 mm/min. However, increased rotational speed caused defects in the composite, particularly at higher traverse speeds. employed response surface methodology (RSM) for process optimization and suggested an optimal rotational speed of 1200 rpm and a traverse speed of 40 mm/min, resulting in the best mechanical properties for the composite. When using other reinforcements such as MWNT, a higher rotational speed range of 1500 to 2000 rpm improved MWNT distribution in the Al 7075 matrix . Ultimately, the optimal range of speeds is highly dependent on the substrate material and the type of reinforcements being used.[89]

10.3. TILT ANGLE :

The tool tilt angle (α), defined as the angle between the tool axis and the processing/welding direction, is an important process parameter in FSW and FSP. Its purpose is to ensure that the tool effectively holds the base material beneath the tool shoulder, allowing it to move efficiently around the pin during welding or modifications. Typically, tilt angles between 0° and 3° are chosen [3,5]. Dialami et al. [33] conducted experiments testing two tilt angles (0° and 2.5°) and concluded that the tool tilt angle has an impact on increasing stress within the leading edge of the tool on the workpiece, as well as on raising the temperature in the neighboring zone of the FSW tool on the rear advancing side. They also observed that changes in the tilt angle can reduce material flow stress on the rear advancing side, promote

material flow behind the tool, and enhance the material stirring action at the trailing edge on the advancing side. Moreover, the tilt angle directly affects the plunge depth of the tool.

10.4. INSERTION DEPTH :

Determining the appropriate "insertion depth" in FSP is primarily dependent on the length of the probe, and it can significantly impact the quality of the resulting surfaces. [9] conducted a study to investigate the influence of FSP tool insertion depth on the quality of a newly formed composite. The reinforcement material used was SiC powder, which was distributed within an Al AA6061-T6 matrix plate measuring 5 mm x 60 mm x 200 mm. The powder was inserted into a groove with a depth and width of 2 mm. The groove was closed using a pin-less tool made of H13 tool steel. The FSP process parameters employed were a tool tilt angle of 2.5°, a traverse speed of 40 mm/min, and a tool rotational speed of 1400 rpm. It was observed that a low plunge depth resulted in limited material flow and the formation of cavities at the center of the stirred zone. This occurred due to the low heat generation resulting from the small contact area between the tool shoulder and the workpiece. The authors proposed 0.25 mm as the optimal plunge depth (with a 20 mm shoulder diameter). If the penetration depth exceeded the optimal value, issues such as workpiece-tool shoulder sticking, ejection of the reinforcement powder, thinning of the workpiece, and even significant damage occurred.

10.5.TOOL GEOMETRY :

the pin geometry of the FSW/FSP tool is a significant factor in the FSW/FSP process. Various tool pin variations exist, with the most common ones being the conical round bottom pin, columnar (cylindrical) pin, threaded columnar pin, threaded columnar pin with flutes, triangular pin, and square pin [2,4,32,34] (refer to Figure 25). The threaded cylindrical, triangular, and square pin profiles are commonly applied according to the literature. Probes without threads are particularly suitable for processing harder alloys or metal matrix composites as threaded features tend to wear away more easily. Additionally, the outer surfaces of the probe can feature flutes or combinations of flutes and threads [2]. Some pin profiles also facilitate a pulse-type processing approach. Tools with a higher number of flat surfaces tend to exhibit a more pulsating work principle, resulting in a finer grain size. Threads and flutes can further enhance heat input into the material compared to flat-surfaced tools since they promote better material mixing through improved stirring.

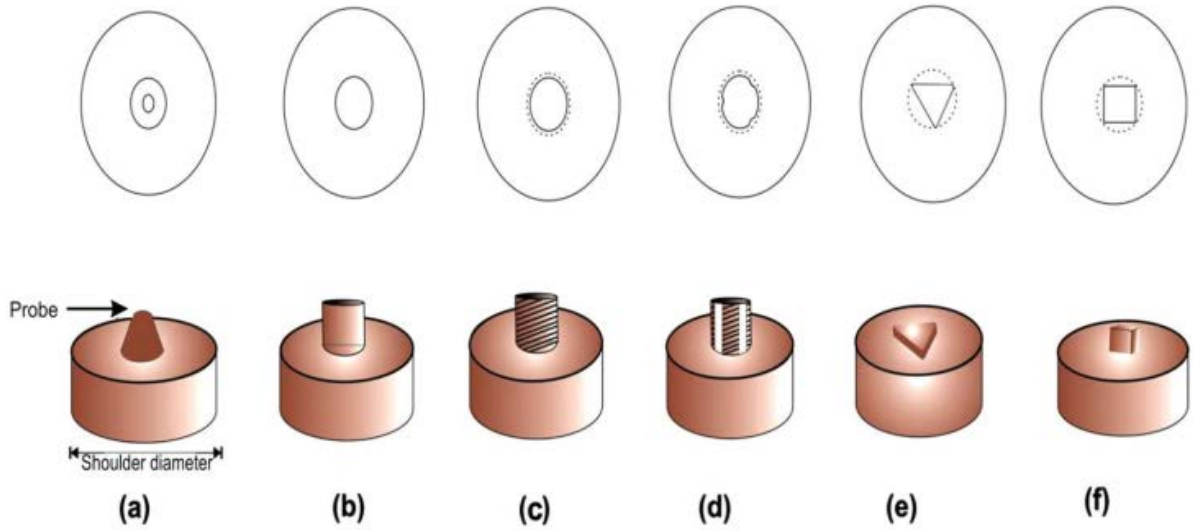

Figure 3.11:Profle of FSP tool probes a conical, b cylindrical, c threaded cylindrical, d threaded cylindrical futes, e triangular, f square [33]

various tool pin geometries including straight, taper (conical), threaded cylindrical, square, and triangular profiles were compared [32]. They found that the square pin profile exhibited defect-free zones regardless of the welding speeds. Moreover, they concluded that the optimal welding speed, irrespective of the pin profile, combined with the best pin profile, irrespective of the welding speeds, resulted in maximum tensile strength, hardness, and a finer grain structure. In terms of surface composite fabrication using FSP, it was observed that the square pin tool achieved the most uniform dispersion of reinforcement particles throughout the matrix compared to cylindrical (threaded and non-threaded) and triangular profiles [34]. Furthermore, the square pin profile yielded the finest grain structure. However, it should be noted that the squared tool exhibited the highest wear rates, leading to the deposition of iron debris within the aluminum matrix. compared the effect of different tool pin profiles on particle distribution in AZ31/Al2O3 surface composite. They concluded that the threaded columnar probe resulted in no defects when compared to the non-threaded and fluted cylindrical probe, due to better material flow and stirring.

10.6. NUMBER OF PASSES:

[10] conducted a study on Al/Al2O3 composite using single-pass FSP and found that the non-uniformity of the composite was more pronounced in terms of grain structure, tensile properties, and particle distribution. However, with the second pass, a higher level of homogeneity was achieved. [13] achieved relatively uniform TiB2 distribution by performing four passes. [14] investigated one- and two-pass FSP processes and found that two passes yielded better results in terms of hardness and wear resistance compared to a single pass. [16] examined the influence of multi-pass FSP on AA5803/ZrO2 composite and discovered that

increasing the number of passes consistently improved tensile properties while reducing wear rate. However, the friction coefficient was higher in the case of eight-pass FSP compared to the substrate material. [17] evaluated the effects of multi-pass FSP on AA2024/Al2O3 surface composite and obtained similar results, achieving a 40% increase in surface hardness due to grain refinement. It was also concluded that a single pass is insufficient to form a surface composite, which aligns with findings reported in other literature [20]. In the FSW process, increasing the number of passes (rewelding) enhances the mechanical characteristics of the weld joint [36]. However, it is important to note that a higher number of passes can lead to increased deformation due to higher heat inputs.

11. ADVANTAGE OF FSP METHOD:

The FSP method offers several advantages in materials processing. Some of the key advantages include:

Microstructural Refinement: FSP allows for the refinement of the material's microstructure, leading to improved mechanical properties. The stirring action of the FSP tool breaks down large grains into smaller, more uniform grains, resulting in enhanced strength, hardness, and durability.[49]

Densification and Homogeneity: FSP promotes densification of the material, reducing porosity and improving its overall density. Additionally, it helps achieve a homogeneous distribution of alloying elements, resulting in consistent properties throughout the processed material.

Elimination of Porosity and Casting Defects: Unlike traditional liquid metallurgical routes, FSP avoids the formation of porosity and casting defects. The solid-state nature of FSP prevents the entrapment of gases and impurities that often lead to defects in cast components.

Simplicity and Cost-Effectiveness: FSP offers a simpler and more cost-effective alternative to conventional processing methods. It eliminates the need for melting and casting, reducing energy consumption and associated costs. Additionally, it avoids the complexities of mold design and maintenance.

Tailored Material Properties: FSP allows for precise control over material properties. By adjusting FSP parameters such as tool rotation speed, traverse speed, and applied pressure, the microstructure, mechanical strength, and other properties can be tailored to specific requirements.

Versatility and Flexibility: FSP is applicable to a wide range of materials, including metals, alloys, and composites. It can be used to modify existing materials, repair damaged components, or create new structures with desired properties. The versatility and flexibility of FSP make it suitable for various industries, including aerospace, automotive, and manufacturing.

APPLICATION OF FSP TECHNIQUE:

The incorporation of additional metals or alloys to provide support and enhancement to the primary material has proven to be a beneficial approach, particularly in the automotive, armors, defense, and aerospace industries. This method enables the establishment of new materials with improved wear resistance, creep resistance, and fatigue properties [51]. Several successful examples of composites developed using the FSP technique include combinations such as AA 6082/stainless steel, AA 6082/TiC, AA 6063/SiO2, Al5083/Ni, Al 5083/Ti, and AA 7075/TiB2 [51]. These composite materials, achieved through FSP, demonstrate the effectiveness of this technique in creating customized materials with enhanced characteristics for various applications.

12. (FSP) EFFECTS ON THE MECHANICAL PROPERTIES:

12.1 MICROSTRUCTURE EFFECTS :

FSW/FSP surfaces typically exhibit four distinct microstructure zones: the stirred zone (SZ), which is also referred to as the "nugget zone" (NZ), the thermomechanically affected zone (TMAZ), the heat-affected zone (HAZ), and the base material (BM). These zones can be observed in **Figure 26** [39].

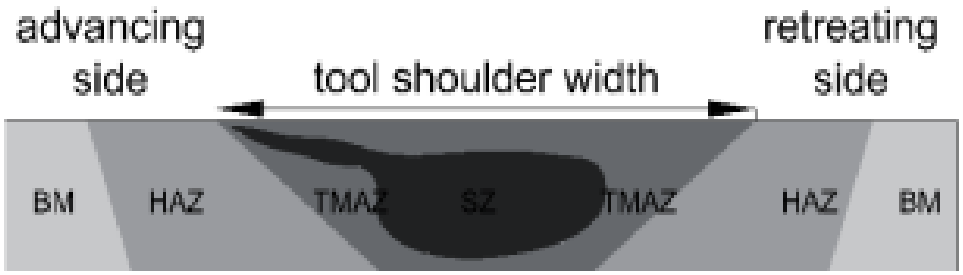

Figure 3.12: Microstructural zones in transverse crosssection of the FSW/FSP material. BM – substrate material; HAZ – heat affected zone; TMAZ - thermomechanically affected zone; SZ – stirred zone.

The size of grains in the stirred zone (SZ) is directly influenced by the peak temperature experienced [40]. When there is adequate stirring action and high temperature, a significant number of fine recrystallized grains can be generated. Rathee et al. [9] conducted microscopic observations and found that smaller tool plunge depths (TPD) resulted in defects in the center

of the stir zone, whereas increasing the TPD led to a uniform distribution of powder and a defect-free stir zone. However, a larger increase in TPD (0.35 mm) caused the appearance of defects. In the case of certain material combinations, such as TiC-reinforced Al7075-T651 aluminum alloy, minimal cracks and voids were observed within the stir zone [14]. [15] discovered that TiB2 and BN particles were evenly dispersed throughout the aluminum matrix. Zahmatkesh et al. [37], during microstructural analysis of FSP workpieces, identified four distinct zones: the base material (BM), heat-affected zone (HAZ), thermomechanically affected zone (TMAZ), and stirred zone (SZ). Their study revealed the absence of defects and a uniform distribution of reinforcements. Several research studies have shown that FSP leads to a reduction in grain size, and the incorporation of reinforcements such as CNTs and B4C further contributes to grain size reduction [19,20,25].

12.2.HARDNESS:

The average hardness of the Al7075/B4C composite was found to be 1.3 to 1.6 times higher than that of the metal substrate, [11]. [21] observed a 4.5 times increase in hardness for the AA583/SiC composite compared to the base material, using a speed ratio of 1400 rpm to 40 mm/min. However, increasing the rotational speed while keeping the traverse speed fixed resulted in lower hardness values. The addition of TiB2 particles to the AA6063 matrix led to a hardness increase from 55 HV to 140 HV (2.5 times) [13]. I [14], the substrate material Al7075 exhibited higher hardness compared to the Al/TiC composite fabricated through FSP.

12.3. WEAR PROPERTIES :

The reduction in the coefficient of friction for aluminum can be achieved by creating a thin composite layer on the surface using an AA1050 matrix reinforced with Al2O3 particles. This reduction is attributed to the increased strength and wear resistance of the composite, as well as a decrease in the contact area between the steel counterpart and the fabricated composite, without significant alterations in the material structure [10]. However, it should be noted that in a separate study, an increase in the wear rate coefficient was observed when comparing the composite to the Al 7075 substrate. On the other hand, [15] conducted research where they utilized the Friction Stir Processing (FSP) technique to incorporate TiB2 powder as reinforcement into AA7075. This resulted in a notable enhancement in sliding wear resistance. Moreover, the addition of TiB2 significantly improved the mechanical and wear

properties of the AA7075 matrix, with further improvements observed after the FSP process. The inclusion of reinforcement particles altered the wear mechanism from adhesive to abrasive, while FSP contributed to a more uniform wear pattern and finer debris formation.

12.4.TENSILE STRENGTH :

The tensile strength of AA6063 can be significantly increased, up to 70%, through the addition of TiB2-Al particles and the application of FSP. Similar findings have been reported in [24]. Additionally, improvements in tensile strength have been achieved through multi-pass processing, particularly at lower rotational speeds and medium traverse speeds. FSP has been shown to enhance both the tensile and yield strength of unreinforced materials [19,25] as well as composites produced through the compocasting process [19,20,25]. However, further research is needed to thoroughly understand the mechanical performance and the influence of various other factors on composites processed using the FSP method.

12.5. FRACTURE AND DEFECTS FORMATION :

In astudy , [24] observed that the addition of TiB2 particles to AA7075 alloy resulted in a reduction in void size on the fracture surface, and this refinement was further enhanced after FSP. Similarly, [16] compared the fracture surfaces of eight-pass FSP processed material with the base material and found a similar structure characterized by ductile fracture features, such as networked dimples and voids. FSP has been proven to be an effective method for addressing porosity defects that occur during casting, particularly in terms of reducing shrinking cavities [25]. The selection of the tool pin profile also plays a significant role in porosity and defect formation. However, finding the optimal pin profile that ensures maximum material flow and low wear rates remains a challenge.

- 2024 Aluminum Alloy after Friction Stir Processing:

The Al 2024 alloy was obtained from Alu-Stock as rolled plates with a thickness of 3 mm in the T351 temper condition. The nominal chemical composition in wt.% is presented in Table 1.

Table4.cominal chemical composition of the Al 2024 alloy.

Elment	Cu	Mg	Mn	Si	Fe	Zn	Ti	Cr	Al
Wt.%	4.3	1.5	0.6	<0.5	<0.5	0.15	0.03	0.007	Balance

The 2024-T351 aluminum alloy underwent heat treatment at various temperatures, heating times, and cooling conditions. It was found that subjecting the alloy to a temperature of 280 °C for 48 hours, followed by slow furnace cooling , resulted in the minimum hardness. This specific temper condition was designated as TT or Al 2024-TT.

Subsequently, the material in the TT condition was subjected to Friction Stir Processing (FSP) along the initial rolling direction. The FSP was performed using a tool made of MP159 nickel superalloy, comprising a scrolled shoulder with a diameter of 9.5 mm and a concentric threaded conical pin with flutes measuring 4.7-4.1 mm in diameter and 1.8 mm in length. The objective of the FSP was to achieve ultra-fine grain sizes in the aluminum alloy, and to accomplish this, a steel backing plate was utilized during the processing. The processing conditions were selected to have low heat input (HI), which was achieved by employing low tool rotation speed (r or ω) and high traverse speed (v). It is known that HI $\propto r^2/v$ [24,25], thus choosing lower HI values resulted in more severe processing conditions. The specific processing conditions, involving different traverse speeds and rotational speeds, are detailed in Table 5.

Table 5.disinations and values of the FSP processing conditions.

r (rpm)	v(mm/min)	HI(rpm^2/(mm/min))	Designation
1000	1000	1000	10r10v
700	1000	490	07r10v
700	1400	350	07r14v

The microstructural characterization involved the use of light microscopy (OM) with an Olympus BH-2 microscope and scanning electron microscopy (SEM) and electron backscattered scanning diffraction (EBSD) with a Hitachi ColdFEG S-4800 and a JEOL JSM 6500 F , respectively. For OM analysis, samples were prepared by conventional polishing methods and etched at room temperature using the Keller reagent (1.5% HCl, 1% HF, 2.5% HNO3, and 95% distilled water). SEM and EBSD samples were prepared by electropolishing at 15 V and 25 °C using a solution of 30% HNO3 and 70% CH3OH.

The mechanical characterization involved the use of constant crosshead speed tensile tests (CCST) at an initial strain rate of 10^{-2} s^{-1}. Additionally, strain rate change tensile tests (SRCT) were conducted to evaluate the material's behavior over a range of strain rates from $10^{-1}$to 10^{-5} s^{-1} at temperatures ranging from room temperature to 450 °C. The tests were performed using a universal Instron 1362 testing machine equipped with a four-lamp ellipsoidal furnace. Planar dog-bone tensile samples with dimensions of 6.5 × 2 × 1.7 mm^3 were obtained through electro-discharge machining, ensuring that their longitudinal axis was parallel to the initial

rolling or FSP direction. The upper surfaces of the tensile samples were mirror-polished to a final thickness of 1.6 mm to enable the monitoring of microstructural changes post-testing. The true strain (ε) was calculated using the formula $\varepsilon = \ln(1 + e)$, where $e = (l - lo)/lo$, and lo is the initial gage length while l represents the instantaneous length. The true stress (σ) was defined as $\sigma = F/Ao(1 + e)$, where Ao represents the initial cross-sectional area of the sample, and F denotes the applied load during the tensile testing.

RESULTS AND DISCUSSION :

3.1. Microstructures

Figure 27 displays a light micrograph showcasing the Al 2024 alloy in the TT temper condition. It is evident from the micrograph that the alloy exhibits coarse grain structures following this tempering process.

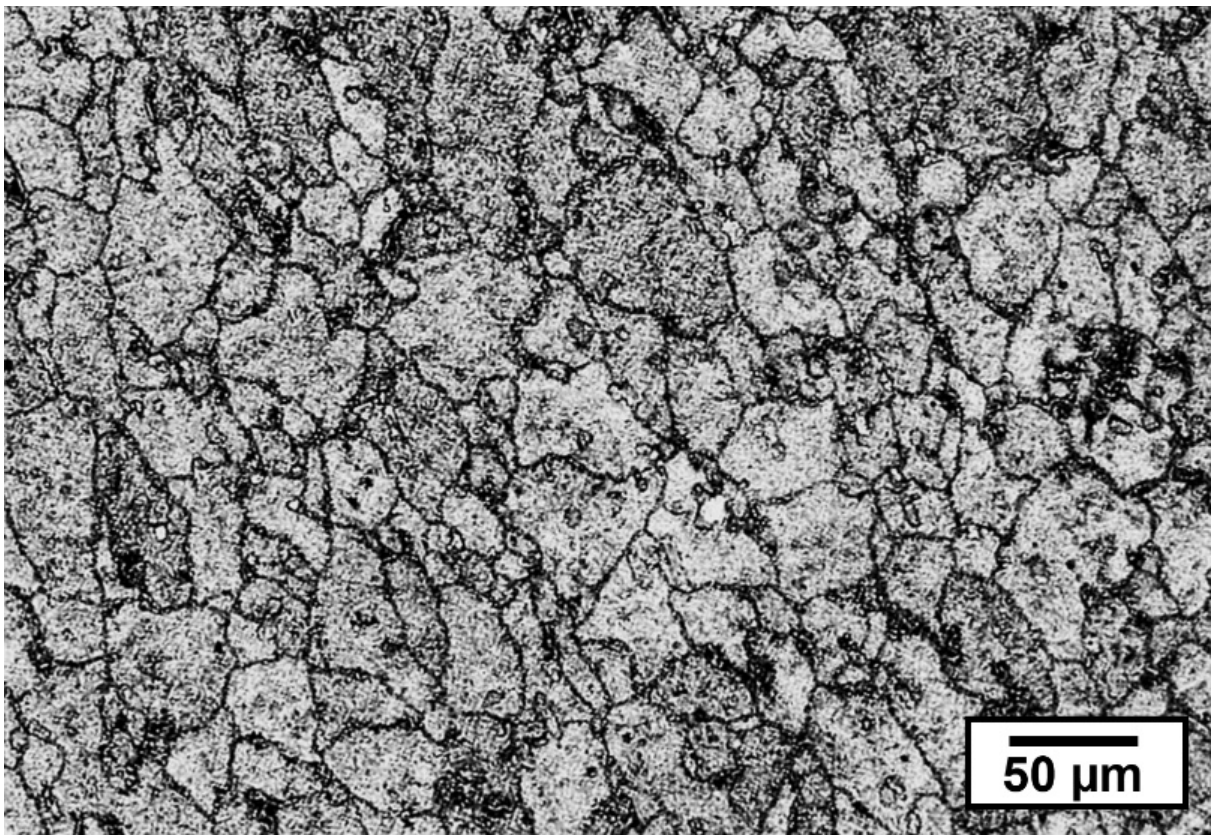

Figure 3.13:Light micrograph of the Al2024 alloy under TT temper.

The majority of the grains observed in the Al 2024 alloy were approximately 20 µm in size, with some grains even larger, reaching around 50 µm. The grains exhibited a slightly elongated shape. However, significant changes in the microstructure were observed following friction stir processing (FSP). Figure 28 illustrates an EBSD crystallographic orientation map

of an FSP sample processed at 1000 rpm and 1000 mm/s. The microstructure of the processed material exhibited a very fine-grained structure, with an average grain size of approximately 1 μm. It also displayed a high density of high-angle grain boundaries and nearly random misorientations. The average grain sizes, measured using the Feret diameter (DF), were 1.12 μm, 1.05 μm, and 0.93 μm for the 10r10v, 07r10v, and 07r14v conditions,respectively.

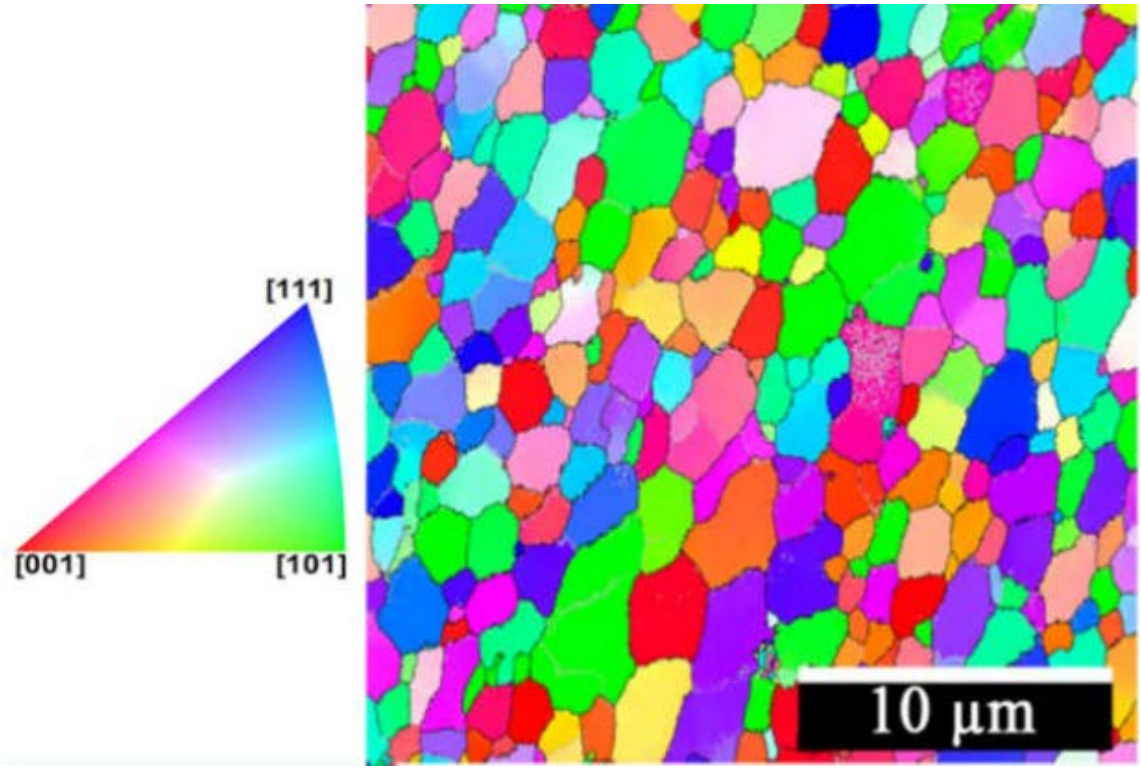

Figure 3.14: EBSD OIM micrograph of Al 2024-TT FSP sample 10r10v (processed at 1000 rpm and 1000 mm/s).

3.2. TENSILE TESTS AT MEDIUM AND HIGH TEMPERATURE:

Figure 29 presents the true stress–true strain curves for the Al 2024 alloy in the TT temper, obtained at an initial strain rate of 10−2 s−1 and temperatures ranging from 200 to 450 °C. Generally, it can be observed that the stress values exhibit a drastic decrease as the temperature increases. The ductility of the alloy shows an increasing trend with rising temperature; however, at 450 °C, the elongation to failure experiences a substantial decrease. The highest tensile ductility is observed at 400 °C for all three severe conditions, accompanied by the lowest stress values.

Furthermore, Figure 30 illustrates the elongation to failure curves at an initial strain rate of 10−2 s−1 as a function of temperature for both the TT and FSP conditions. The ductility continuously increases with temperature up to 400 °C. At this temperature, the ductility exceeds 400% for all FSP-processed materials. Similar values are observed for the three FSP

processing conditions, followed by a significant decrease in ductility at 450 °C. This phenomenon will be discussed further. In contrast, the non-processed material shows a moderate increase in ductility up to 450 °C, with values lower than 100%. These values are much lower than those observed for the processed materials, indicating the presence of different deformation mechanisms.

Figure 31 presents the flow stress as a function of temperature at an initial strain rate of 10−2 s−1 for both the TT temper and FSP conditions. The figure demonstrates a significant decrease in stress with increasing temperature for all FSP-processed materials. The stressvalues start at very high levels at 200 °C and gradually decrease to very low values at 350 °C. In contrast, the non-processed Al2024-TT material exhibits a moderate and continuous decrease in stressvalues,with the stress at 450 °C being the same as that observed for the FSP materials.

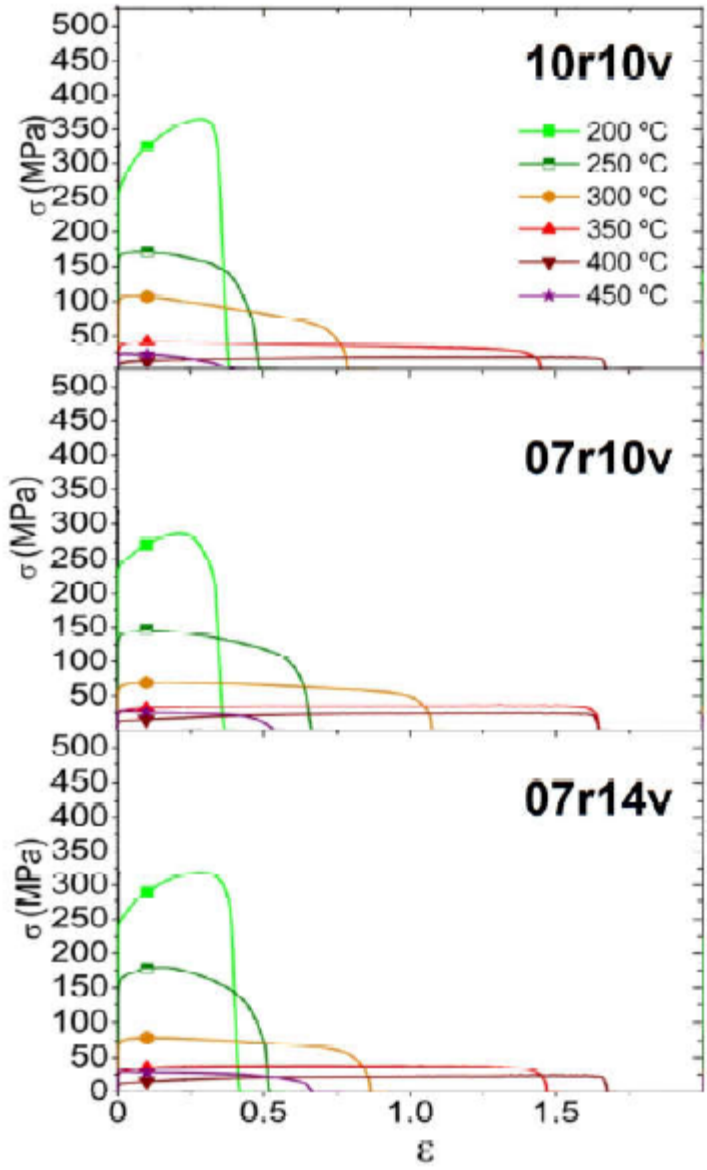

Figure 3.15:Stress as a function of strain at 10−2 s−1 for the Al 2024-TT in three FSP conditions and temperaturesfrom 200 to 450 °C.

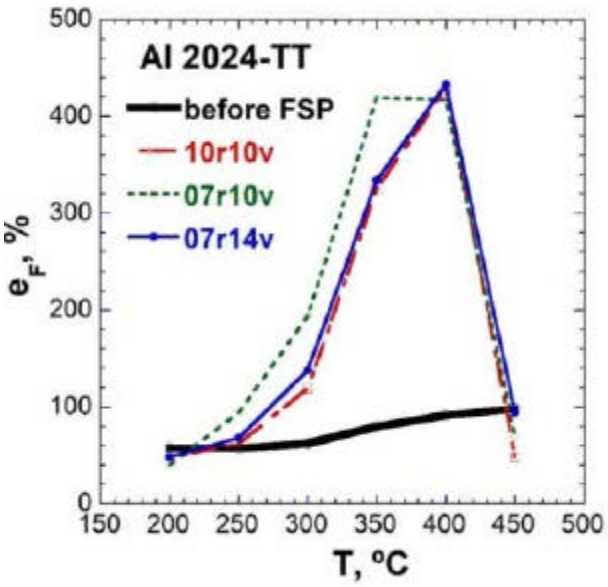

Figure 3.16:Elongation to failure as a function of temperature at 10−2 s−1 for the three FSP conditions and the non-processed Al 2024-TT.

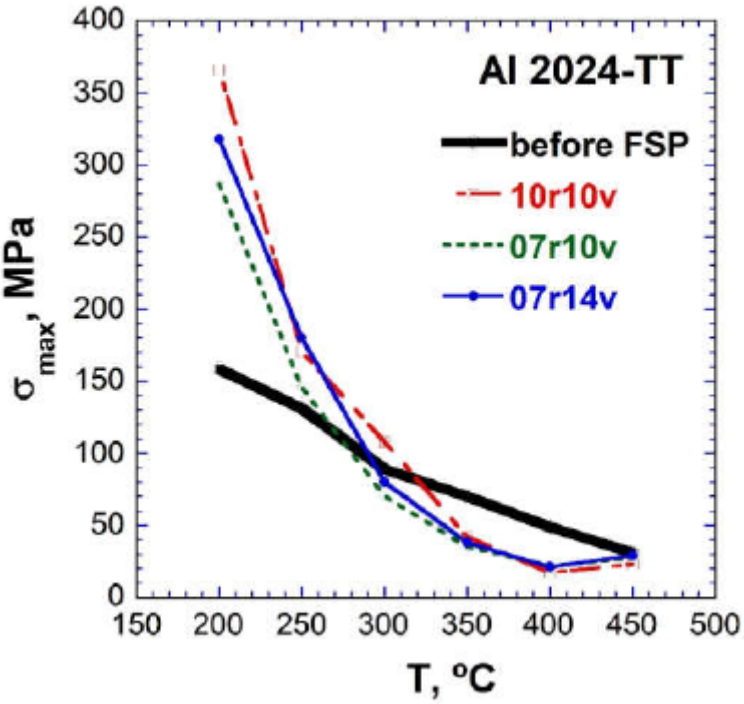

Figure 3.17:The flow stress, σmax, as a function of temperature at 10^{-2} s^{-1} for the Al 2024-TT before and after FSP conditions.

3.3. STRAIN-RATE CHANGE TENSILE TESTS:

To investigate the deformation mechanism in the FSP Al 2024-TT materials at different temperatures, a series of strain-rate change tests were performed for three FSP conditions.

These tests aimed to determine the stress exponents and activation energies. Figure 32 depicts the strain rate–true stresscurves at temperatures of 300, 350, 400, and 450 °C.

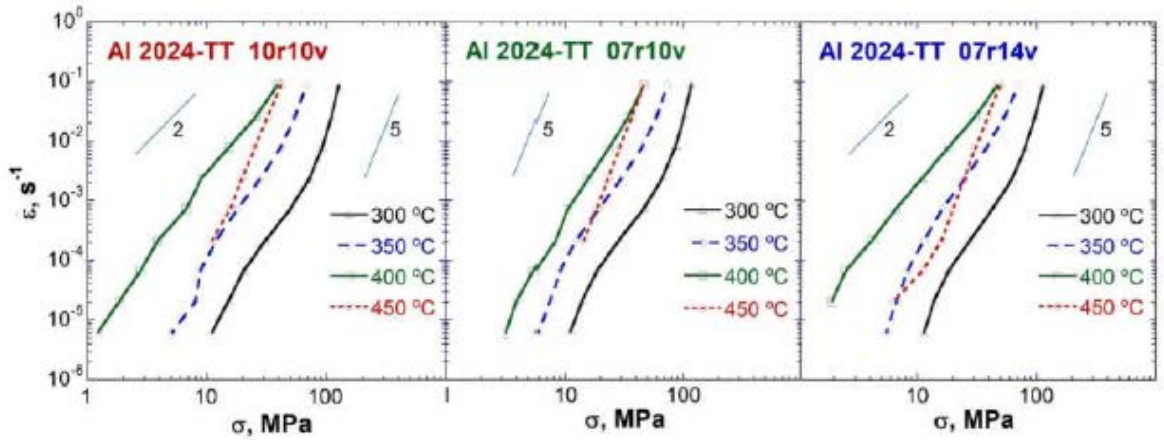

Figure 3.18:Double logarithmic scale representation of the strain rate−stress pairs at different test temperaturesof the three FSP Al 2024−TT alloys.

3.4. **MICROSTRUCTURES AFTER TESTING:**

Upon testing at high temperatures, the microstructures of the FSP materials reveal a rapid coarsening of grain size, as illustrated in Figure 33 for testing conducted at 350 and 400 °C. At 350 °C, the grain size measures approximately 3 μm, which subsequently increases to around 4 μm at 400 °C. It is worth noting that the grain size among the three FSP conditions remains highly similar at each temperature, indicating a consistent behavior across the different processing conditions.

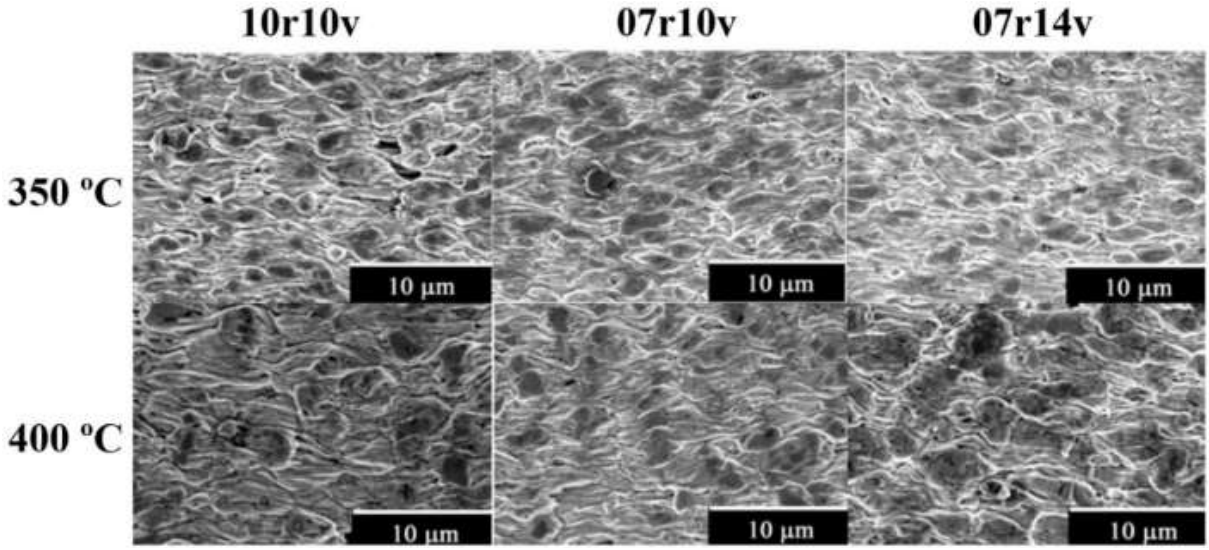

Figure 3.19:Microstructures of FSP Al 2024-TT samples after tensile testing at 10−2 s−1 at 350 and 400 °C.

The microstructure of the 07r10v material at 450 °C is depicted in Figure 34, serving as an illustrative example since similar microstructures were observed for the other FSP conditions. It is evident that the material exhibits relatively large grains that exceed the defined threshold of 20 μm for the activation of Grain Boundary Sliding (GBS). This finding helps to elucidate

the observed low elongation to failure, as shown in Figure 3, and the anomalous behavior displayed in the strain-rate change tests depicted in Figure 6, specifically at the testing temperature of 450 °C.

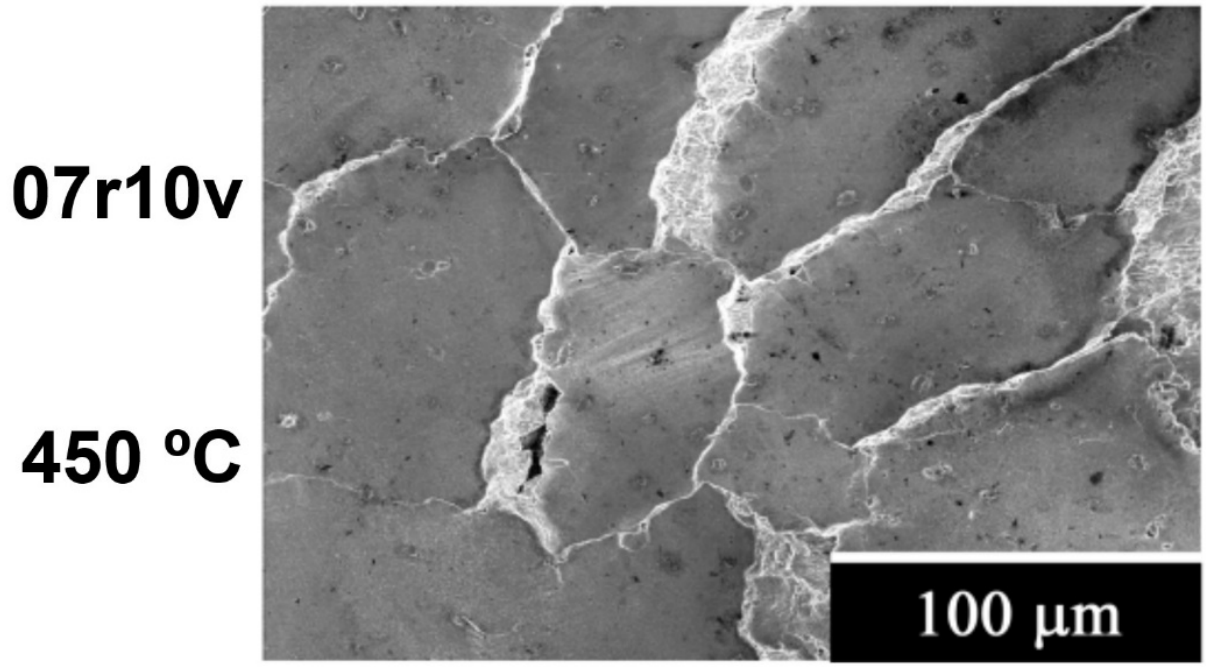

Figure 3.20:Microstructure after tensile testing at 10−2 s−1 and 450 °C the Al 2024-TT FSP 07r10v materialshowing very coarse grains.

All FSP conditions exhibit similar activation energy values for deformation, approximately around 140 kJ/mol within the superplastic range. Remarkably, this value closely aligns with the activation energy associated with the self-diffusion of aluminum, which is approximately142 kJ/mol [26].

Deformation Mechanisms.

The stress exponent values were determined by analyzing the slopes of the curves shown in Figure 32 for each temperature, and most of them fall within the range of n = 2 to 3. A stress exponent of 3 is commonly associated with solute drag or viscous glide creep [27]. During plastic deformation at high temperatures, dislocations interact with solute atoms, impeding their motion. It is important to note that the rate of dislocation movement is governed by the slower of the two sequential stages: glide along the slip plane and climb to overcome obstacles such as second-phase particles. While climb is typically the slower stage in many cases, in materials with relatively high solute concentrations, glide can be slower and become the rate-controlling process. Under such conditions, a power law with an exponent of three naturally emerges:

$$\dot{\varepsilon} = A_1 D_{SOL}/b_2(\sigma/E)^3 \quad (1)$$

In the equation mentioned, A1 represents a constant, b denotes the Burgers vector, and E refers to the average unrelaxed polycrystalline Young's modulus. In the case where the stress exponent is n = 3, it is associated with a mechanism such as solute drag or viscous glide

creep. On the other hand, grain boundary sliding (GBS) is characterized by a stress exponent of n = 2. However, in the present FSP Al2024 materials, the grain size (L) is much smaller than the typical threshold of 20 μm, which is considered the maximum grain size for GBS activation. The constitutive equation that describes this particular mechanism is [28]:

$$\dot{\varepsilon} = A_2 D_L/L^2(\sigma/E)^2 \quad (2)$$

In the given equation, A2 is a constant equal to A= $2\cdot10^9$, which is applicable for materials with high stacking-fault energy, including aluminum and its alloys. At high temperatures, the associated grain size exponent, denoted as p, typically takes a value of p = 2. On the other hand, for coarse grains and high strain rates, slip creep becomes the dominant mechanism. This mechanism can be described by the following equation [29]:

$$\dot{\varepsilon} = A_3 D_L/b^2(\sigma/E)^5 \quad (3)$$

where A3 is a constant, n = 5 and p = 0 (grain size independent, as for the solute drag mechanism in Equation (1).

The stress exponents for the materials under consideration exhibit values of approximately 5 or higher, indicating that the deformation is primarily governed by slip creep in the power law breakdown region. This phenomenon occurs at elevated temperatures and high strain rates. In contrast, at lower strain rates, the stress exponents fall within the range of 2 to 3, making it challenging to determine whether dislocation glide or grain boundary sliding (GBS) is the dominant deformation mechanism. Therefore, it becomes necessary to identify additional features or characteristics that can help differentiatebetween these two mechanisms.

At 400 °C, the FSP-processed materials demonstrate a remarkable improvement in ductility, reaching approximately 400% according to Figure 4. Meanwhile, the stress values exhibited by these materials are considerably low, as evident from Figure 31, which stands in contrast to the non-FSP Al 2024-TT samples. Notably, at this temperature, the stress exponent values (n) for the 10r10v and 07r14v FSP conditions closely approximate 2. A previous study by [16] proposed that the dominant rate-controlling mechanism in Al-2024 alloys is dislocation glide. This is attributed to the significant disparities in size between the solute and matrix atoms in Al-Mg and Al-Cu alloys. Interestingly, even in materials with very fine grains resulting from processes like equal channel angular pressing (ECAP), dislocation glide was observed despite elongations to failure exceeding 500%. These elongations are typically higher than what is associated with dislocation glide or solute-drag mechanisms at high strain rates.

Upon closer examination of our findings, a different interpretation emerges regarding the deformation behavior of the Al 2024 alloy. Our data consistently support the involvement of a grain boundary sliding (GBS) mechanism under specific temperature and strain rate conditions. As illustrated in Figure 4, the maximum elongations are observed at 400 °C for the FSP materials, surpassing those of the coarse-grained Al 2024-TT alloy. However, beyond this temperature, the rapid coarsening of the FSP materials' microstructure hinders the activation of GBS, resulting in a significant reduction in ductility. This dependence on grain

size contradicts the expectations of dislocation glide as the governing mechanism. Furthermore, Figure 31 demonstrates the lowest stress values for all three FSP materials at 400 °C, followed by higher stress values at 450 °C. This trend is further supported by the strain-rate change test results depicted in Figure 32, which show higher stress values at 450 °C compared to 400 °C, and even at 350 °C for certain strain rates (indicated by the dotted red lines). This behavior, combined with substantial grain coarsening as evidenced in Figure 8, again contradicts the grain-size independence typically associated with the dislocation glide mechanism.

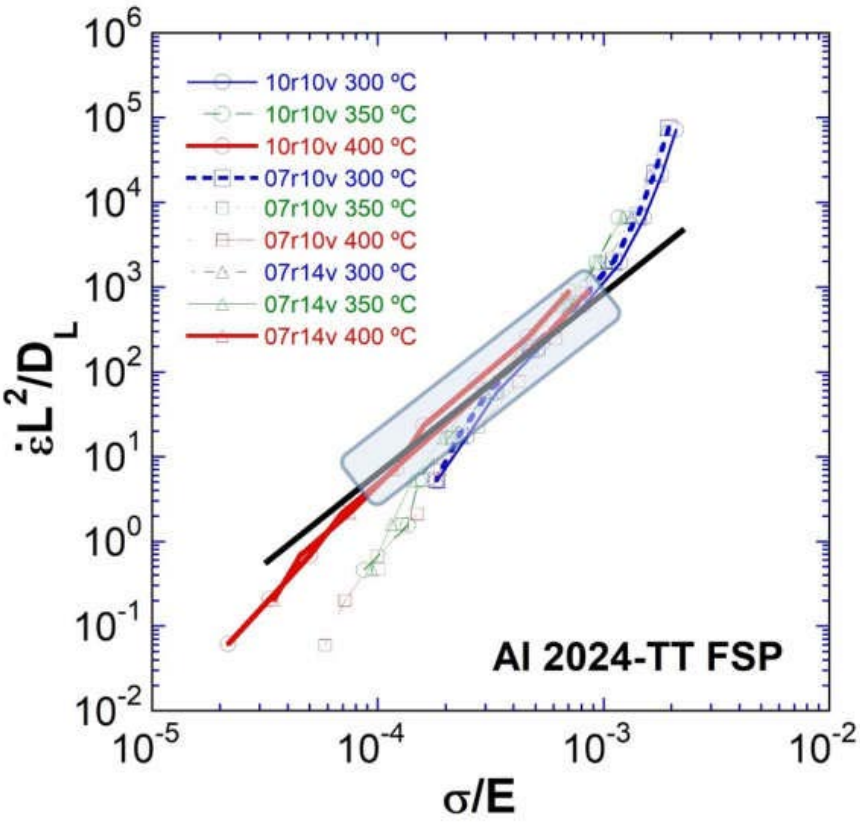

Figure 3.21:Diffusion− and grain−size−normalized strain rate as a function of modulus−compensated stress for the FSP conditions (L = 4 μm) at three temperatures.

Figure 35 presents a thick black line indicating a pre-exponential constant, A, with a value of 6×108. This value is notably lower than the typically accepted value for superplastic materials, which is around 2×109. Additionally, the figure includes data from other superplastic alloys with compositions similar to that of Al 2024, obtained from various studies [13,30–37]. These alloys exhibit comparable resistance within the superplastic regime, leading to similar A values. Moreover, other aluminum superplastic alloys with stress exponents close to 2 and significant elongations to failure also fall within the colored band of Figure 9 [38–41]. These alloys deform through grain boundary sliding when their microstructures consist of fine, equiaxed, and highly misoriented grains, demonstrating

behavior similar to the processed materials. Comparing with other aluminum alloys highlights similar high-temperature resistance despite distinct precipitation characteristics, emphasizing the crucial role of grain size in controlling superplastic behavior. Consequently, friction stir processing (FSP) serves as an appropriate technique for achieving ultrafine microstructures, enabling improved formability at high strain rates and intermediate temperatures, even for highly resistant aeronautical aluminum alloys.

A tempered 2024 aluminum alloy underwent three different friction stir processing (FSP) conditions. The initial tempering treatment, referred to as TT, involved heating the alloy to 280 °C for 48 hours, followed by slow cooling to achieve minimal hardness.

The microstructure of the TT-tempered alloy consisted of coarse grains with minimal elongation. However, severe FSP processing significantly reduced the grain size to approximately 1 μm.

A distinct trend was observed in the stress-temperature relationship for the FSP-processed materials. The stress exhibited a rapid decrease from 200 °C to 350 °C across all FSP conditions. In contrast, the non-processed Al 2024-TT material displayed a slower decrease in stress, with stress values at 450 °C matching those of the FSP materials.

Ductility demonstrated a substantial increase with temperature, particularly up to 400 °C, for all FSP-processed materials. At this temperature, the ductility exceeded 400% for the FSP materials. However, a significant decline in ductility occurred at 450 °C due to extensive grain coarsening, indicating that grain boundary sliding was no longer the dominant deformation mechanism. Conversely, the coarse-grained non-processed Al 2024-TT alloy exhibited a moderate increase in ductility up to 450 °C, but with values lower than 100%.

Similar strain rates were observed for a given stress within the superplastic regime, suggesting comparable grain sizes in the three FSP materials during deformation.

The deformation mechanism prevailing in the low-stress regime was grain boundary sliding, which aligns with the presence of fine, equiaxed, and highly misoriented grains resulting from friction stir processing.

Overall, these observations indicate the effectiveness of FSP in refining the microstructure and enhancing ductility in the 2024 aluminum alloy, while grain boundary sliding serves as the primary deformation mechanism in the low-stress regime.

MAX PHAS :

MAX phases take their name from their chemical composition Mn+1AXn where M

is a transition metal from groups IIIB to VIB (Ti, Cr,Zr, Nb,Hf,.....), A is an element from groups IIIA to VIA (Al, Si, P, S, Ga, Ge, As, In, Sn or

element from groups IIIA to VIA (Al, Si, P, S, Ga, Ge, As, In, Sn.....) and X is

nitrogen (N) or carbon (C) or a combination of both. The

Figure 1 shows the main elements making up the MAX phases synthesised so far.

to date.

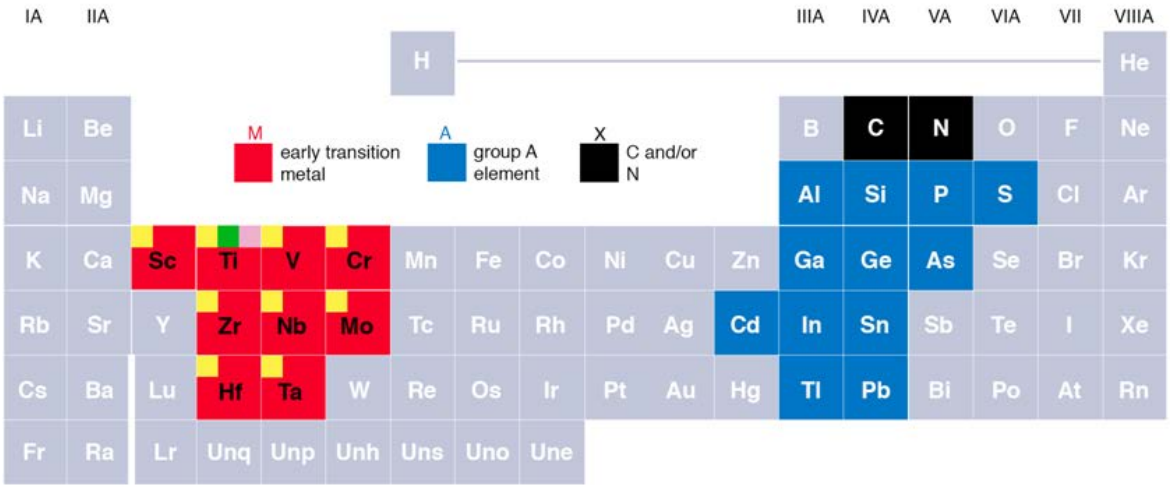

Figure3.22: Components of MAX phases

For the main phases known and studied, the index n varies from 1 to 3. Thephases thus formed are of the :

- M2AX for n=1 or 211
- M3AX2 for n=2 or 312
- M4AX3 for n= 3or 413.

In recent years, other phases of the MAX type, with more complex structurestype phases with more complex structures have been synthesised, and the n index has taken on values from 1 to 6 [4].

The MAX phases have a lamellar structure with a hexagonal mesh whose space group is P63/mmc. Their elementary cell structure is shown inFigure I.2 for the 211, 312 and 413 phases.

The crystal structure of MAX phases can be described simply asstacks of M6X octahedra separated by planes of A atoms. In theM6X octahedra, the element X occupies the octahedral sites. Figure I.2 showsthat the three structures differ in the number of layers of octahedral (each made up of 2 planes of red M atoms) separating the A layers (blue, A atoms).blue atoms, A). In structure 211, between two successive planes of A, there is anoctahedron (i.e. 2 planes of M containing 1 plane of X), while in thestructure 312, the number of octahedra is 2 (i.e. 3 planes of M containing2 planes of X) between two planes A. For structure 413, the number of octahedra is3 (i.e. 4 planes of M containing 3 planes of X) between two planes A.

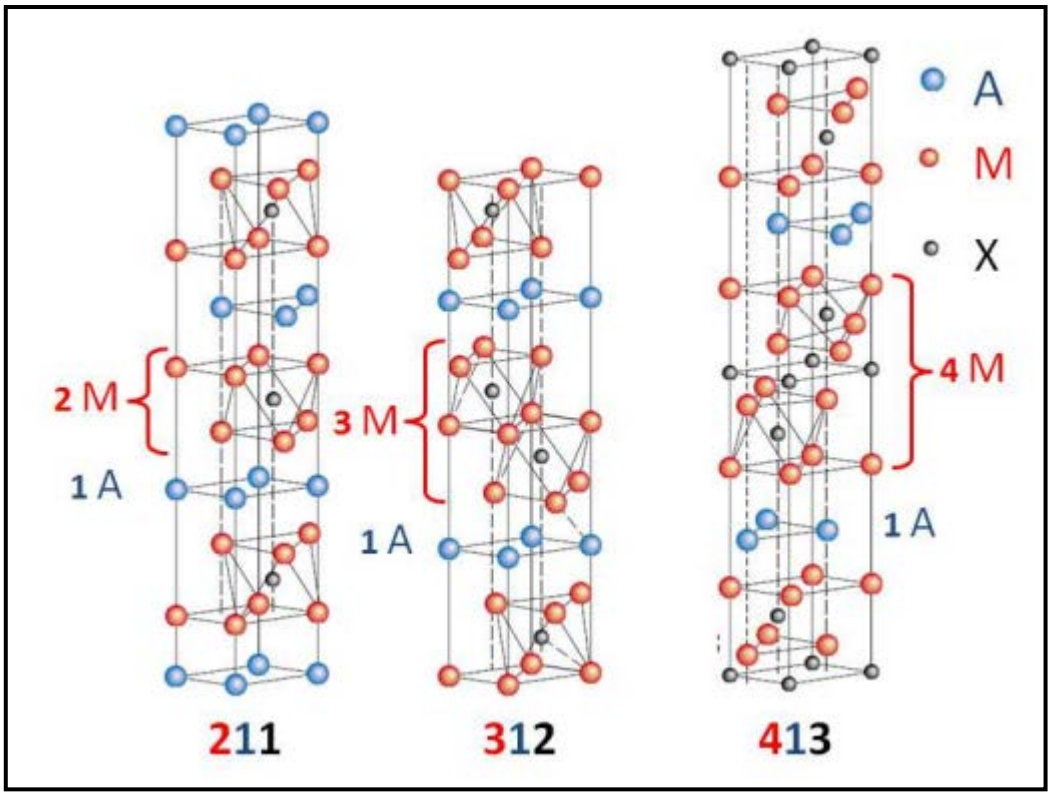

Figure 3.23: Crystal structure of MAX phases

Figure 38 shows an example of the hexagonal crystal structure of theTi3AlC2 phase (type 312) compared with that of Ti2AlC (type 211). Thelengths of the a and c parameters in Ti3AlC2 (i.e. the lattice parameters) areparameters) are 3.08 and 18.58 Å respectively, whereas these parameters are3.04 Å and 13.59 Å for the Ti2AlC phase [3].of some MAX

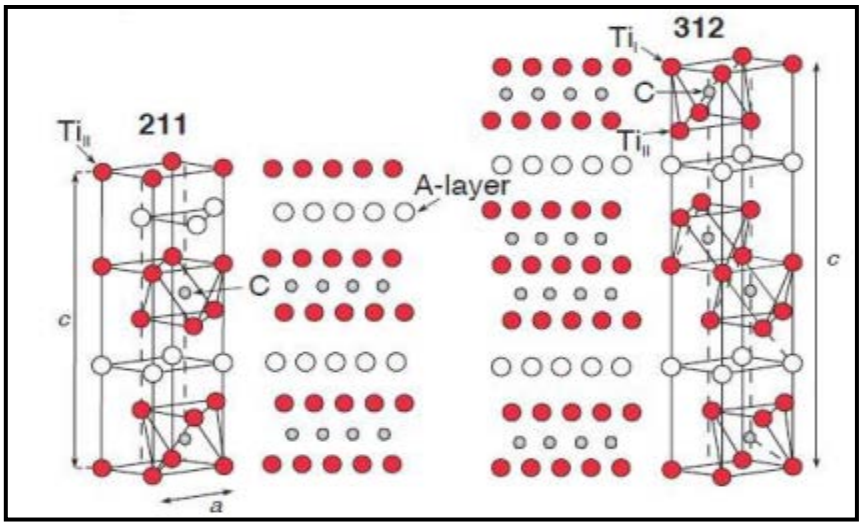

Figure3.24: Comparison between 122 and 213. [3]

Table 5: Mesh parameter values for some MAX phases

Phase	Paramètre a (Å)	Paramètre c (Å)	Rapport a/c
Ti2AlN	2,99	13,61	4,55
Ti2AlC	3,04	13,60	4,47
Cr2AlC	2,86	12,80	4,47
Ti2SC	3,22	11,20	3,47
Ti3SiC2	3,07	17,67	5,75
Ti3AlC2	3,08	18,58	6,03
Ti3SnC2	3,14	18,65	5,93
(V0,5Cr0,5)3AlC2	2,89	17,73	6,13
Ta3Al0,6Sn0,4C2	3,09	19,13	6,19
Ti4AlN3	2,99	23,27	7,78
Ti4SiC3	3,05	22,67	7,43
Ti4GaC3	3,05	23,37	7,66
Ti4GeC3	3,08	22,85	7,41
α-Ta4AlC3	3,11	24,12	7,75
β-Ta4AlC3	3,09	23,70	7,66
Nb4AlC3	3,13	24,12	7,70
V4AlC3	2,92	22,69	7,77

This particular structure means that MAX phases can be described as nano-lamellar materials. Figure 39shows thenanolamellar structure of the MAX Ti3SiC2 phase observed by high-resolutionhigh resolution transmission electron microscopy (HRTEM). An alternation ofTi3C2(octahedra) and silicon planes[1].

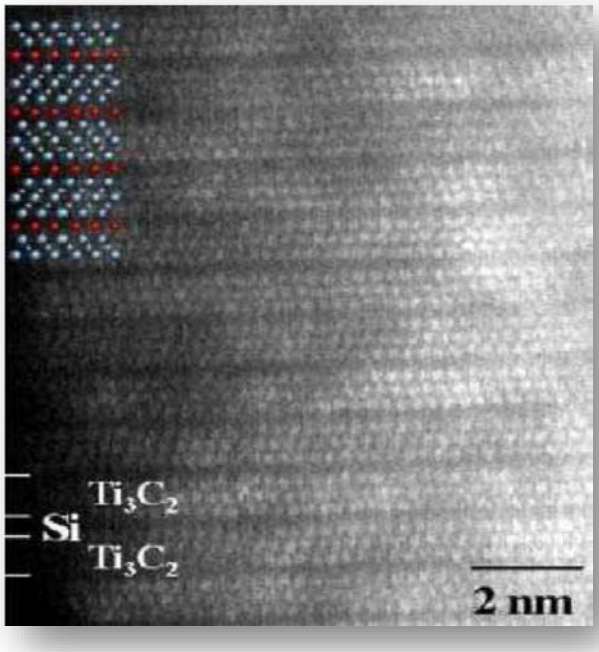

Figure3.25: Structure of the Ti3SiC2 phase observed by METHR [1].

The phases make it possible to form a large number of solid solutions ofsubstitutions on the M, A and X sites or by combinations. For example, it is form Ti2AlC0.8.XNX, with x between 0 and 0.8 by heat treatment atat 1490°C. Other examples include solid solutions of (Ti-Cr)2AlC, (Ti-V)2SC,(Nb-Zr)2AlC, and (Ti-Nb)2AlC[3].properties as a function of composition, for materials with identical and geometricallygeometrically similar crystalline structures[1].

MAX phases are new materials appreciated for their exceptionalproperties due to their ceramic-metal duality. The Ashbyndiagrams in figure I.5 show that these phases are located in the ceramic-metalceramic-metal domain. Like metals, MAX phases can be machined,

they are thermally and electrically conductive, impact resistantlike ceramics, they are rigid and resistant to thermal shockmechanically at high temperatures, they are refractory (high decomposition temperatures)refractory (high decomposition temperatures), resistant to oxidation and low density

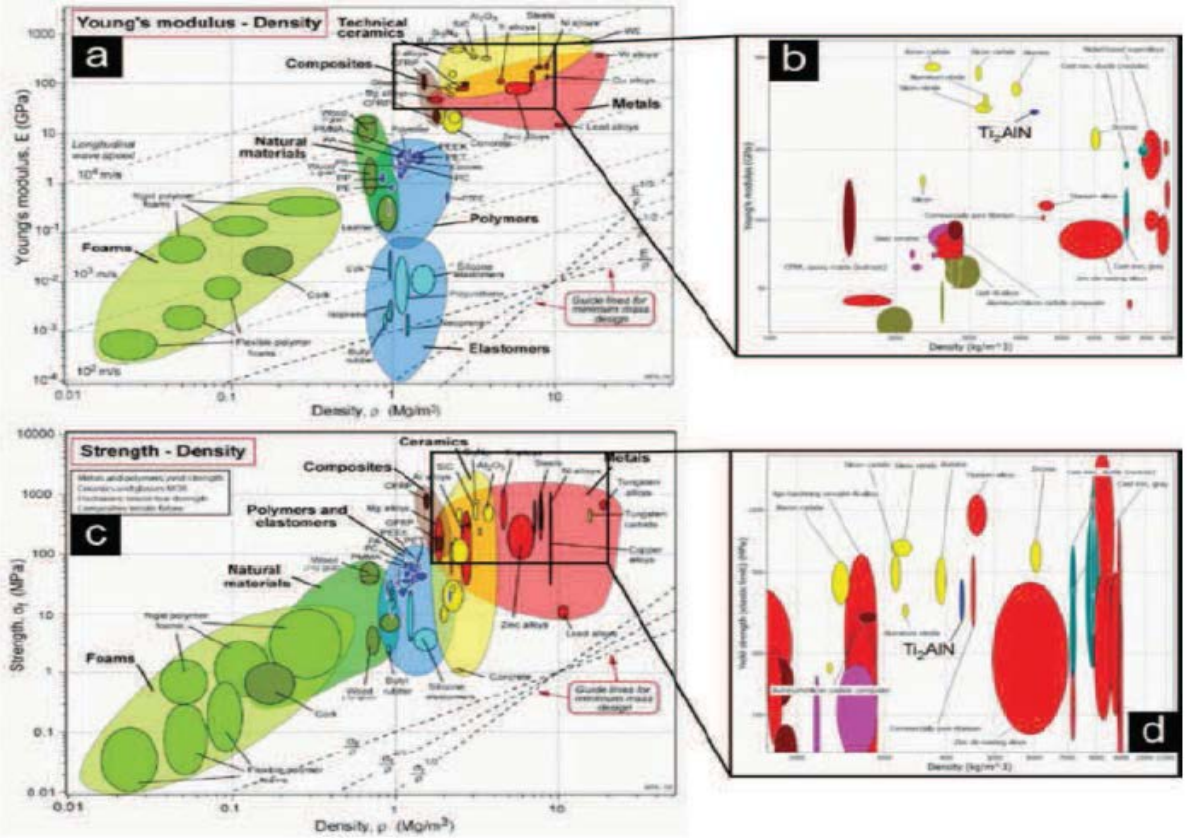

Figure 3.26: Ashby diagrams showing a MAX phase, Ti2AlN

MAX phases are used as heating elements in various atmospheres, as pressing tools and as structural materials.atmosphere, as press tools and as structural materials for high temperatureand many other specific applications. shows some examples of applications of MAX phases. shows a heating resistor made in the MAX phase, heated here to 1350°C.. shows, under a scanning electron microscope, a dense, adherent layer ofadherent oxide layer on the surface of a MAX phase subjected to atmosphericatmospheric oxidation of 10000 thermal cycles between 1350°C and room temperature.[1]

PROPRETIES OF MAX phase :

Mechanical propertieMAX phases have surprising and very interesting mechanical properties.interesting mechanical properties.Low hardness: the hardness of MAX phases is low and rather anisotropiccompared with the hardness of isotropic materials. The hardnesses of thesephases synthesised to date are generally between 2 and 5GPa. The highest value is 5.5 GPa, observed in the case ofTi3AlC0.5N0.5[5]. High rigidity marked by a Young's modulus that varies withn; around 300GPa for phases with n > 1, although this value is intermediateintermediate compared with carbides. The 211 phases, with fewerM-X bonds

than the others, are slightly less rigid (E211 = 200GPa). TheTi3SiC2 has a Young's modulus of approximately 320GPa and a shear modulus of 140GPa.The Poisson's ratio is of the order of 0.2 for the MAX phases synthesised.phases synthesised [1].

MAX phases are polycrystalline and highly anisotropic. Deformation occursessentially by sliding in the base planes (kink-band theorytheory put forward by Barsoum) [13]. Dislocation slip systemsdislocation slip systems that are particularly simple and active at room temperature are veryfavoured and generate deformations in the planes that can be assimilated toassimilated to sheet deformations as shown in Figure 41 (partsa. and b.). Parts c. and d. illustrate the effect of plane deformations on thepaddle-shaped grain of the MAX phase. Parts e. and f. schematize the evolution of the deformation in the case of a compressive stress on a MAX phase grain.while parts g. and h. show the deformation mode induced by compound

induced by compound loads (compression-flexion). Slidingalong the basic planes causes the other planes to move outside the basic planes, as shown inshown in Figure 42This mode of deformation provides MAX phases withimpact strength and resistance to crack propagation.

resistance. Recently, a team of French researchers have demonstrateddisplacement of dislocations outside the base planes [14].

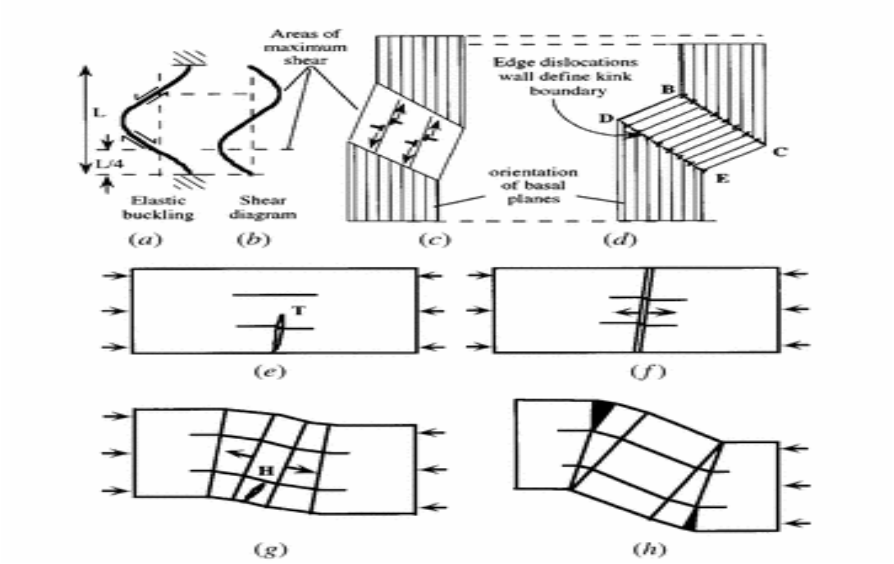

Figure 3.27: Mode of disclocation growth in MAX phases: kink-band theorykink-band theory [13]

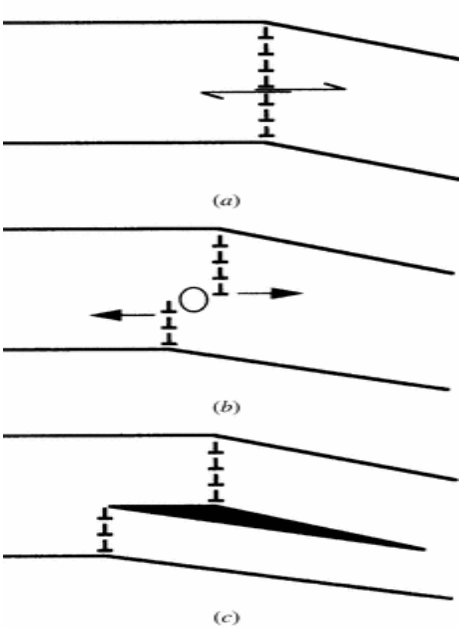

Figure 3.28: Displacement of dislocation lines in nanolamellae of MAX phases [13]

In addition to their strength properties, MAX phases are characterised by theirvery good machinability. Machining this type of material involves breaking and removing microscopic particles in the form of flakes.and removal of microscopic particles in the form of flakes, unlike metalsmetals, where machining is carried out by plastic deformation [1].

43shows a tiny screw-nut pair machined from a piece of sintered Ti3SiC2.

Figure3.29: Screw-nut system machined from Ti3SiC2

CHAPTER 4
EXPERIMANTAL PART

1.Objective of the experiment:

The purpose of this illustrative part is to learn how to make lubricant from kaolin in five different method

2.EQUIPMETS USED:

2.1.Tribometer: (Anton paar)

Tribometer or tribotester is a generic name for a device used to simulate friction and wear at the interface between surfaces in relative motion under controlled conditions. The 1989 edition of the Oxford English Dictionary defines a tribometer as an instrument for estimating sliding friction. The earliest reference provided by this dictionary is in the writings of Goldsmith in 1774, who used the word tribometer to refer to a "friction meter". In 1877, Knight defined it as a sled-like device used to estimate the friction of rubbing surfaces Tribometers are developed and used for a variety of purposes, including:

- simulating the tribocontact situation in a particular machine
- evaluating candidate bearing materials for a friction-critical application
- evaluating lubricants for a particular application
- qualifying lubricants for use based on established criteria
- monitor surface contamination of a product
- Acquire non-ecosystem specific (generic) friction data to compare and develop new materials, coatings or lubricants
- investigate the fundamental nature of friction of solids or lubricated solids

2.2.Ultrasonic Machining:(ISOLAB)

Ultrasonic machining is a material reduction manufacturing process, which means that material is removed from the surface of a part through the pounding of abrasives on the surface of the material using a high frequency, low amplitude vibrating tool.Ultrasonic vibration processing is usually used for brittle materials and materials with high hardness and is often used for piercing, cutting, welding, polishing, and cleaning processes.

2.3.Homogenizer:(Wis TIS)

A homogenizer is a laboratory device used to mix, emulsify, and homogenize liquids. It can be used to break up large particles in a liquid and evenly distribute them, creating a homogenous mixture. Homogenizers can be used in a variety of applications, including food and beverage production, pharmaceuticals, and biotechnology. The most common types of homogenizers are mechanical homogenizers, which use high pressure and shearing forces to break up particles, and ultrasonic homogenizers, which use high-frequency sound waves to create a cavitation effect that breaks up particles.

2.4. Analytical balances:(X ADAM)

Analytical balances are precision measuring instruments used in quantitative chemical analysis, to determine the mass of solid objects, liquids, powders and granular substances. Today, electronic balance use the principle of magnetic force restoration, offering readability up to .0001 g

2.5.Optical microscope:

In materials engineering, the optical microscope plays a crucial role in the analysis and characterization of materials. It is used to examine the microstructure, surface features, and defects present in various types of materials. Additionally, the optical microscope is used in materials engineering for the examination of non-metallic materials such as polymers, ceramics, and composites. It allows for the observation of surface morphology, particle distribution, fiber alignment, and other characteristics that influence the material's behavior and functionality.

2.6.Micro hardness:(Innovatest falcon 400)

The FALCON 400 improves on the conventional hardness testing methods by focusing on elimination of user influence on the test results. The advanced force sensor technology utilizes an electronically controlled loadcell closed loop system with force feedback to achieve absolute accuracy, reliability and repeatability, on all of the forces used for a testing. The innovative software functions of I-TOUCH™ workflow control, allows file storage, test program setting and storing, limit settings, conversions to other hardness scales, system setup

and convex and concave sample test settings that contribute to the exceptional repeatability and reproducibility of test results.

2.7. PROFILOMETER : (Tylor Hobson)

A profilometer, also known as a surface profilometer or surface roughness tester, is a precise instrument used to measure the surface texture or roughness of an object. It provides quantitative data about the height variations of a surface at a microscopic level.Taylor Hobson is a well-known manufacturer of metrology instruments, including profilometers. The company specializes in the design and production of high-precision measurement equipment for various industries, such as automotive, aerospace, electronics, and manufacturing. Taylor Hobson profilometers are widely used in research, quality control, and manufacturing processes to ensure surface integrity and meet specific requirements for smoothness or roughness.

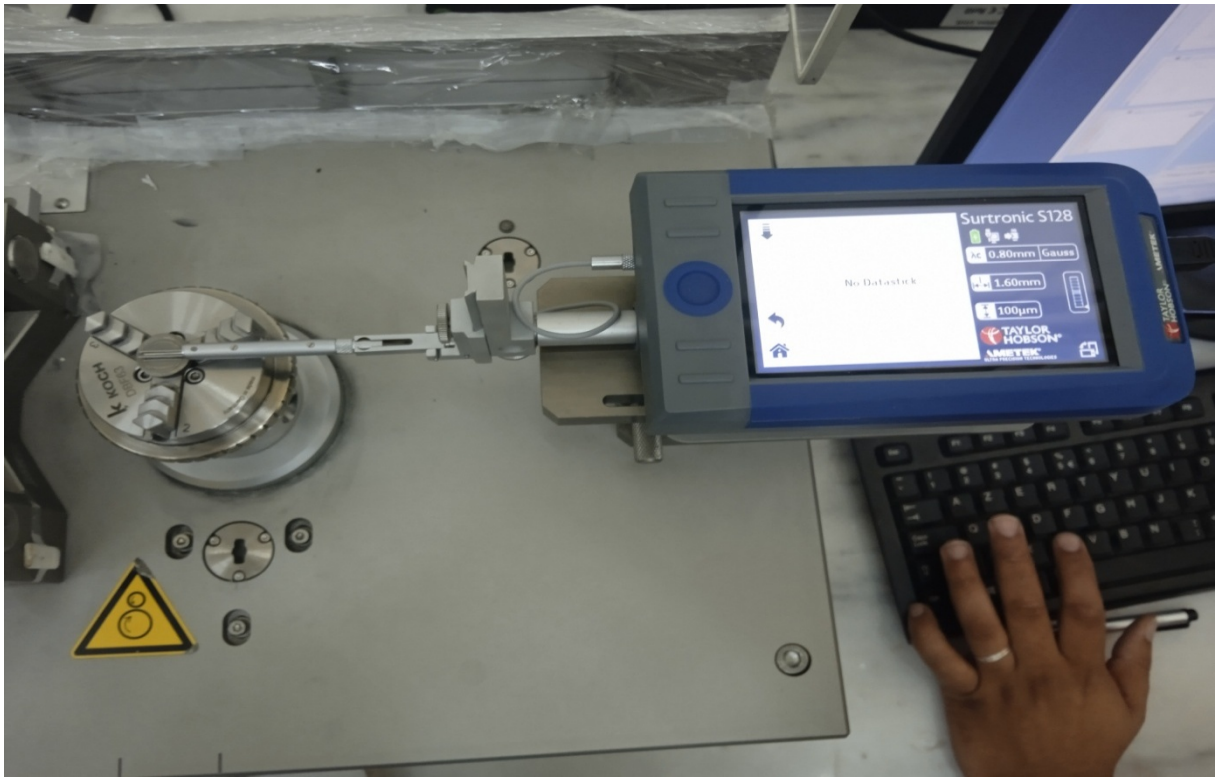

Fig4.1: profilometer

THRUST BEARING Balls :((FAG)

FAG is one of the leading brands in the field of ball bearings and offers a wide range of products, including ball bearings, roller bearings, bearing housings and power transmission solutions. The brand is renowned for its quality and innovation in bearing systems**.**

FAG brand bearing balls are essential components in ball bearings produced by the German company FAG (Fischer Aktien-Gesellschaft). The bearing balls are steel spheres, usually made from a high quality steel such as 100Cr6, which is an alloy of chromium and carbon.

Figeur4.2 :THRUST BEARING 100Cr6

Paraffin oil :

Paraffin oil, also known as white oil, is a type of mineral oil produced through the distillation of crude oil. It is primarily composed of paraffin, a saturated hydrocarbon, and finds wide usage as a lubricant, processing oil, baby oil, laxative, and skin emollient. It is also employed as a dielectric insulator in electrical transformers and as a heat transfer fluid in heating systems. Paraffin oil has low viscosity and is relatively inexpensive compared to other types of oils, making it popular in numerous industrial and commercial applications

Figure4.3: paraffine oil**.**

2-Chemical product:

To carry out our work, which consists in modifying the crystalline structure of kaolin to obtain better properties as well as lubrication additives, we used several chemical products.

2-2 Ethanol:

Ethanol, or ethyl alcohol or simply alcohol, is an alcohol with the semi-developed formula CH_3-CH_2-OH. It is a colourless, volatile, flammable liquid that is miscible with water in all proportions. It is a psychotropic drug, and one of the oldest recreational drugs, in the form of an alcoholic drink.

Figure 4.4 : Ethanol

Acetone:

Acetone is a colorless, volatile liquid compound with the chemical formula (CH3)2CO. It is a ketone and belongs to the group of organic solvents. Acetone is characterized by its strong, sweet-smelling odor and its ability to mix well with water and many organic solvents. It is highly flammable and evaporates quickly at room temperature. Acetone is commonly used as a solvent in various industries, including pharmaceuticals, cosmetics, and chemical manufacturing. It also finds applications as a cleaning agent,

Figure4.5 :acetone

RAW MATERIALS:

2.8. Steel 100Cr6:

For our tests we used 100Cr6 steel. 100Cr6 steel is a steel used in more than 90% of rolling bearings, thanks to its properties : High resistance to adhesive wear, also due to lubrication; resistance to abrasive wear, due to the small non-metallic inclusions and the uniformity in the distribution of the carbide disc, which crushes the inclusions; good resistance to fatigue due to the homogeneity of the structure: the steel is core-hardened due to the presence of chrome.

Chemical Composition :

	C	Mn	Si	P	S	Cr
Min	0.95	0.25	0.15	-	-	1.35
Max	0.10	0.45	0.35	0.030	0.030	1.65

Heat Treatments-Approximate Temperateurs :

Annealed ºC	Quenched ºC	Tempered ºC
720-800	830-870 Oil	150-300

mechanical properties:

Young modulus (MPa)	210000	965
Poisson coefficient	**0.3**	**0.35**
Plastic flow stress (MPa)	**-**	**26**
Hardness (HV)	**800**	**94**

Figure 3-1: Cylindrical bar of 100cr6 Steel.

3. Experimental part :

We used the aditive that Drouiche Mohamed Redaand ElarbiHadjala (thesis Intercalation and exfoliation of kaolinite: application as solid lubricants).preparated last year wichis CTAB and DMSO and Kurea , KNO_3 of added to oil

3.1.SAMPLE PREPARATION:

For our tribological tests we used 100Cr6 steel recovered from sarlmoussaoui which was cut by laser

3.1.1. POLISHING :

then we went to polishing to have a smooth and finished surface using abrasive paper p280 ; p400 ; p600 ; p800 ; p1200 ;p1500;p2000and p3000.We change the abrasive paper when all the scratches getin one direction then we change the orientation of the sample and use the next abrasive paper.

Figure4.6: Polisher

The sample is scrubbed on tissue polishing disks for alumina solution for to mak scratches a ppear.

Figure4.7: polishing disks

so that we can see the scratches and treat them withdiamond suspensionLMD 3µ , LMD 1µ , LMD 0.25µ.

Figure4.8 :diamond suspension.

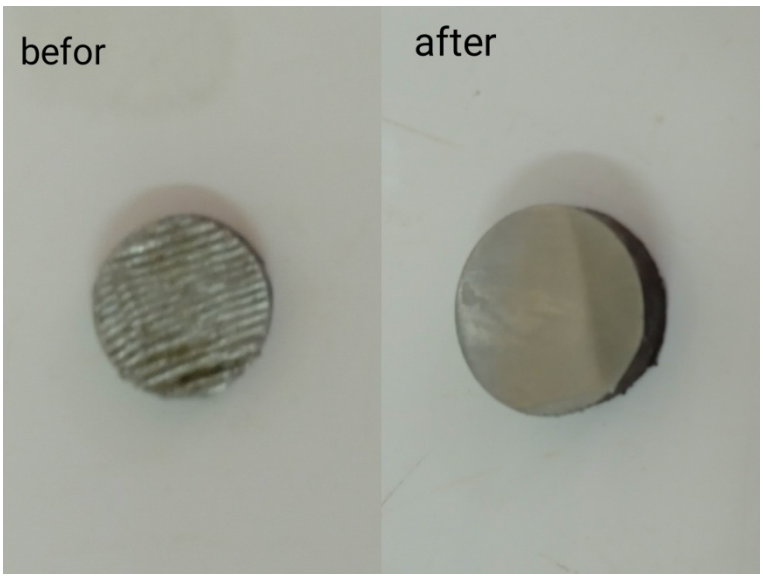

Figeur 4.9:polishing result sample before polishing sample after polishing

LUBRICANT PREPARATION:

THE WEIGHING:

In measuring cylinder We weigh 20 moles, which is equivalent to 16 grams ofparafin oil.We also weigh in watch glass 0.1% which is the equivalent 0.016 g of $KM_{10}I_2$ powder .

Figure 4.10: the weighing of oil anskaoilnit

Homogenization of lubricant :

In a becher , put the oil and powder and mix with a homogenizer five times and the ultra sonic cleaner for four time each and alternatively (2 min in each time).when all steps followed we immediattely test it on the tribometer to prevent the powder from sedimentation.

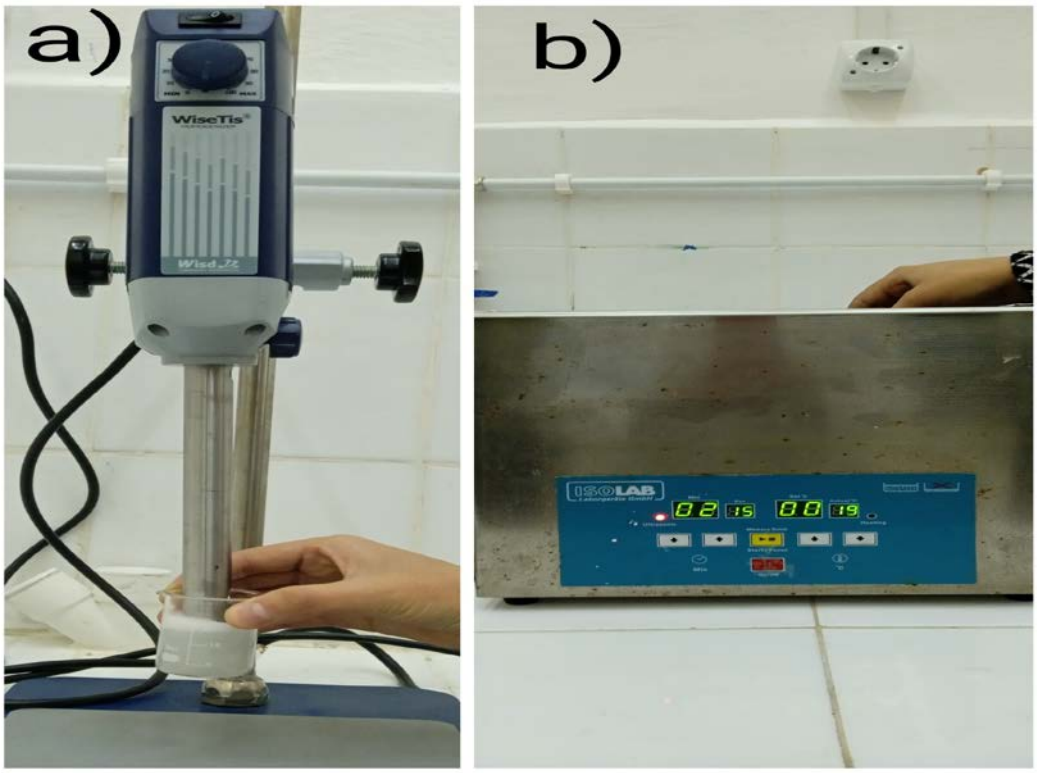

Figure4.11:(a) mixing the solution with a homogenizer (b) dispersing the solution with an ultrasonic bath.

TRIBOMETER :

Firstly we set up the machine by entering the following informations :

Table : Parameters of the tribological tests

Instrument	Partenaire statique	Echantillon	Lubricant
- TRB3 - Serial number 1000108567 - Tribometer / Version 9.0.12 - Date of measurment: 06/02/2023 11:35:46	- Substrat: 100Cr6 - Dimension: 6,00 [mm] - Geometry: Bille	- Coating: KNT-20N-100Cr6-NV-0.1pourcent - Substrat: 100 cr6	- Type: paraffine - Volume: 20,00 [ml] - Application method

Environment	Séquence
- Lab temperature: 14.6 [°C] - Target temperature: 15.0 [°C] - Humidity: 75 [%]	- Repetitions: 1 - Single-way mode - Radius: 5.19 [mm] - Lin. Speed: 10.00 [cm/s] - Acquisition rate: 20.00 [Hz] - Cycles sampled: 1/1 - Pause: 3 [s] without acquisition - Homing at begin: Yes - Normal load: 20.00 [N] - Unload at end: No - Stop condition: 1000.00 [m] or Mu > 2.00 - Effective Stop:Meters

TRIBOMETER TEST:

After we import the information to , we glued the sample on the tribometer funnel and add the lubricant inside it then we put down the ball holder containing a contact ball brought from a thrust bearing with a load of 20 N, then start the test with constant observation in case of accident ,with the saving of the data obtained.

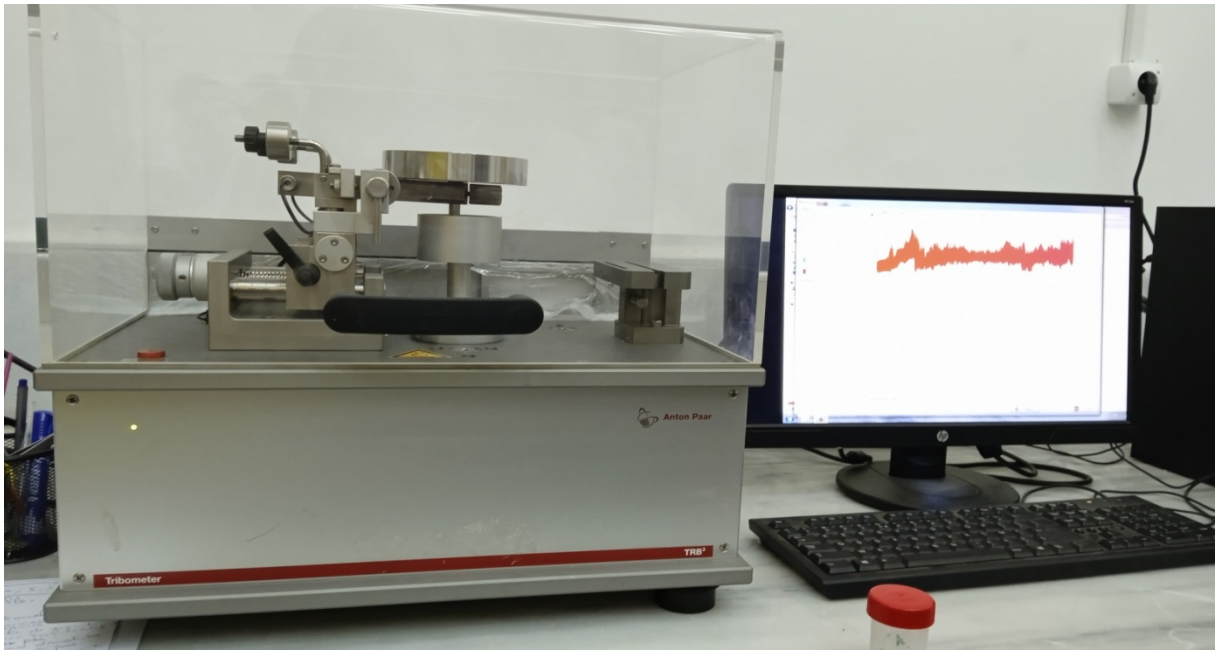

Figure 4.12: the tribometer

MICROSTRUCTURE:

We submerge the sample in acetone to clean it with utilizing the ultrasonic cleaner ,then we dry it with dryer to test it on the optical microscope and choose 100µm as a scale ,then we go find the mark of the wear on the sample and measure it.

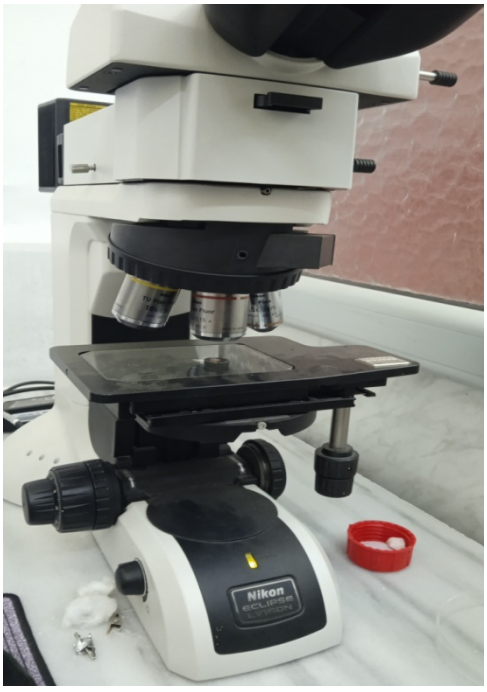

Figure 4.13:an optical microscope

PROFILOMETER:

We firstly reclean the sample to make valid output data represented by a graph, this graph is imported to a program called “GetData Graph Digitizer”, and then the data treated with the program is imported to another program called “Origin” which gives us a graph of the wear curve.

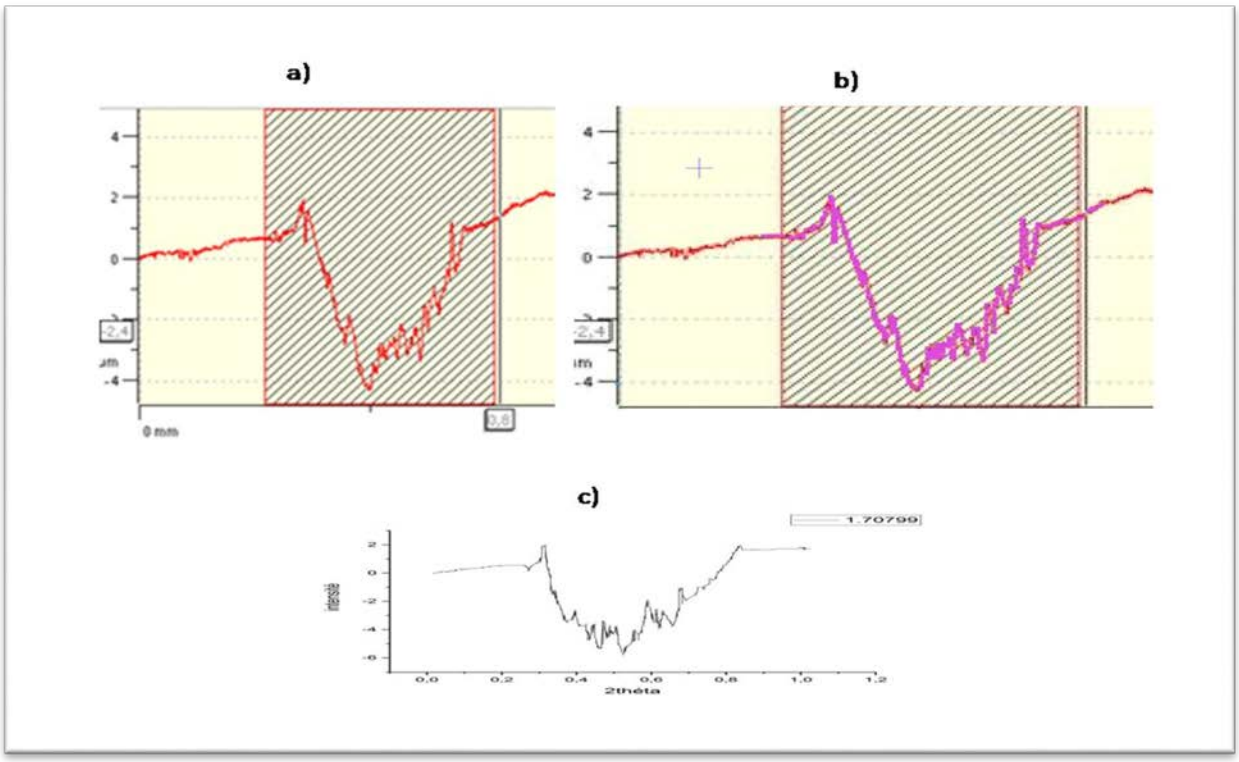

Figure 4.15: 0.5 % KNT 20 N , a) graph in prophilo , b) Graph in Digitizer , c) graph in origin.

PART 2

USED PROCESSORS :

FRICTION STIR PROCESSING

Friction stir processing (FSP) is a variation on FSW. A spinning, non-consumable tool is translated along the surface of a material to form a modified region with improved properties compared to the base material.

QUENCHING:

This is a process of heating and maintaining then fast cooling to retain the beneficial properties it gained through the heating process.

THE THERMAL TREATMENTS:

The termal treatments are carried out in a furnace where the metal parts are heated to high temperature in a controlled gas atmosphere and chosen according to the properties that one wishes to modify: surface hardness, ductility, wear resistance, aesthetic appearance, etc. The final step in a heat treatment cycle is quenching, which is a controlled cooling of parts to bring them to room temperature. The objective is to obtain parts with different mechanical characteristics from the initial parts.

EQUIPMENTS USED:

MILLIN MACHINE :

A milling machine is a machine tool used to machine all types of mechanical parts, individually or in series, by removing material from blocks or sometimes stamped or molded blanks, using a tool called strawberry.

BENCH VISE :

A metal or wooden jaw consisting of two parts that can be brought together by means of a screw to grip the object to be shaped.

METAL CUTTING SAW

The saw is a tool designed to cut.

AN OVEN:

It is a laboratory equipment allowing elements to be heated at regulated temperature by atmospheric pressure or vacuum pressure. Common applications when using an oven are drying, sterilization and hot preservation .

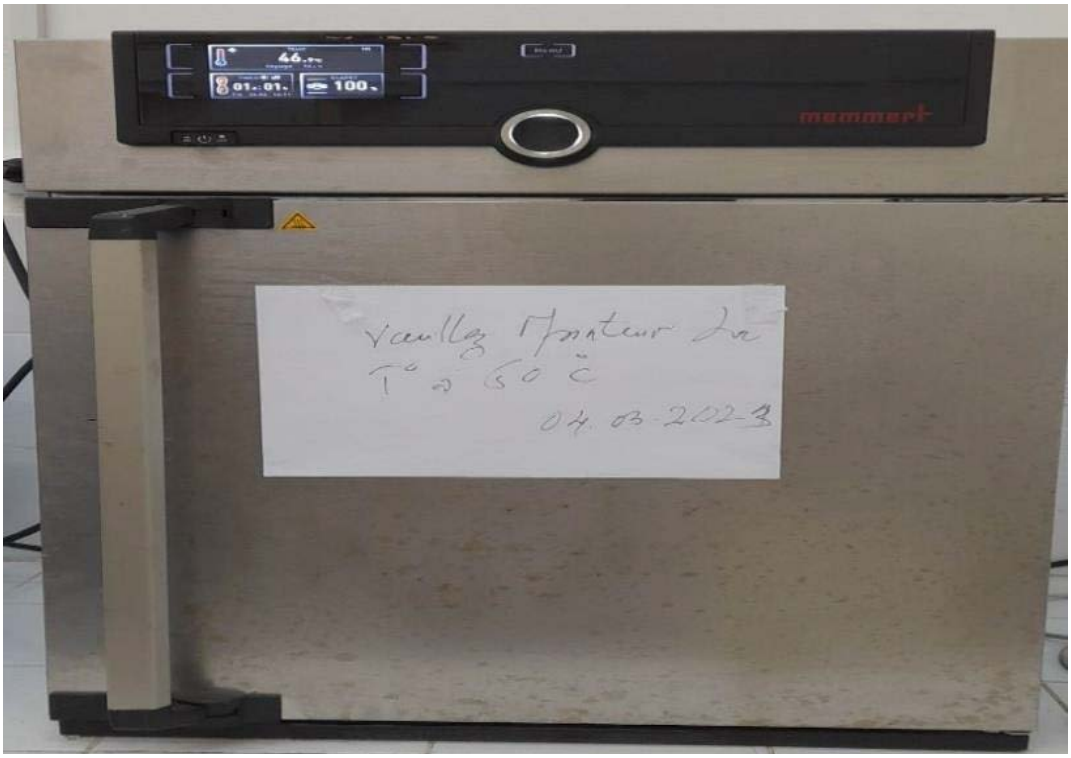

Figure 4.16: An Oven

RAW MATERIAL (2024 Aluminum Alloy):

2024 Aluminum Alloy is a high-strength aluminum alloy primarily composed of aluminum and copper, along with smaller amounts of other elements. It is known for its excellent strength-to-weight ratio and is commonly used in aerospace and structural applications.

General characteristics

Characteristics	Appraisal
Strength	High
Corrosion resistance	Poor
Weldability and brazability	Poor
Workability	Good
Machinability	High

Physical Properties :

Proprety	2024-T3	2024-4,T351	2024-T851
Density	2.78g/cc |0.100 lb/in^3	2.78g/cc |0.100 lb/in^3	2.78g/cc |0.100 lb/in^3

MechanicalProperties :

Property	2024- T3	2024-4, -T351	2024-T851
TensileStrength	483 MPa | 70000 psi	469 MPa | 68000 psi	>=455 MPa | 66000 psi
YieldStrength	345 MPa | 50000 psi	324 MPa | 47000 psi	>=400 MPa | 58000 psi
Modulus of Elasticity	73.1 GPa| 10600 ksi	73.1 GPa | 10600 ksi	72.4 GPa | 10500 ksi

Thermal Properties :

Property	2024-T3	2024-4, -T351	2024-T851
Coefficient of Thermal Expansion @20.0 - 100 °C Temp	23.2 µm/m-°C | 12.9 µin/in-°F	23.2 µm/m-°C | 12.9 µin/in-°F	23.2 µm/m-°C | 12.9 µin/in-°F
Thermal Conductivity	121 W/m-K | 840 BTU-in/hr-ft²-°F	121 W/m-K | 840 BTU-in/hr-ft²-°F	151 W/m-K | 1050 BTU-in/hr-ft²-°F

Chemical Composition :

Element	Minimum %	Maximum %
Silicon	NO MIN	0.5
Iron	NO MIN	0.5
Copper	3.8	4.9
Manganese	0.5	0.6
Magnesium	1.2	1.8
Chromium	NO MIN	0.1
Zinc	NO MIN	0.25
Titanium	NO MIN	0.15
OtherElements	NO MIN	0.05 each, 0.15 in total

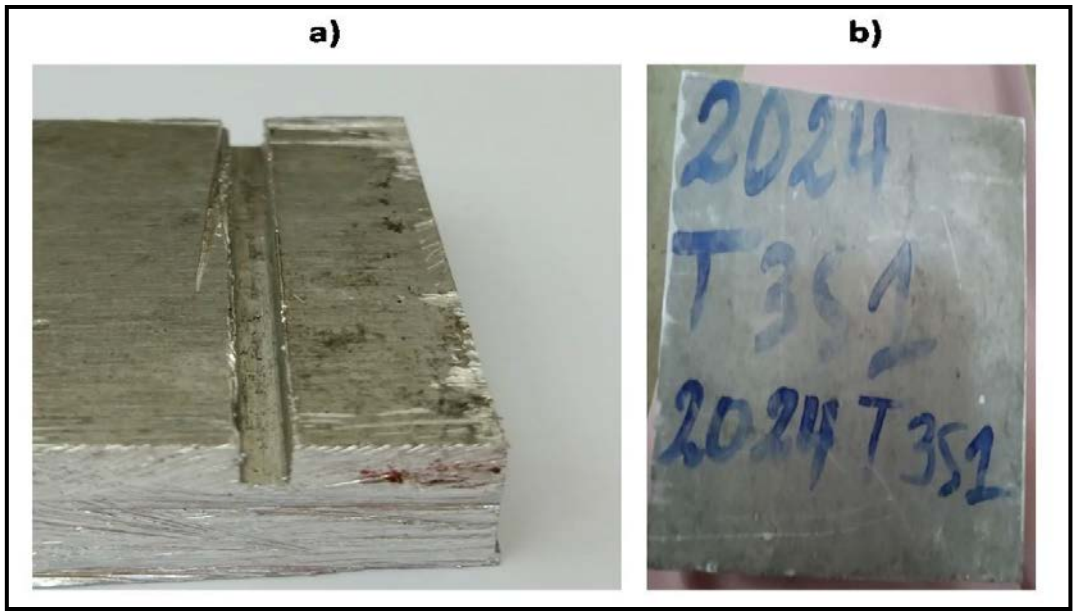

Figure4.17:Al 2024

EXPERIMENTAL SETUP:

- Prepar the Al 2024(put powder): We have used 2024 aluminum alloy as the primary material a tool with rails (2 mm depth), a kUrea rail, a Cr2 AlC rail, and a third rail as a witness.

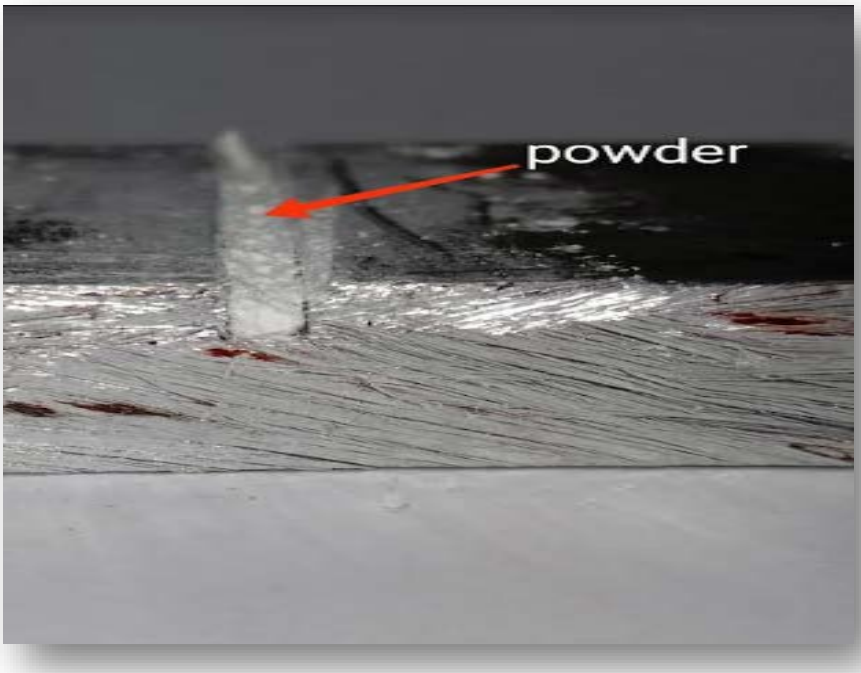

Figure4.18:put the powder in rail

- **Opiration of FSP**

After the bridle of tool we programmed the milling machine with this information :

- rotational speed :1400 Rad/S
- forward speed:60 min/s
- passes:6

Figure 4.19: a) Result of FSP b)During the operation of FSP

3- SAMPLE CUTTING:

We used the vise to hold the raw material and cut it to 21 small samples, We cutted these samples with the hand saw in different zones(zone KUrea , zone Cr_2AlC, zone witness)and different sizes to test each one on different test machine.this 21 samples (12 for microhardness test and 9 for tribology test)

Figure4.20 :the hand saw

THERMAL TREATMENT:

To prepare samples which is one with urea and one with Cr2AlC and one as a reference for hardness testing and a tribometer, we wanted to experiment with changing their properties. The first stage is to put the three samples in the oven at 480 degrees Celsius for one hour, then quickly cool them in water inside a beaker , and in the second stage we put them back In the oven 180 . for 8 hours (thermal treatment)

We repeat the same process with a change in the oven temperature in the first stage, once to 500° and again to 530°.

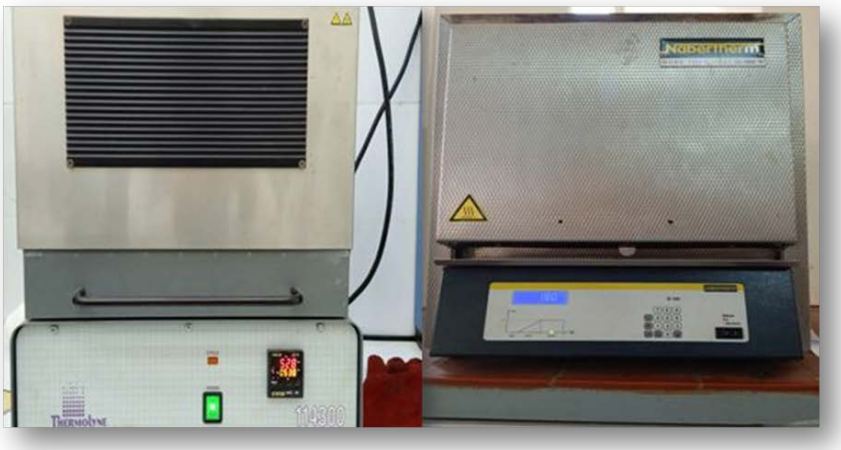

Figure4.21:the ovens used

Figure 4.22: the quenching

Polisng : Due to sample distortion and to ensure accuracy of results and flatness of them, we performed embedding .We start by preparing the resin, put 65% epoxy or 35% hardener, mix well until the color changes, then the mixture is ready to be used in the coating Sample .

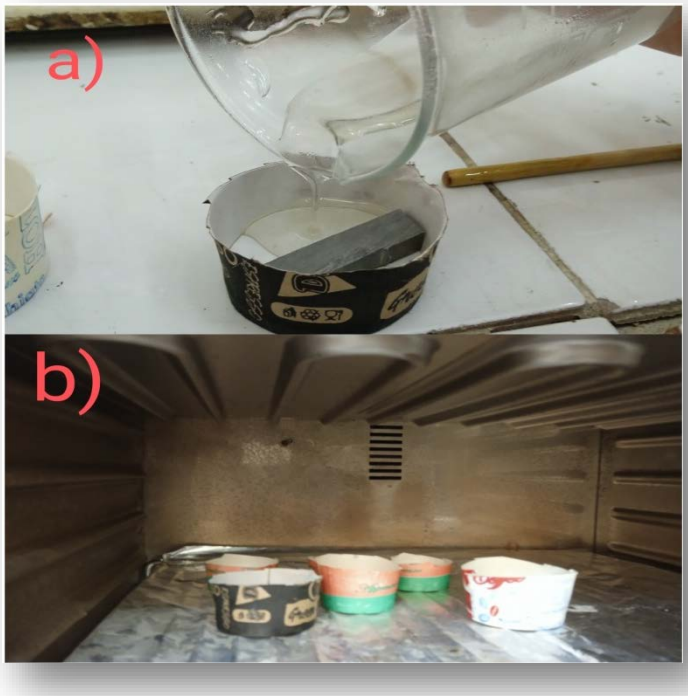

Figure 4.23:a) prepar the coating Sample. b) we put them in an oven

after coating the samples we polishing with abrasive papers from 80µm to 1500 µm.then we pases to the paste diamenti from 3 µm to 0.25 µm to have a final meror state.

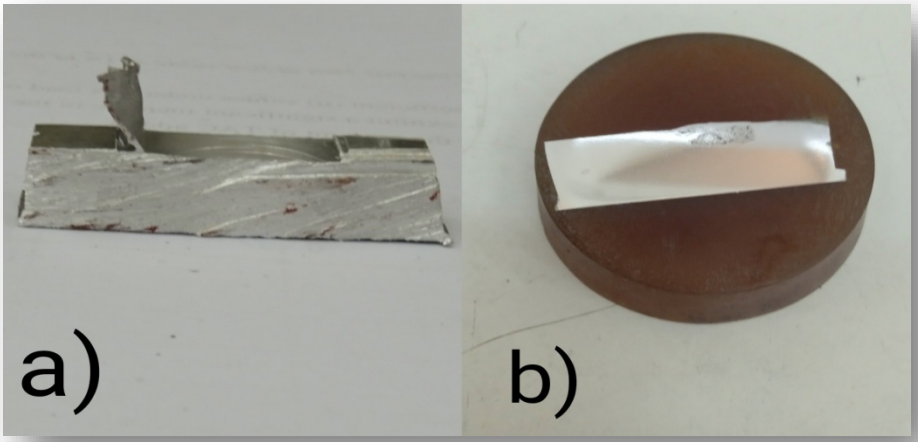

Figure 4.24: a) before coating b) after polising and coating

microhardness test:

After preparing the samples, one of the most important prerequisites for using the Micro Hardness device was that the sample be flat (for the safety of the penetrator, which is a material made of diamond) and also that the sample be wiped with acetone to clean it. After collecting the points and using the Origin program, we draw the evolution of aluminum hardness before and afterthermal thretment.

Figure4.25 :microhardness machin

Trebology test :

Due to time constraints, we were unable to complete all samples. We tested only two samples, one as a witness and a KUrea. We prepared the sample for the tribological test, but this time the contact between the ball and the aluminum was without a lubricant. The test starts at the same time. It records the data of this test to draw the friction graph in terms of time.

Figure4.26: the tribometer

PROFILOMETER:

We reclean the sample to test it with profilometr to make valid output data represented by a graph, this graph is imported to a program called “GetData Graph Digitizer”, and then the data treated with the program is imported to another program called “Origin” which gives us a graph of the wear curve.

CHAPTER 5
Interpretation and Results

1.INTRODACTION:

In this last chapter, we will discuss the results obtained during the different experimental techniques used in our study (tribology, profilometer, microhardness, etc.) and will provide relevant interpretations concerning wear, wear marks and microhardness.

Part one:

1.TRIBOLOGY TEST:

The friction coefficients of the samples are shown in the following figures:

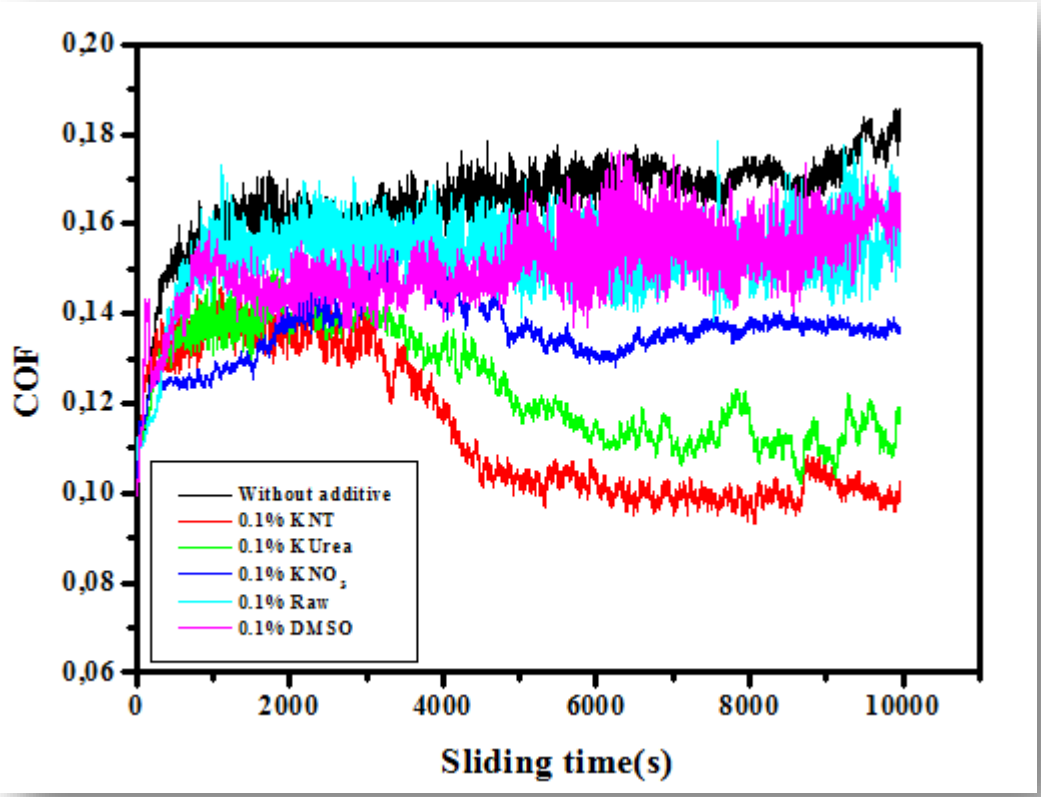

Figure5.1:variation in coefficient of friction for pure oil and oil of parafine+ 0.1% by weight of Kaoilnite Raw 0.1% of $KN0_3$ 0.1% of DMSO 0.1% of KUrea 0.1% of KNT

Table : coefficient of friction as a function of percentage of exfoliated kaoilnite KNT :

% of KNT	0.1% dmso	0/1%Raw	0.1%KUrea	0.1%KNO_3	0.1%KNT	Without additive
COF	0.15	0.15	0.12	0.13	0.11	0.17

COF:**C**oefficient **O**f **F**riction

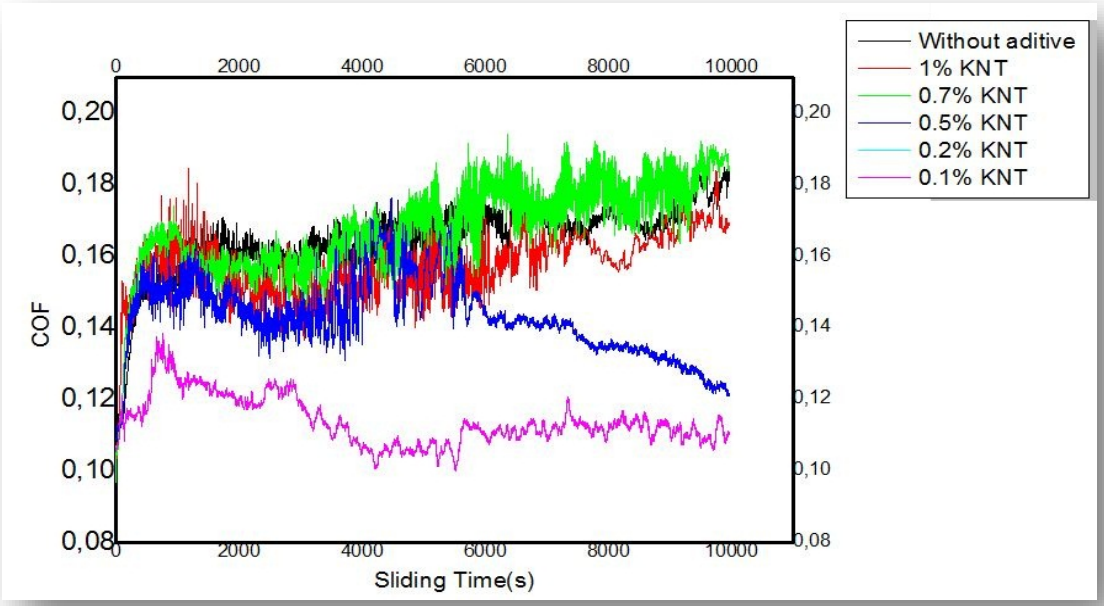

Figure5.2:variation in coefficient of friction for pure oil and oilparafine with deffrent % of kaoilnitenanotube KNT1% 0.7%0.5%0.2% and0.1%

Table : coefficient of friction as a function of percentage of exfoliated kaoilnite KNT :

% of KNT	1%	0.7%	0.5%	0.2%	0.1%	Without additive
COF	0.16	0.15	0.14	0.11	0.11	0.17

COF:Coefficient **O**f **F**riction.

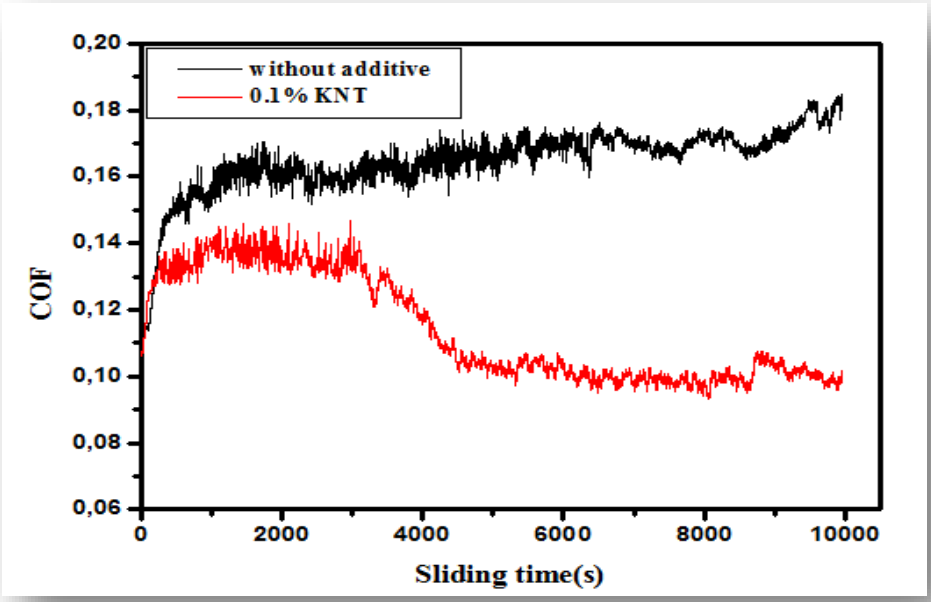

Figure 5.3:variation in coefficient of friction for pure oil and oil with 0.1% of KNT best result

2. PROFILOMETRE TEST:

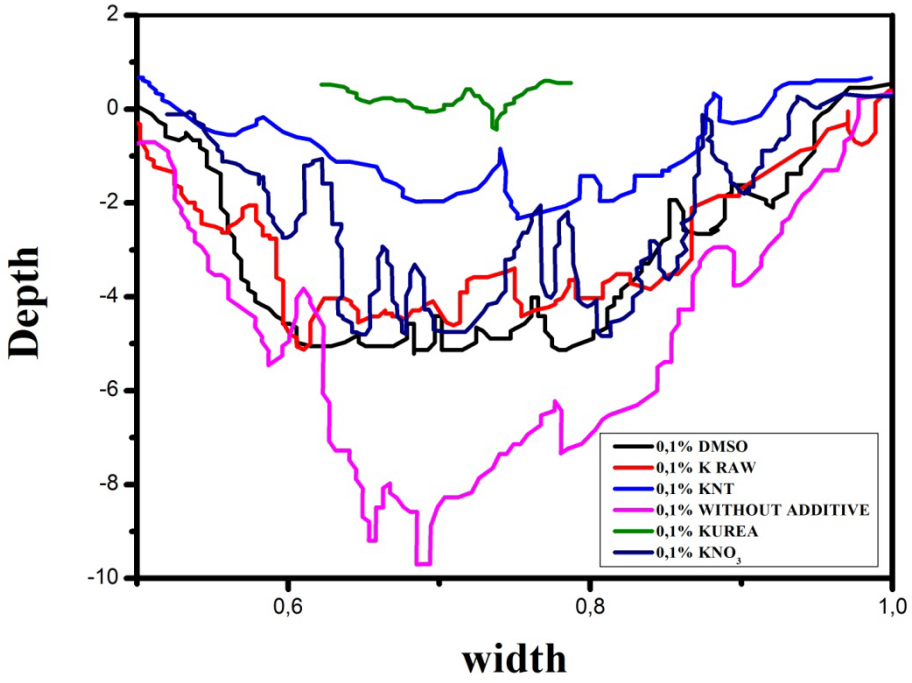

Figure 5.4:trace of wear for worn surfaces lubricated by oil and oil + 0.1% of all expolatedkaoilnite powder ($KN0_3$ DMSO KNT KUrea Raw)

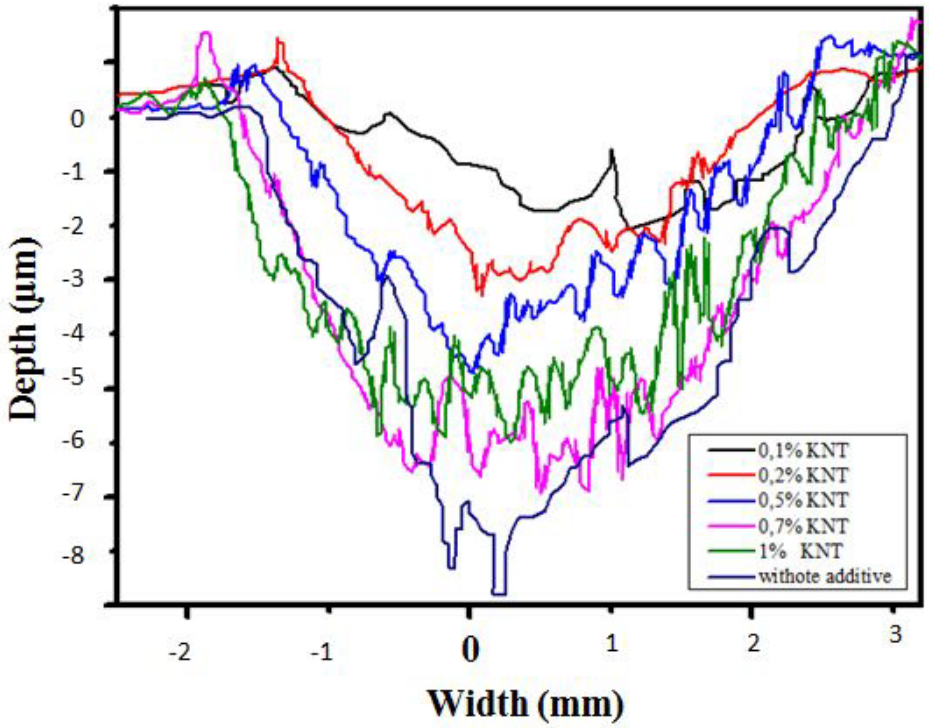

Figure 5.5:wear trace for worn surfaces lubricated by oil and oil + different concentration of KNT

2.1. WEAR RATE CALCULE:

To calculate the rate of wear, we applied the law below:

$$WR = \frac{2\,\pi\,R\,S}{F\,d} = mm^3/Nm$$

S:track area ($mm^{2)}$R :radius (m) π:constant F :charge (N) d : distance (m)

Tabel:wear friction 0.1% All powder kaoilnite

%	Without additive	0.1% $KM_{10}I_2$	0.1% KNO_3	0.1% K urea	0.1% K Raw	0.1% KNT
track area(mm^2)	$1{,}773.10^{-3}$	$2{,}062.10^{-3}$	$1{,}264.10^{-3}$	$1{,}048.10^{-4}$	$2.049.10^{-3}$	$9{,}502.10^{-4}$
Radius(mm)	5,07	5	5,12	6,20	5,07	5,19
Force(N)	20	20	20	20	20	20
Distance(m)	1000	1000	1000	1000	1000	1000
wear ratemm^3/Nm	$2{,}823.10^{-6}$	$3{,}238.10^{-6}$	$2{,}032.10^{-6}$	$2{,}042.10^{-7}$	$3{,}263.10^{-6}$	1,548.10-6

Tabel:represent all the % of KNT

KNT	Without additive	0.1%	0.2%	0.5%	0.7%	1%
track area(mm^2)	$1{,}773.10^{-3}$	$9{,}502.10^{-4}$	$9{,}275.10^{-4}$	$9{,}840.10^{-4}$	$2{,}287.10^{-3}$	$1{,}988.10^{-3}$
Radius(mm)	5,07	5,19	5,19	5,18	5,07	5,02
Force(N)	20	20	20	20	20	20
Distance(m)	1000	1000	1000	1000	1000	1000
wear ratemm^3/Nm	$2{,}823.10^{-6}$	$1{,}548.10^{-6}$	$1{,}511.10^{-6}$	$1{,}600.10^{-6}$	$3{,}641.10^{-6}$	$3{,}135.10^{-6}$

3.THE OPTICAL MICROSCOPY:

3.1.Trace wear samples:

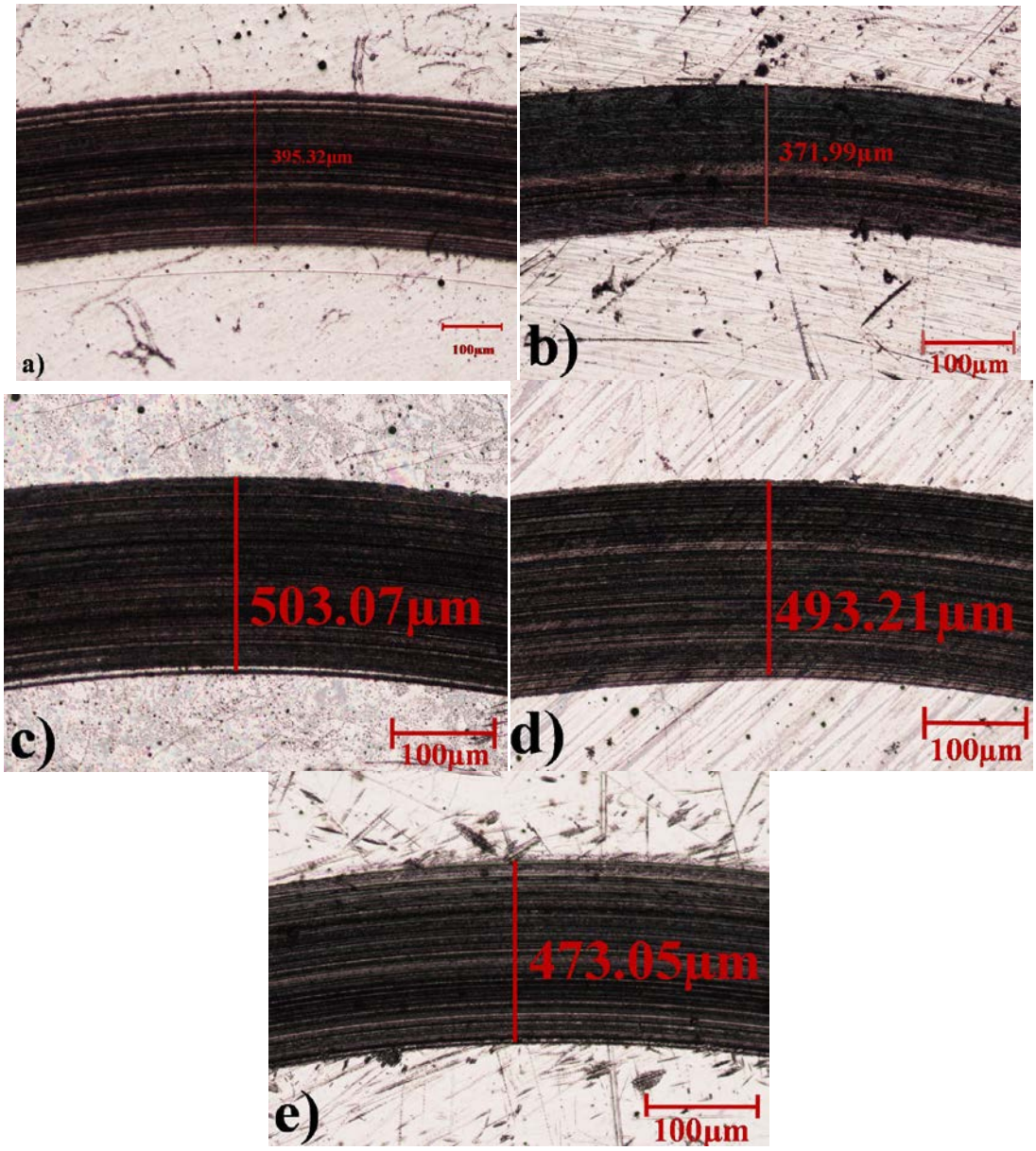

Figure 5.6:a). b). c.) d). e). f) shows the optical microscopy of the wear marks for the different samples a of KNT 1% 0.7% 0.5% 0.2% 0.1%

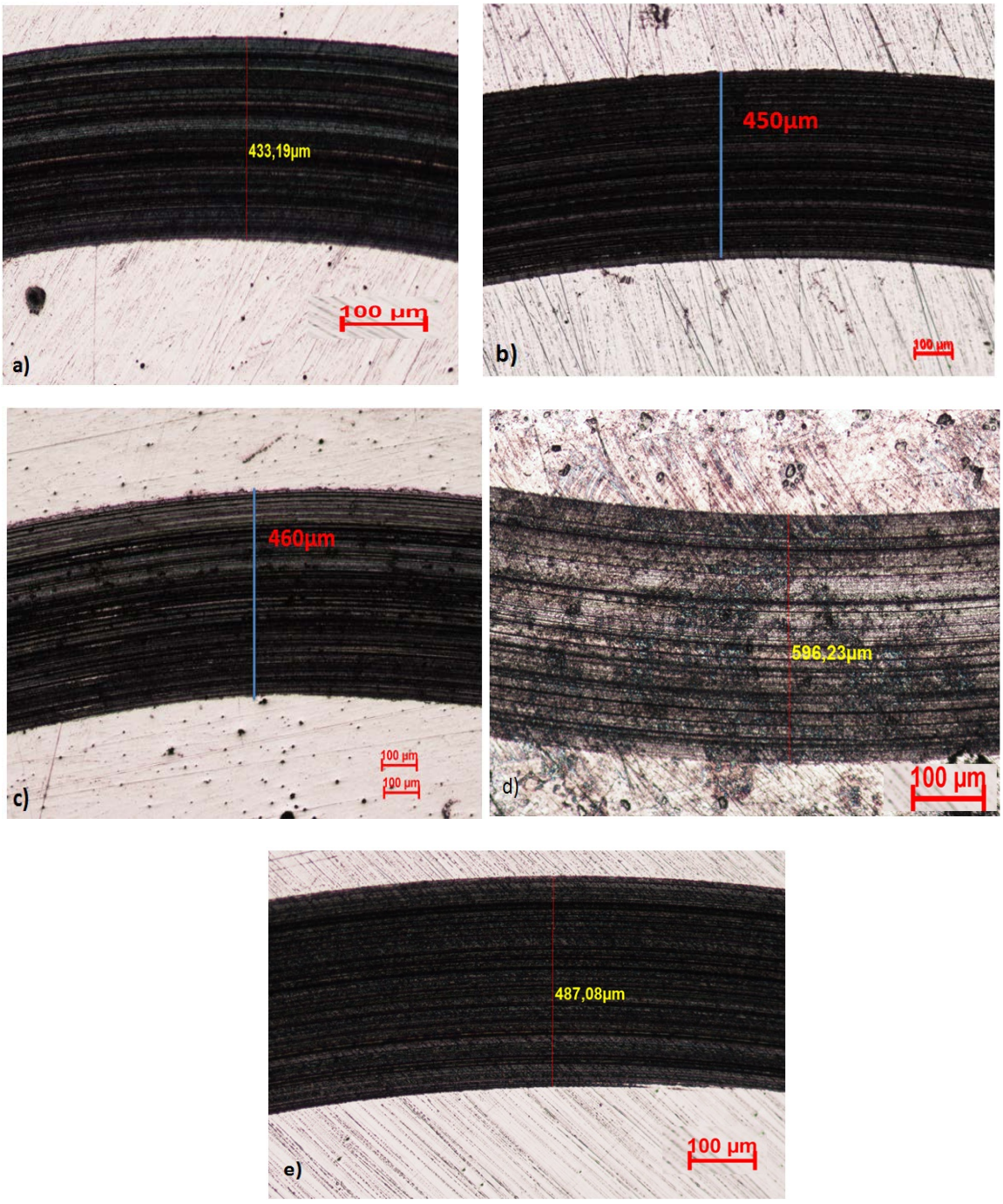

Figure 5.7:a) .b).c.)d).e).f)shows the optical microscopy of the wear marks for the different samples ofpawderkaoilniteexfolié.

3.2. WEAR MARKS OF BALLS:

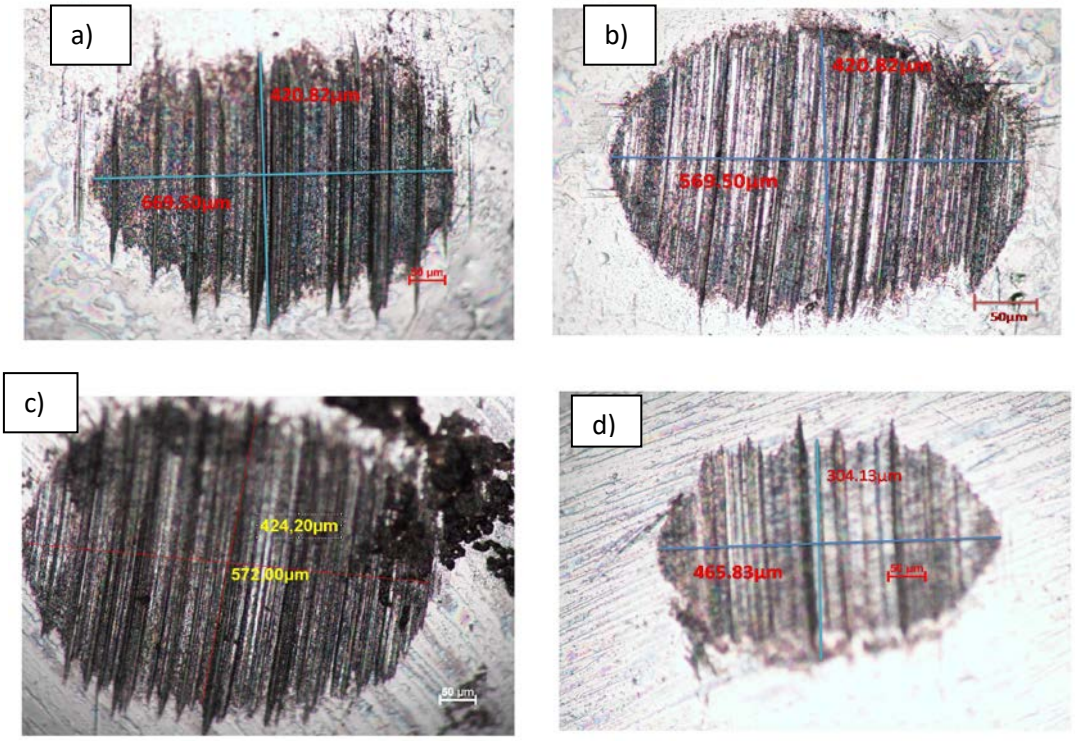

Figure 5.8: Optical microscopy of wear marks of 100Cr6 steel balls a)Kno_3 b)DMSO C) Raw d)kuera

This is what happened in our experience:

When the ball comes into contact with the surface, it exerts pressure, causing the ball to penetrate the surface and move in a circular path. This phenomenon is called "running-in" and leads to increased friction between the ball and the surface. During this contact, two types of wear mechanisms take place. The first one is adhesive wear, which occurs when the ball rubs against the surface, generating particles that form a powder. This powder consists of eroded particles from the surface. The second mechanism is abrasive wear, facilitated by the movement of these powder particles. The powder deposits onto the sample's surface, resulting in material transfer between the ball and the sample. In this experiment, both the ball and the sample are made of 100 CR6 material.

To mitigate these wear mechanisms, a lubricant (oil + additive "kaolinite") is applied. The purpose of the oil is to create a protective film called a tribofilm, which reduces direct contact between the ball and the sample. When kaolinite is added to the oil, it infiltrates the tribofilm, composed of kaolinite and iron oxide. This infiltration of kaolinite helps decrease the coefficient of friction and wear between the ball and the sample.

The kaolinite particles fill in any surface irregularities or tiny gaps between the ball and the sample, resulting in a smoother contact surface. This filling effect reduces the chances of asperity collisions and abrasive wear. Additionally, kaolinite itself possesses inherent anti-wear properties due to its structure and composition. It can form a protective layer that resists wear and prevents direct metal-to-metal contact.

Overall, the combination of oil and kaolinite diminishes friction by providing lubrication, forming a protective tribofilm, filling surface irregularities, and exhibiting anti-wear properties. These combined effects work together to reduce the coefficient of friction and minimize wear between the ball and the sample.

Part 2

1.Optical microscope:

Figure5.9: image from inkscapepresent optical microscope result showing the FSP of Al2024 Cr2 AlC

Figure5.10: image from inkscapepresent optical microscope result showing the FSP of Al2024 KUrea

2.Microhardnes:

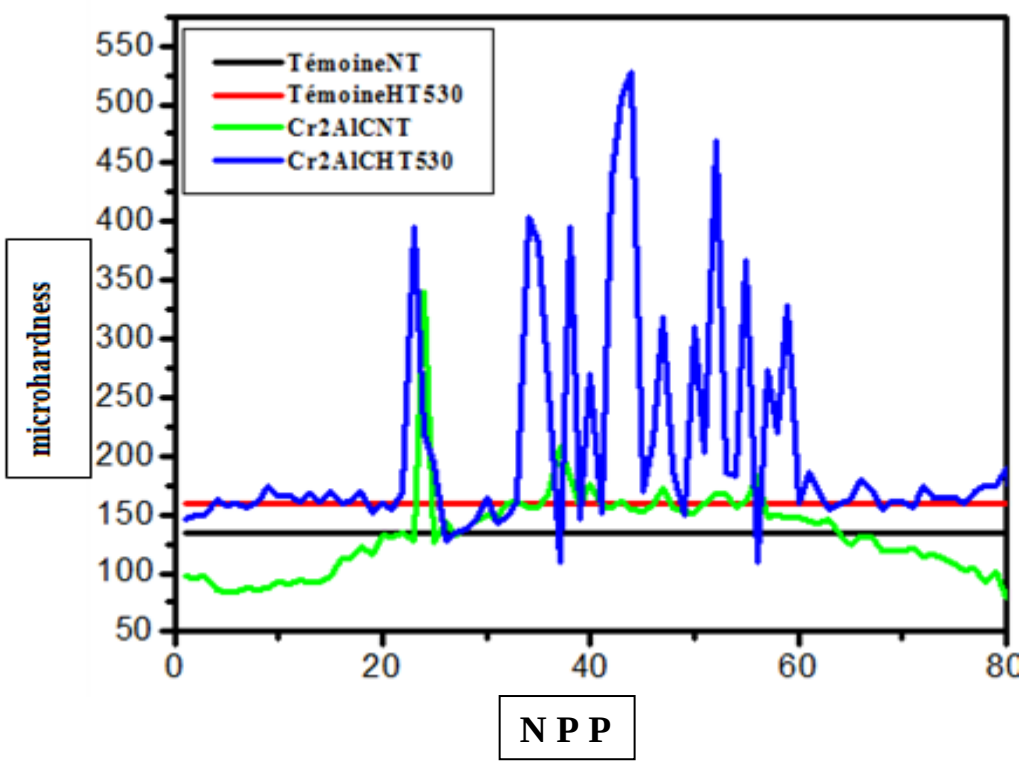

Figure5.11: The varaition hardness changes in each of these samples witness not heat treated ,witness heat treated Al2024 530 °, Cr_2AlC not heat treated and Al2024 Cr_2AlC heat treat530°

N P P:Number of**P**enatration**P**oints

From these results, it can be seen that the Cr_2AlC HT 530 sample showed the highest hardness value; This increase is probably due to decomposition of the grain size of Al 2024 composite with Cr_2AlC due to FSP and number of passes of FSP

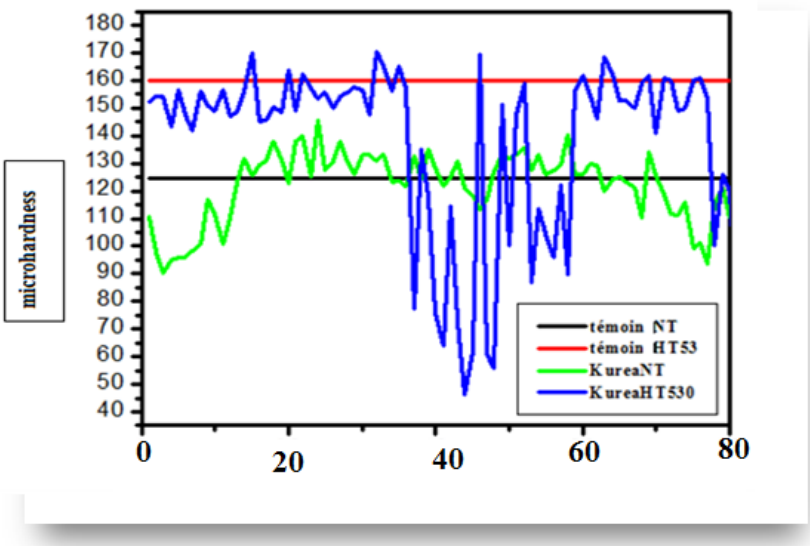

Figure5.12: The varaition hardness changes in each of these samples witness not heat treated, witnessheat treated 530 °, Al2024 +KUreanot heat treated and Al2024+KUrea heat treat 530°.

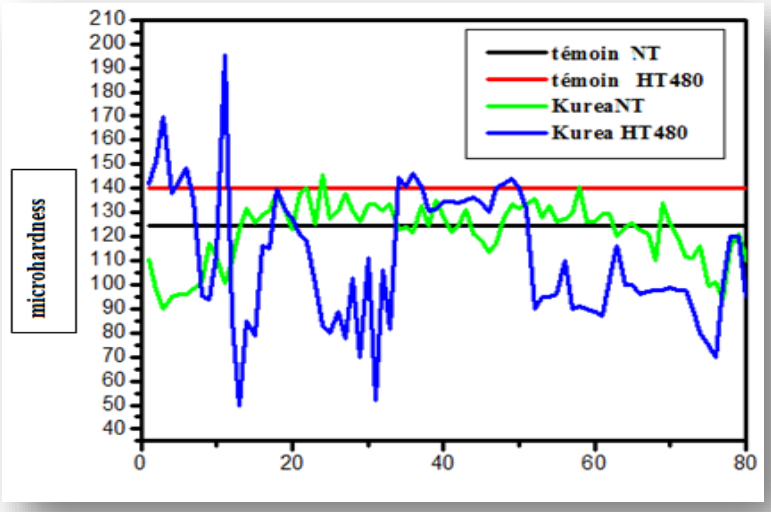

Figure5.13: The varaition hardness changes in each of these samples witness not heat treated ,witness heat treated 480 °, Al2024 +KUreanot heat treated and Al2024+KUrea heat treat 480°.

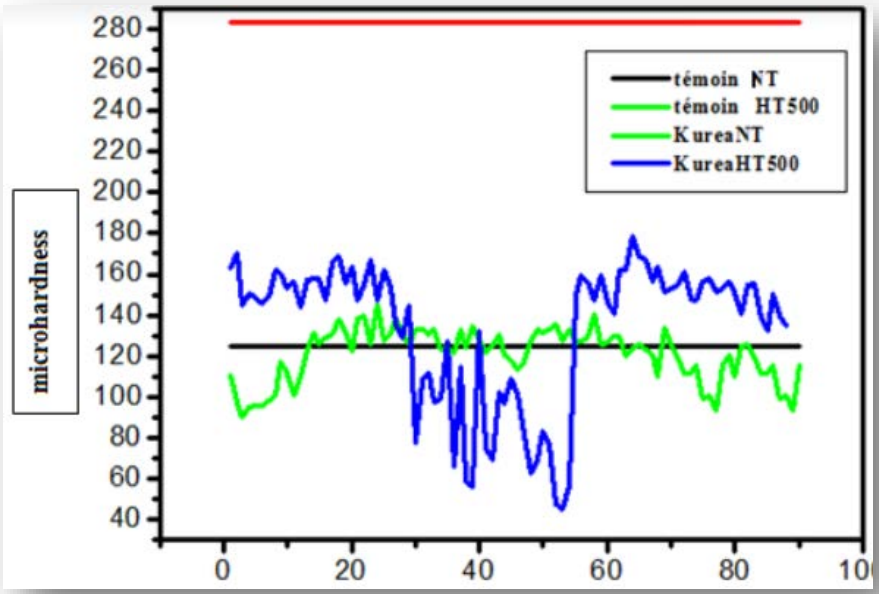

Figure 5.14: The varaition hardness changes in each of these samples witness not heat treated ,witness heat treated 500 °, Al 2024 KUrea not heat treated and Al 2024 KUreaheat treat500°.

3.TRIBOLOGY TEST:

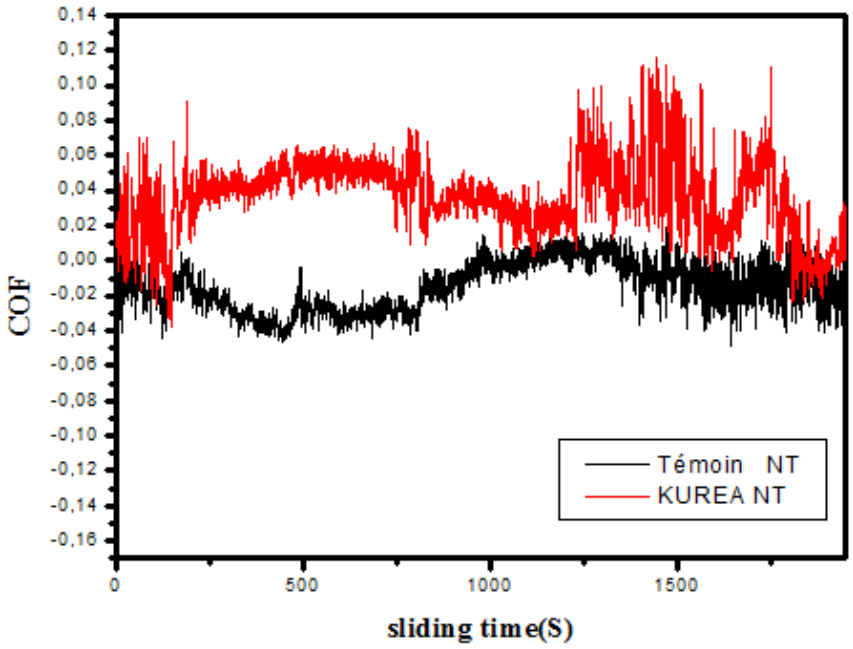

Figure 5.15:variation in coefficient of friction for Al 2024 witout friction stir processing and Al 2024 +KUrea with FSP

4.PROFILOMETRE TEST:

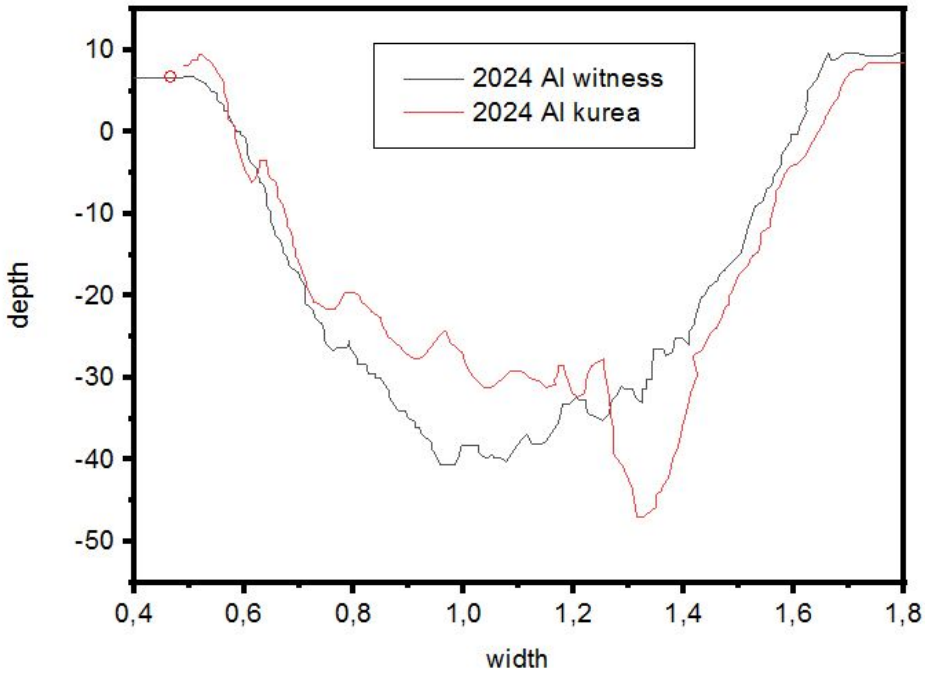

Figure5.16: wear trace for worn surfaces for Al 2024 witout friction stir processing and Al 2024 +KUrea with FSP

The reduction in grain size typically results in an increase in microhardness after friction stir treatment. Smaller grain sizes mean a higher density of grain boundaries, which act as obstacles to dislocation movement. The increased number of grain boundaries and their interaction with dislocations impede their movement and contribute to the material's increased hardness.

In addition to the grain refinement effect, friction stir treatment can also lead to the formation of fine-scale precipitates or other microstructural changes that can further contribute to the increase in microhardness.

It is important to note that the relationship between microhardness and grain size after friction stir treatment can vary depending on the specific material as we Kurea give bad result and 2024Al + Cr2 AlC Micro-hardness augmentation in FSP-treated areas, process parameters, and other factors. However, in general, a decrease in grain size tends to be associated with an increase in microhardness due to the effects of grain boundary strengthening and impediment of dislocation motion.

Conclusion:

The aim of this work is to study the behavior and tribological properties of the 2D kaolinite as an additive in paraffine oil.

The 4 different 2D kaolinites prepared by different methods were added in the oil according to different pourcentages. The effect of content as well as the synthesis method of the 2D kaolinite was studied.

The results revealed that the wear rate varied depending on the type and proportion of additive used.

All the 2D Kaolinite materials decreased the friction coefficient and the wear rate of the 100Cr6/100Cr6 steel contact. The best preparation method was the samples named K-CTAB and K-Urea.

The lubricant K-Urea and K-CTAB gave the best results in reducing the coefficient of friction and wear, while the results were not good when using the KUrea as a reinforcment in Al 2024.

The results were compared with the MAX phase Cr_2AlC, the latter gave the best results after heat treatement, the microhardness results increased up to 500Hv.

REFERENCES

1. Clay minerals, including kaolinite, montmorillonite and illite, arelayered silicate minerals, which are important materials widely used in industrial products, such as ceramic, plastic, paint, paper, rubber and cosmetic [1].
2.
3. On the origin of the name kaolin and the kaolin deposits of the Kauling and Dazhou areas, Kiangsi, China [1]

4. Y. Hu, X. Liu, Chemical composition and surface property of kaolins, Miner. Eng.16 (2003) 1279–1284. (2)

5. G.B. West, Further consideration of the crystal structure of kaolinite, Mineral.
6. Mag. 31 (1958) 781–786.[3]

Siretanu, D. van den Ende, F. Mugele, Atomic structure and surface defects at
7. mineral-water interfaces probed by in situ atomic force microscopy, Nanoscale
8. 8 (2016) 8220–8227.[4]

9. H. Cheng, J. Yang, Q. Liu, J. Zhang, R.L. Frost, A spectroscopic comparison of
10. selected Chinese kaolinite, coal bearing kaolinite and halloysite—a mid-infrared
11. and near-infrared study, Spectrochim. Acta A 77 (2010) 856–861.[5]

12. S.A. Carroll-Webb, J.V. Walther, A surface complex reaction model for the pH-dependence of corundum and kaolinite dissolution rates, Geochim. Cosmochim. Acta 52 (1988) 2609–2623[6]

13. C. Ma, R.A. Eggleton, Surface layer types of kaolinite: a high-resolution transmission electron microscope study, Clay Clay Miner. 47 (1999) 181–191.[7]

14. R. Duarte-Silva, M.A. Villa-García, M. Rendueles, M. Díaz, Structural, textural
15. and protein adsorption properties of kaolinite and surface modified kaolinite
16. adsorbents, Appl. Clay Sci. 90 (2014) 73–80.[8]

17. H. Cheng, Q. Liu, J. Yang, J. Zhang, R.L. Frost, Thermal analysis and infrared
18. emission spectroscopic study of halloysite-potassium acetate intercalation compound,Thermochim. Acta 511 (2010) 124–128. [9]

19. H. Cheng, J. Yang, Q. Liu, J. He, R.L. Frost, Thermogravimetric analysis-mass
20. spectrometry (TG-MS) of selected Chinese kaolinites, Thermochim. Acta 507–
21. 508 (2010) 106–114.[11]

22. S. Tosoni, K. Doll, P. Ugliengo, Hydrogen bond in layered materials: structural
23. and vibrational properties of kaolinite by a periodic B3LYP approach,
24.
25. ChemInform 37 (2006) 2135–2143.[15]

26. T. Attila, K. Róbert, R.K. Szilágyi, The positions of inner hydroxide groups and

27. aluminium ions in exfoliated kaolinite as indicators of the external chemical environment, Phys. Chem. Chem. Phys. 16 (2014) 25830–25839.[0]

28. B. Ndlovu, S. Farrokhpay, E. Forbes, D. Bradshaw, Characterisation of kaolinite
29. colloidal and flow behaviour via crystallinity measurements, Powder Technol.
30. 269 (2015) 505–512.[16]

31. S.W. Bailey, R.B. Langston, Anauxite and kaolinite structures identical, Clay Clay Miner. 17 (1969) 241–243.[17]

32. D.M.M. Krishantha, R.M.G. Rajapakse, D.T.B. Tennakoon, H.V.R. Dias, AC impedance analysis of polyaniline–montmorillonite nanocomposites, Ionics 12
33. (2006) 287–294.[18]

34. G.S. Sen, K.G. Bhattacharyya, Adsorption of heavy metals on kaolinite and montmorillonite: a review, Phys. Chem. Chem. Phys. 14 (2012) 6698–6723.
35. [19]

36. K. Sakurai, A. Teshima, K. Kyuma, Changes in zero point of charge (ZPC), specific surface area (SSA), and cation exchange capacity (CEC) of kaolinite and[20].

37. E. Reinoso-Maset, J. Ly, Study of major ions sorption equilibria to characterize
38. the ion exchange properties of kaolinite, J. Chem. Eng. Data 59 (2014)
39. 4000–4009[21]

40. D.B. Ward, Effect of Al and organic acids on the surface chemistry of kaolinite,
41. Clay Clay Miner. 46 (1998) 453–465.[22]

42. D.H. Everett, W.A. House, Adsorption on heterogeneous surfaces, Surf. Sci. 42
43. (2007) 552–564.[23]

44. K.O. Adebowale, I.E. Unuabonah, B.I. Olu-Owolabi, Adsorption of some heavy
45. metal ions on sulfate- and phosphate-modified kaolin, Appl. Clay Sci. 29 (2005)
46. 145–148.[24]

47. V. Gupta, Surface Charge Features of Kaolinite Particles and their Interactions,
48. (Dissertations & Theses), Gradworks, 2011.[25]

49. C. Appel, L.Q. Ma, R.D. Rhue, E. Kennelley, Point of zero charge determination
50. in soils and minerals via traditional methods and detection of electroacoustic
51. mobility, Geoderma 113 (2003) 77–93.[26]

52. K. Khawmee, A. Suddhiprakarn, I. Kheoruenromne, B. Singh, Surface charge
53. properties of kaolinite from Thai soils, Geoderma 192 (2013) 120–131.[27]

54. Y. Yukselen-Aksoy, A. Kaya, A study of factors affecting on the zeta potential of kaolinite and quartz powder, Environ. Earth Sci. 62 (2011) 697–705.[28]

55. E. Reinoso-Maset, J. Ly, Study of major ions sorption equilibria to characterize
56. the ion exchange properties of kaolinite, J. Chem. Eng. Data 59 (2014) 4000–4009.[30]

57. P.B. Lorenz, Surface conductance and electrokinetic properties of kaolinite beds, Clay Clay Miner. 17 (1969) 223.[31]

58. [1] I. Naghmouchi, F.X. Espinach, P. Mutjé, S. Boufi, Polypropylene composites based on lignocellulosic fillers: How the filler morphology affects the composite properties, Materials & Design, 2015; 65: 454–461

59. [3] I. Naghmouchi, P. Mutjé, S. Boufi, Olive stones flour as reinforcement in polypropylene composites: A step forward in the valorization of the solid waste from the olive oil industry, Industrial Crops and Products, 2015; 72: 183–191.

60. [7] H. Djidjelli, A. Boukerrou, R. Founas, A. Rabouhi, M. Kaci, J. Farenc, J.J. Martinez-Vega, D. Benachour, Preparation and characterization of poly (vinyl chloride)/virgin and treated sisal fiber composites, Journal of Applied Polymer Science, 2007; 103: 3630-3636.

61.] T.J. Madera-Santana, H. Soto Valdez, M.O.W. Richardson, Influence of surface treatments on the physicochemical properties of short sisal fibers: Ethylene vinyl acetate composites, Polymer Engineering and Science, 2013; 53: 59-68.

[61] V. Sharma, U. Prakash, B.V.M. Kumar, *Surface composites by friction stir processing: A review*, Journal of Materials Processing Technology, vol. 224, pp. 117–134, 2015, doi: 10.1016/j.jmatprotec.2015.04.019

[62] R.S. Mishra, P.S. De, N. Kumar, Friction Stir Welding and Processing, Springer, 2014. doi: 10.1007/978-3-319-07043-8

[63] S. Bharti, N.D. Ghetiya, K.M. Patel, A review on manufacturing the surface composites by friction stir processing, Materials and Manufacturing Processes, vol. 36, iss. 2, pp. 135–170, 2021, doi: 10.1080/10426914.2020.1813897

[64] R.A. Gite, P.K. Loharkar, R. Shimpi, Friction stir welding parameters and application: A review, Materials Today: Proceedings, vol. 19, pp. 361– 365, 2019, doi: 10.1016/j.matpr.2019.07.613

[65] S. Rathee, S. Maheshwari, A.N. Siddiquee, M. Srivastava, *Effect of tool plunge depth on reinforcement particles distribution in surface composite fabrication via friction stir processing*, Defence Technology, vol. 13, iss. 2, pp. 86–91, 2017, doi: 10.1016/j.dt.2016.11.003

[66] I. Dinaharan, N. Murugan, A. Thangarasu, Development of empirical relationships for prediction of mechanical and wear properties of AA6082 aluminum matrix composites produced using friction stir processing, Engineering Science and Technology, an International Journal, vol. 19, iss. 3, pp. 1132–1144, 2016, doi: 10.1016/j.jestch.2016.02.004

[67] R.D. Bourkhani, A.R. Eivani, H.R. Nateghi, *Through-thickness inhomogeneity in microstructure and tensile properties and tribological performance of friction stir processed*

AA1050-Al2O3 nanocomposite, Composites Part B: Engineering, vol. 174, Available online, 2019, doi: 10.1016/j.compositesb.2019.107061

[68] H. G. Rana, V. J. Badheka, A. Kumar, Fabrication of Al7075 / B4C Surface Composite by Novel Friction Stir Processing (FSP) and Investigation on Wear Properties, Procedia Technology, vol. 23, pp. 519–528, pp. 519–528 2016, doi: 10.1016/j.protcy.2016.03.058

[69] M. Narimani, B. Lotfi, Z. Sadeghian, *Investigating the microstructure and mechanical properties of Al-TiB2 composite fabricated by Friction Stir Processing (FSP)*, Materials Science and Engineering: A, vol. 673, pp. 436–442, 2016, doi: 10.1016/j.msea.2016.07.086

[70] F. García-Vázquez, B. Vargas-Arista, R. Muñiz, J.C. Ortiz, H.H. García, J. Acevedo, *The Role of Friction Stir Processing (FSP) Parameters on TiC Reinforced Surface Al7075-T651 Aluminum Alloy*, Soldagem&Inspeção, vol. 21, iss. 4, pp. 508–516, 2016, doi: 10.1590/0104-9224/si2104.10

[71] S.S. Mirjavadi, M. Alipour, A.M.S.Hamouda, A. Matin, S. Kord, B.M. Afsharif, P.G. Koppad, *Effect of multi-pass friction stir processing on the microstructure, mechanical and wear properties of AA5083/ZrO2 nanocomposites*, Journal of Alloys and Compounds, vol. 726, pp. 1262–1273, 2017, doi: 10.1016/j.jallcom.2017.08.084

[72] E. Moustafa, Effect of Multi-Pass Friction Stir Processing on Mechanical Properties for AA2024/Al2O3 Nanocomposites, Materials, vol. 10, iss. 9, p. 1053, 2017, doi: 10.3390/ma10091053

[73] P. Ebrahimzad, M. Ghasempar, M. Balali, Friction Stir Processing of Aerospace Aluminum Alloy by Addition of Carbon Nano Tube, Transactions of the Indian Institute of Metals, vol. 70, iss. 9, pp. 2241–2253, 2017, doi: 10.1007/s12666-017-1062-5

[74] N. Yuvaraj, S. Aravindan, Vipin, *Fabrication of Al5083/B4C surface composite by friction stir processing and its tribological characterization*, Journal of Materials Research and Technology, vol. 4, iss. 4, pp. 398–410, 2015, doi: 10.1016/j.jmrt.2015.02.006

[75] V. Sharma, Y. Gupta, B.V.M. Kumar, U. Prakash, Friction Stir Processing Strategies for Uniform Distribution of Reinforcement in a Surface Composite, Materials and Manufacturing Processes, vol. 31, iss. 10, pp. 1384–1392, 2016, doi: 10.1080/10426914.2015.1103869

[76] D.K. Lim, T. Shibayanagi, A.P. Gerlich, *Synthesis of multi-walled CNT reinforced aluminium alloy composite via friction stir processing*, Materials Science and Engineering: A, vol. 507, iss. 1–2, pp. 194–199, 2009, doi: 10.1016/j.msea.2008.11.067

[77] P. Sevvel ,V. Jaiganesh, Effects of axial force on the mechanical properties of AZ80A Mg alloy during friction stir welding, Materials Today: Proceedings, vol. 4, iss. 2, pp. 1312–1320, 2017, doi: 10.1016/j.matpr.2017.01.152

[78] N. Busu, M.S. Jaffarullah, C.Y. Low, M.S.B. Shaari, Armansyah, A. Jaffar, A Review of Force Control Techniques in Friction Stir Process, Procedia Computer Science, vol. 76, pp. 528–533, 2015, doi: 10.1016/j.procs.2015.12.331

[79] O.P. Abolusoro, E.T. Akinlabi, S.V. Kailas, Tool rotational speed impact on temperature variations, mechanical properties and microstructure of friction stir welding of dissimilar high-strength aluminium alloys, Journal of the Brazilian Society of Mechanical Sciences and Engineering, vol. 42, iss. 4, pp. 1–12, 2020, doi: 10.1007/s40430-020-2259-9

[80] F.J. Liu, L. Fu, H.Y. Chen, Effect of high rotational speed on temperature distribution, microstructure evolution, and mechanical properties of friction stir welded 6061-T6 thin plate joints, The International Journal of Advanced Manufacturing Technology, vol. 96, iss. 5–8, pp. 1823–1833, 2018, doi: 10.1007/s00170-018-1736-0

[81] J. Luo, J.F. Xiang, L. Yuan, H.X. Lin, X.R. Wu, D.Z. Xie, Heat transfer and metal flow behavior of AA7075 high-strength aluminum alloy in a new currentinduced friction stir welding with a multi-physics field model based on the inverse method and parameter scanning batch processing technique, The International Journal of Advanced Manufacturing Technology, vol. 111, iss. 9–10, pp. 2615–2635, 2020, doi: 10.1007/s00170-020-06249-y

[82] K. Elangovan,V. Balasubramanian, Influences of tool pin profile and welding speed on the formation of friction stir processing zone in AA2219 aluminium alloy, Journal of Materials Processing Technology, vol. 200, iss. 1–3, pp. 163–175, 2008, doi: 10.1016/j.jmatprotec.2007.09.019

[83] N. Dialami, M. Cervera, M. Chiumenti, *Effect of the Tool Tilt Angle on the Heat Generation and the Material Flow in Friction Stir Welding*, Metals, vol. 9, iss. 1, pp. 1–17, 2018, doi: 10.3390/met9010028

[84] E.R.I. Mahmoud, M. Takahashi, T. Shibayanagi, K. Ikeuchi, *Effect of friction stir processing tool probe on fabrication of SiC particle reinforced composite on aluminium surface*, Science and Technology of Welding and Joining, vol. 14, iss. 5, pp. 413–425, 2009, doi: 10.1179/136217109X406974

[85] D.B. Darmadi, M. Talice, *Improving the strength of friction stir welded joint by double side friction welding and varying pin geometry*, Engineering Science and Technology, an International Journal, vol. 24, iss. 3, pp. 637–647, 2021, doi: 10.1016/j.jestch.2020.11.001

[86] A.C. Ferreira Magalhães, *Thermoelectric Measurements for Temperature Control of Robotic Friction Stir Welding*, PhD thesis, University West, Trollhättan, Sweden, 2020.

[87] P. Upadhyay, A.P. Reynolds, *Effects of thermal boundary conditions in friction stir welded AA7050-T7 sheets*, Materials Science and Engineering: A, vol. 527, iss. 6, pp. 1537–1543, 2010, doi: 10.1016/j.msea.2009.10.039

[88] MA., Z.Y. (2008). Friction stir processing technology: A review. Metallurgical and Materials Transactions A, 39(3): 642-658. https://doi.org/10.1007/s11661-007- 9459-0

[89] a*Faculty of Engineering, University of Kragujevac, SestreJanjic 6, 34000 Kragujevac, Serbia,* bIMW *Institute, Aleja Milanovic bb, 34325 Luznice, Serbia,*
c*AMM Manufacturing, Aleja Milanovic bb, 34325, Luznice, Serbia.*